Modelling and Experimental Evaluation of an Active Thermal Energy Storage System with Phase-Change Materials for Model-Based Control

Vasken Dermardiros

A Thesis

in the Department

of

Building, Civil and Environmental Engineering

Presented in Partial Fulfillment of the Requirements

for the Degree of Master of Applied Science (Building Engineering) at

Concordia University

Montréal, Québec, Canada

September 2015

© Vasken Dermardiros 2015

CONCORDIA UNIVERSITY

CONCORDIA UNIVERSITY

School of Graduate Studies

This is to certify that the thesis prepared

By: Vasken Dermardiros

Entitled: Modelling and Experimental Evaluation of an Active Thermal Energy Storage System with Phase-Change Materials for Model-Based Control

and submitted in partial fulfillment of the requirements for the degree of

Magistrate of Applied Science (Building Engineering)

complies with the regulations of the University and meets the accepted standards with respect to originality and quality.

Signed by the final Examining Committee:

_____ Chair
Dr. Fariborz Haghighat

_____ Supervisor
Dr. Andreas K. Athienitis

_____ Examiner
Dr. Marius Paraschivoiu External (to program)

_____ Examiner
Dr. Fariborz Haghighat

_____ Examiner
Dr. Radu G. Zmeureanu

Approved by _____
Dr. Fariborz Haghighat, GPD
Department of Building, Civil and Environmental Engineering

_____
Dr. Amir Asif, Dean
Department of Building, Civil and Environmental Engineering

Date _____

Abstract

Modelling and Experimental Evaluation of an Active Thermal Energy Storage System with Phase-Change Materials for Model-Based Control

Vasken Dermardiros

This thesis presents an experimental and numerical investigation of an active thermal energy storage (TES) system utilizing phase-change material (PCM). The PCM-TES intended for building integration consists of PCM panels with active air circulation between the panels. Air is drawn through a channel to charge and discharge the PCM enabling the system to be used for both heating and cooling purposes – conditioned air, room air or outdoor air for night cooling can be utilized. This creates the possibility of a low thermal mass building to operate more like a high mass building and thereby gaining advantages commonly associated with traditional TES systems such as an ability to incorporate peak load reducing and shifting strategies without the significant weight of a traditional high mass building.

A prototype PCM-TES is built and tested in an environmental chamber. The experimental data collected is used for model validation. A 30th order non-linear model with varying thermal capacitance {C(T)} is developed and compared for fitness to experimental data. A simplified 2nd order model is shown to adequately predict the dynamic response of the system for thermal charging/discharging and can be incorporated into model-based control systems, which are effective in peak load reducing and shifting strategies. Simplified models are easier to implement and calibrate since they contain fewer parameters to adjust which could be learned in real time (online calibration) by using measurements from the building automation system to compensate for installation and construction tolerances.

The model was extended to investigate the effect of increasing the exposed surface area to the air stream by having more air circulation channels while keeping the total air mass flow rate and convective heat transfer coefficients constant. Increasing the exposed area resulted in faster responding systems.

A case study was simulated to demonstrate the use of the simplified 2nd order non-linear PCM-TES model for heating peak load reduction. The PCM-TES was shown to reduce the peak by at least 50% for the simulated conditions.

Acknowledgements

First and foremost, I would like to thank my supervisor Prof. Andreas K. Athienitis for giving me the privilege to work with him. Throughout these past 2 years, you have granted me innumerable enriching experiences: the ICEBO Workshop, SNEBRN AGM, the Solar Canada Conference in Toronto and the Pivotry Workshop in 2013; the eSim Conference in Ottawa and the PhD Summer School in 2014; the 6th Annual IBPC in Torino Italy in June 2015, the CZEBS-iiSBE-APEC Symposium in August 2015 and the Energy Forum on Advanced Building Skins Conference in Bern Switzerland in November 2015. In between these notable events, we had numerous meetings under our CZEBS/SNEBRN Network and the NSERC/Hydro-Québec Industrial Research Chair. Throughout these meetings, I have met research leaders from around the world, have collaborated with them and have enriched my understanding of the many facets of building physics. Thank you for your support!

I would like to thank the late Prof. Paul Fazio. You were a pioneer and a visionary. By creating the Building Engineering program in Concordia, you aspired many young students to follow their passions. Our research laboratory, the Paul Fazio Solar Simulator Environmental Chamber facility, bears your name and though you are no longer with us, your legacy lives on.

I would like to acknowledge and thank the financial support received through the Concordia Graduate Scholarship in Natural Sciences and Engineering Research, the Faculty of Engineering and Computer Science Graduate Scholarship, the Concordia University 25th Anniversary Fellowship Entrance Scholarship and the financial support directly from Prof. Athienitis.

This work is part of an ongoing research project at Concordia University funded by a Natural Sciences and Engineering Research Council (NSERC) & Hydro Québec Industrial Research Chair. The research program aims to optimize operation and improve energy efficiency in buildings. The chair benefits from a close partnership of Hydro-Québec, Concordia University, Régulvar, and Natural Resources Canada CanmetENERGY. I would like to thank Ahmed Daoud, Jocelyn Milette, Eric Dumont and the rest of the Hydro-Québec IREQ LTE team. I would like to thank José Candanedo and Vahid Dehkordi from NRC CanmetENERGY. I would also like to thank Gabrielle Mainville, Carlos Mollinedo, Mathieu Lajoie and Marc Dugré from Régulvar.

From the administrative team, I would like to thank Jiwu Rao, Gerald Parnis, Jacques Payer, Lyne Dee, Jenny Drapeau, Olga Soares, Debbie Walker and Linda Swinden. From the technical team, I would like to thank Luc Desmers, Jaime Yeargans, Tiberiu Aldea and Joe Hrib.

Working at the office was enriching because of the great and enthusiastic people I had the opportunity to be surrounded with. I would like to especially thank Sam Yip and Costa Kapsis for the hours of conversation we have had about architecture, engineering, and an innumerable other subjects. I would like to thank Diane Bastien for our symbiotic relationship! Without you, I would not have had an experiment to work with! Thank you for your hard work on the procurement of the PCM panels, as well as the hours of discussion on the modelling methodologies. Thank you Edvinas Bigaila, Yuxiang Chen, William Gagnon, Ana López-Terradas, James Bambara, Jennifer Date, Stratos Rounis, Tasos Papachritsou, Zissis Ioannidis, Ahmad Kayello, Tingting Yang, Peter Luk, Sophie Yuan, Shahriar Hossain, Ali Saberi, Mathieu Le Cam, Nunzio Cotrufo, Nicholas Zibin, and Andreea Mihai. I would like to thank Scott Bucking for the conversations we have had about advanced simulation/optimization/automation studies; I believe there is indeed a great future in the field. I would also like to thank Francesco Guarino, Maurizio Cellura, Benoit Delcroix and Katherine D'Avignon for our PCM collaborations and discussions.

Finally, I would like to thank my friends and family for believing in me (and for not asking too many questions!). Last, but may perhaps have been first, I want to thank Elsa Monanteras, my girlfriend whom I've practically known longer than I've not known her, for cheering me up during the long hours of work, for motivating me to continue and to stay strong.

To everyone, a firm, Thank You!

Table of Contents

List of Figures

List of Tables

Nomenclature

Scripts

i	nodal index, active
j	nodal index, neighbouring
t	time index

Variables

A	surface or cross sectional area, m^2
A_{PCM}	total PCM surface area in contact with the air stream, m^2
$C(T)_i^t$	capacitance as a function of its temperature, $J \cdot K^{-1}$
$C_{p,\,average}$	average specific heat of PCM in the sensible range, $J \cdot kg^{-1} \cdot K^{-1}$
D_h	hydraulic diameter, {defined as: 4·cross_sectional_area·wetted_perimeter^{-1}}, m
E	cumulative energy balance, J
f	friction factor
$F_{i \to j}$	view factor, surface i to j
K	hydraulic loss coefficient
k_{liquid}	conductivity of the liquid phase, $W \cdot m^{-1} \cdot K^{-1}$
k_{solid}	conductivity of the solid phase, $W \cdot m^{-1} \cdot K^{-1}$
L	characteristic linear dimension, m
L_{rough}	absolute roughness, m
M	number of thermal nodes with specified temperatures
$\dot{m}_{air}$	air mass flow rate, $kg \cdot s^{-1}$
N	number of thermal nodes
N_{DR}	diffusivity ratio
P_{fan}	fan power required, W
$\dot{Q}_i$	heat flow into the node, W
R_{ij}	resistance between nodes i and j, $K \cdot W^{-1}$
$skew$	*skewness* factor
$slope$	slope of the transition between phases

T_i^t	temperature, K, unless specified as °C
T_b	bulk air temperature, K, unless specified as °C
T_c	approximate temperature of peak phase change, specific heat equation, °C
T_k	approximate temperature of peak phase change, conductivity equation, °C
T_p	temperature at the center of the pipe, K
$T_{surface}$	average temperature of the front and back PCM surfaces, °C
T_w	average temperature of the channel wall surface, K
U_{ij}	conductance between nodes i and j, $W \cdot K^{-1}$
v	average fluid velocity, $m \cdot s^{-1}$
w	width of the air control volume, m
Δh	enthalpy of fusion, $J \cdot kg^{-1}$
Δp	pressure drop in pipe or duct, Pa
Δt	timestep, s
η_{fan}	combined fan and motor efficiency, %
ε	emissivity
μ	fluid dynamic viscosity, Pa·s
ρ	fluid density, $kg \cdot m^{-3}$
σ	Stefan-Boltzmann constant, $5.67 \cdot 10^{-8}$ $W \cdot m^{-2} \cdot K^{-4}$
ω	temperature range of phase change, °C

Dimensionless Numbers

$$\mathrm{Re} = \frac{\text{inertial forces}}{\text{viscous forces}} = \frac{\rho v L}{\mu}$$

$$\mathrm{Nu} = \frac{\text{convective heat transfer}}{\text{conductive heat transfer}} = \frac{hL}{k}$$

$$\mathrm{Pr} = \frac{\text{viscous diffusion rate}}{\text{thermal diffusion rate}} = \frac{C_p \mu}{k}$$

Acronyms

ASHRAE	American society of heating, refrigerating and air-conditioning engineers
ASTM	American society for testing and materials
BAS	Building automation system
BEMS	Building energy management system
BIPV/T	Building integrated photovoltaic/thermal
CFD	Computational fluid dynamics
CFM	Cubic feet per minute
CMHC	Canadian mortgage and housing corporation
CTF	Conduction transfer function
DSC	Differential scanning calorimetry
FDM	Finite difference method
FPS	Feet per second
HDPE	High-density polyethylene
HVAC	Heating, ventilation and air conditioning
IEA	International energy agency
MBC	Model-based control
MPC	Model-based predictive control
NSERC	Natural sciences and engineering research council [of Canada]
PCM	Phase-change material
PCM-TES	Phase-change material based thermal energy storage
RTD	Resistance temperature detector
SI	System identification
SSEC	[Paul Fazio] Solar simulator-environmental chamber
TABS	Thermo-active building system
TES	Thermal energy storage
TOU	Time-of-use [electrical pricing]
VAV	Variable air volume
WWR	Window-to-wall ratio

Chapter 1

Introduction

The first chapter consists of: the research motivation, a description of the laboratory environment, a conceptual summary, a description of the experimental set-up and finally an overview of the chapters that follow.

1.1 Background

In Québec, 99% of electricity generated originates from renewable sources, almost entirely from hydropower (Hydro-Québec, 2014). However, a 0.9% growth in power demand is expected annually which will be met by gas-operated turbine peaking generators (CNW Telbec, 2015). In the United States and internationally, reducing the peak power demand will avert the construction of new peaking power plants that could alternatively be burning diesel oil or jet fuel. Commercial, institutional and residential buildings account for about 33% of secondary energy consumption in Québec and 51% of the electricity consumption (NRCan-OEE, 2013). Winters are characterized by large electricity demand peaks due to electrically-based heating loads. Thus, there are significant opportunities to reduce and shift peak demand associated with space heating by using the building thermal storage mass and possibly phase change materials (PCM).

Most large commercial and institutional building constructions contain significant thermal mass in the form of exposed concrete. They can store heat and release it at a later time. However, they do so slowly with time constants that can be of the order of 1-3 days, implying that an anticipatory control system is required. (Athienitis, Stylianou and Shou, 1990; Candanedo, Allard and Athienitis, 2011) By modifying zone thermostat setpoints, the charge and discharge of the building thermal mass can be effectively controlled based on predictions of the building response to future weather and occupancy – one or more days ahead. The building mass may be cooled during the night with minimal energy by circulating cooler outside air; during the day, the cooled mass becomes a heat sink and enables the chillers to be activated for less time. In winter, the mass can absorb solar radiation and release it in a controlled manner while avoiding overheating. Potential overall improvements include the reduction of the peak demand for heating and cooling, aiding in demand side management, a decrease in the mechanical room footprint, energy savings, better load matching and enhanced thermal comfort. (Arteconi, Hewitt and Polonara, 2012; Childs and Stovall, 2012; Chen, Athienitis and Galal, 2014)

Traditional lightweight steel and wood-framed buildings, such as small commercial or residential buildings, do not possess significant thermal mass. They can be retrofitted with phase-change material (PCM)-based thermal energy storage (TES) systems placed adjacent to or within the zones they will serve. Within the phase-change temperature range of a thin and light shape-stabilized PCM panel, the panel would store around 12 times energy per weight compared with concrete or brick and has around 2.5 times the thermal capacitance of water[1]. The integration of this material can result in a lightweight building having the equivalent thermal mass of a heavy concrete building. PCMs has the ability to potentially decouple the concept of effective thermal mass from actual physical weight. It can be used to reduce the peak energy demand. However, for PCMs to be fully effective, the controls must ensure that the material undergoes a phase change otherwise it simply acts in its sensible range and thus offers no more thermal capacitance than any other common building material.

---

[1] Δh of DuPont Energain centered around phase change temperature range (18 to 26) °C = 88.67 $kJ \cdot kg^{-1}$
Cp concrete: 0.88 $kJ \cdot kg^{-1} \cdot K^{-1}$, for $\Delta T = 8°C \rightarrow \Delta h = 7.04\ kJ \cdot kg^{-1}$, and so 88.67/7.04 = 12.6x more concrete by weight to equal the same thermal capacitance.
Cp water: 4.18 $kJ \cdot kg^{-1} \cdot K^{-1}$, for $\Delta T = 8°C \rightarrow \Delta h = 33.44\ kJ \cdot kg^{-1}$, and so 88.67/33.44 = 2.65x
Material properties of PCM from (Kuznik, Virgone and Noel, 2008); of concrete and water from (Çengel and Ghajar, 2010)

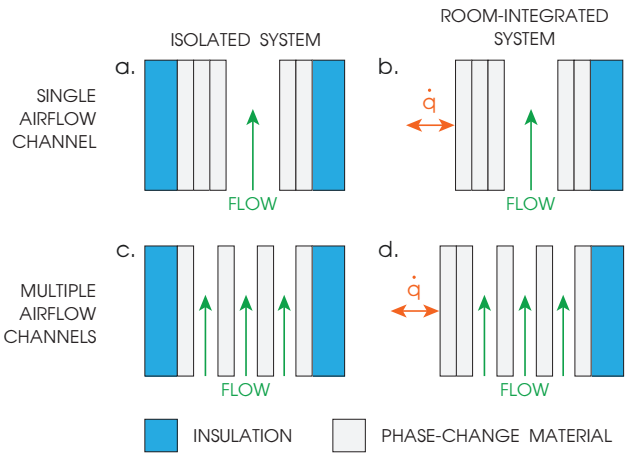

Figure 1.1: The different configurations of a PCM-TES system.

By reducing the peak demand, a smaller capacity thermal plant in the building will satisfy the load at higher efficiencies for longer periods of time. Since building components are typically sized to satisfy peak conditions, extensive upfront construction costs and long-term operating and maintenance costs can be reduced by employing predictive control strategies coupled with TES systems. On the grid scale, by having all buildings follow a flatter power demand curve, utility companies will not need to increase their capacity to meet the peak and will avoid associated environmental concerns. Buildings supplied with power from utilities that either employ a time-of-use (TOU) scheme or charge additional fees for the electrical power demand (e.g.: Hydro-Québec), will benefit significantly from utilizing their thermal inertia in conjunction with a predictive control scheme.

1.2 Phase-Change Material Thermal Energy Storage

The concept of a phase-change material based thermal energy storage (PCM-TES) system can be categorized into four configurations. The PCM-TES can be isolated from the thermal zone, while integrated into the building either independently of or connected to the HVAC network (Figure 1.1.a & .c). For example, PCM-TES can be installed in partition walls, the building enclosure, the floor space (in a raised floor plan) or the ceiling space.

In an alternate configuration, the PCM-TES is room-integrated (Figure 1.1.b & .d) with a surface left exposed to better absorb excess heat. In this case, surface convection and radiation exchange between the room surfaces, occupants and the PCM surface need to be carefully considered.

To actively charge and discharge the PCM-TES, the heat transfer fluid circulates through the system in either a single channel or multiple channels and in single or multiple passes. For shifting and reducing the peak demand associated with residential space heating, the PCM-TES can be used to store solar heat when solar insolation is available and discharge it later during the peak period. The use of air as the heat transfer fluid facilitates the integration of the PCM-TES with HVAC systems and can facilitate the use of outdoor air for free-cooling during the night in order to reduce the space cooling load of the following day. The availability of these energy sources have to be predicted in advance and must be considered by the PCM-TES controller to better match forecasted supply with anticipated demand.

1.3 Experimental Approach

The experiments were conducted in a test room that was fitted with shape-stabilized PCM panels on its back wall. The construction includes an air channel in between the PCM panels to enhance the heat transfer and a plenum fan on the ceiling for circulating the air within this channel. There is a window

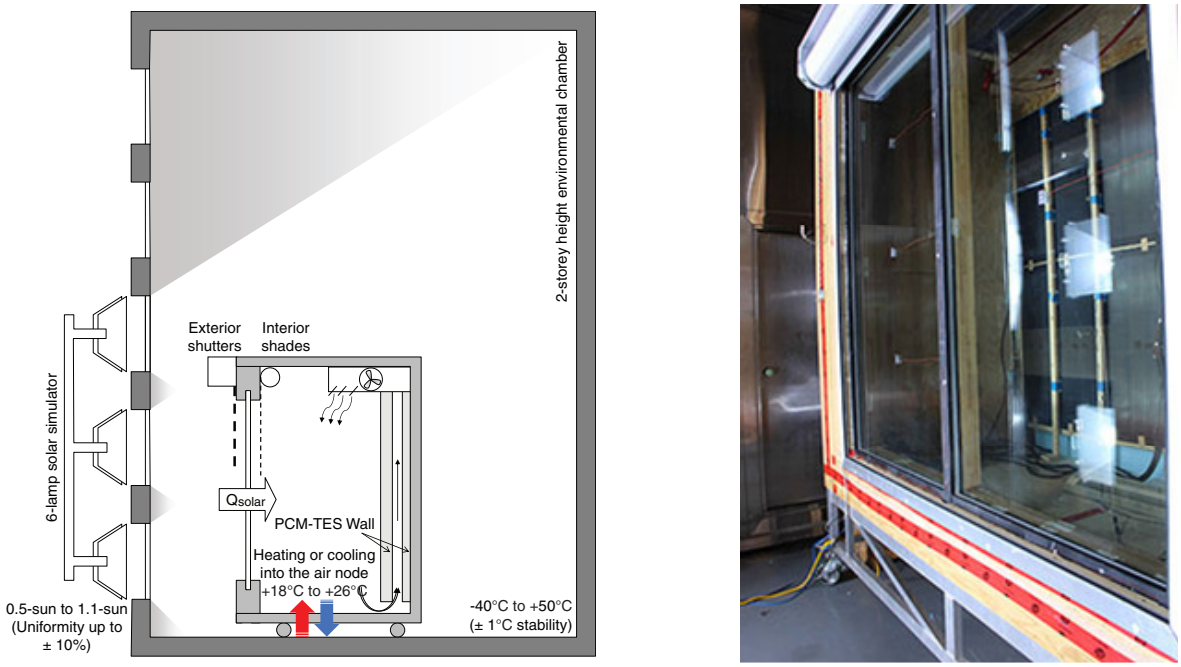

Figure 1.2: (Left) Schematic of the environmental chamber with the PCM test room inside showing the controllable parameters. [Image courtesy of K. Kapsis] (Right) Picture of the test room in the chamber. The reflection of the lamps can be seen from the window. The front surface of the PCM wall is painted black.

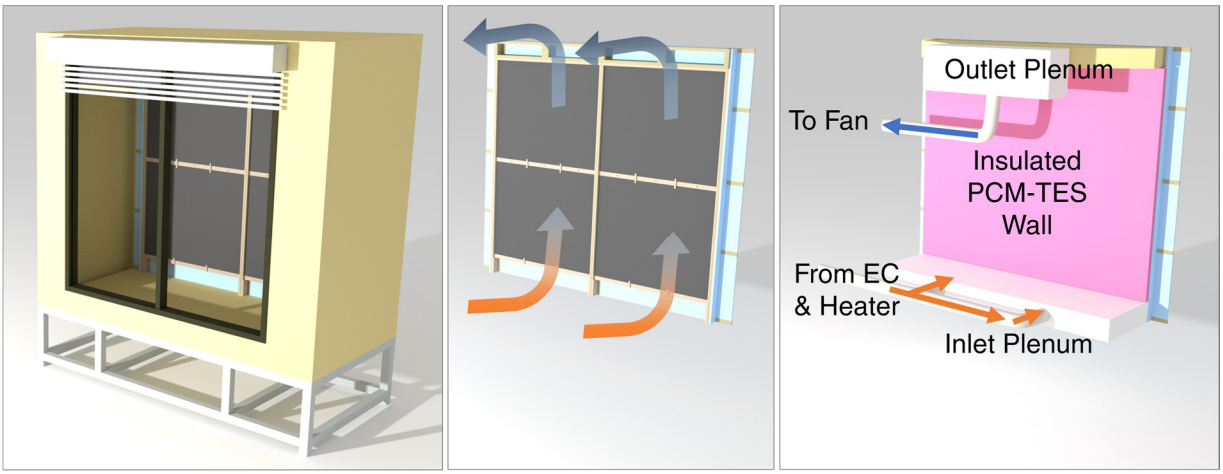

Figure 1.3: Renderings of the PCM test room showing the active PCM-TES system setup (Left) PCM test room; (Center) active PCM wall: warm air enters from the bottom inlet plenum where it exchanges heat to a pre-cooled system and exits cooled through the outlet plenum; (Right) The front of the PCM surface is insulated to isolate the system from the room; the inlet and outlet plenums are ducted.

located on the front wall allowing emulated sunlight to enter. The room is insulated and built on a platform with casters for ease of manipulation. A controllable roller blind and exterior shutters with position feedback are installed. A small forced heater is used to regulate the inside room temperature. A large number of thermocouples, RTDs, and other sensors, are installed to monitor all aspects of the experiment. A schematic and photo of the PCM test room in the SSEC is shown in Figure 1.2.

Experimental work was conducted in the Concordia University Paul Fazio Solar Simulator Environmental Chamber (SSEC) Research Laboratory which has been in operation since December 2011. Federal and provincial governments have invested under the Knowledge Infrastructure Program for the construction of this unique facility. The SSEC enables accurate and repeatable testing of solar systems and advanced building enclosures under standard conditions with a fully emulated sun and fully programmable temperature/humidity/pressurization profiles. (Concordia University, 2011, 2014)

This PCM test room design can be used for various objectives such as determining the performance of a greenhouse/solarium thermal storage system or simulating MPC strategies for commercial buildings.

The aim of this thesis is to study the behaviour of the PCM-TES system in isolation (Figure 1.1.a & Figure 1.3). The prototype PCM-TES has a ducted inlet and outlet and insulation is added to the

front of the PCM wall. Thus, it can be incorporated as interior partition walls during retrofit or in plenums of HVAC systems as a compact thermal storage device.

Phase-change materials integrated into building materials and systems have been studied for more than 30 years (Kuznik *et al.*, 2011). However, they have not been widely adopted due to the lack of rigorous control strategies and the lack of a systematic integration between design and operation of buildings with PCMs. (Zalba *et al.*, 2003; Athienitis and O'Brien, 2015)

1.4 Objectives

The objective of this thesis is to evaluate active air-based thermal energy storage (TES) systems utilizing phase-change materials (PCM) based on experimental and numerical work. The storage system intended for building integration consists of PCM panels with an air circulation between the panels. It can serve for both peak heating and cooling reduction purposes by being able to store energy and release it in a later time. A methodology is to be developed to build models of varying order[2] that capture the behaviour of the system and can potentially be used in model-based control algorithms or for heuristic predictive control – the control algorithms were not implemented in this work. Simplified models are easier to interpret, implement and calibrate. By having less parameters to adjust, the structure of the model would allow these parameters to be adjusted or learned in real time (online calibration) by using measurements from the BAS to compensate for installation and construction toleraces (e.g. as installed PCM properties, contact resistances, heat losses, additional fan pressure losses, etc.). Lastly, the modelling methodology is extended to estimate the behaviour of multi-channel PCM-TES configurations on its impact on peak demand reduction.

1.4.1 Specific Objectives

The specific objectives are as follows:

- Build, install and instrument a test room with PCM panels including a plenum fan used to circulate air within the air channel.

[2] Throughout this thesis, the term "order" refers to the number of capacitances used in the thermal model.

- Install and calibrate thermocouples, RTDs, a pyranometer, and other sensors.
- Design and perform test sequences for studying the dynamic response of the system and for verifying the model.
- Perform an uncertainty analysis on the air stream energy balance due to uncertainties from instrument measurements.
- Investigate PCMs currently used for building applications.
- Describe the limitations and methodologies used to characterize and model the behaviour of PCMs.
- Model the active PCM-TES wall using an implicit finite difference approach. To find simplified methods to input PCM characterization data.
- Reduce the model order (complexity) to facilitate the calibration process and quicken its simulation time, without compromising output accuracy.
- Extend single channel PCM-TES performance results in order to estimate the behaviour of multi-channel PCM-TES configurations with varying number of air channels and overall lengths.
- Simulate a case study to show the potential peak load reduction when using a PCM-TES system.

1.5 Thesis Outline

Chapter 1 contains an introduction to the research topic including background information and descriptions of the laboratory and experimental set up. This chapter contains the thesis objectives.

Chapter 2 presents a literature review focusing on the concept of building thermal energy storage systems without or with PCM. It presents the limitations and methodologies to characterize and model PCM. A brief overview of model-based controls concludes the chapter.

Chapter 3 presents the experiment along with the simplifications and assumptions. Experimental results are analysed.

Chapter 4 presents the numerical modeling of the PCM-TES. The thermal network and corresponding heat transfer equations are presented. Equations representing the specific heat and conductivity of the PCM are formulated.

Chapter 5. The single-channel PCM-TES model is verified against experimental measurements. Simplified control-oriented models are described. This is followed by a parametric study and investigation of the performance of multi-channel systems.

Chapter 6 presents concluding remarks, a summary of the contributions and possible extensions to this research.

Chapter 2

Literature Review

This section presents background information about building simulation and modelling. It introduces historical and modern thermal energy storage systems with sensible or latent storage along with their modeling considerations. Model-based controls are briefly introduced at the end.

2.1 Background

Building simulation software such as TRNSYS, EnergyPlus, ESP-r, EQuest and the like require the building modeller to enter a panoply of data concerning the building enclosure construction, internal loads, occupancy schedules, equipment schedules, weather, etc. in order to simulate the energy use and thermal behaviour of the modelled zone. Many of these variables, possibly unknown, are either left to the default values or, at worst, erroneously input by the modeller. The objective of building simulation is to obtain insight on how a building reacts to various internal and external profiles in order to assess as to what would be the best solution or most economical satisfying the occupants' comfort requirements, the Code, or other special needs prescribed by the client.

Depending on the focus of study, some parameters will be more influential than others and so having a very detailed model will not necessarily be justifiably better for the modeller's goal(s). A

simplified practical model concentrating on those specific parameters would be favourable. Simplified models have less parameters and thus the calibration process would be simplified as well. They could benefit from online calibration where the model parameters can be tuned over time to match the behaviour of the installed system. Simplified models would be more effective for model-based control algorithms due to their computational speed.

Chwif, Barreto and Paul (2000) have discussed that inexperienced modellers will tend to try to include everything they can in a model since they feel *insecure* as to what is essential. Another reason to make a model more complex is to *show off*; here, complexity adds a perceived value to the modeller's work. Finally, with the advancement of computational power and distributed/cloud computing, there exists a *possibility* factor: we have the capacity to do it, so why not? All of these factors are symptoms of a modeller that does not fully understand the goal(s). If a simple model could represent reality, then it should suffice. If more detail is needed afterwards, it could be added. If the model is complex, could it be made simpler? Could the scope of the model be reduced as to have many but simpler models?

Having discussed the nature of modelling, moving forward, how thermal energy storage (TES) systems are analysed experimentally, modelled and how they are used in buildings are presented. Sensible TES systems are presented first, followed by phase-change material (PCM) based TES systems. Finally, literature on advanced control strategies like model-based controls (MBC) and model-based predictive controls (MPC) are reviewed.

2.2 Thermal Energy Storage

There are various applications for thermal energy storage systems. Some are in the industrial or district scale for very large capacities or for long-term (seasonal) storage, whereas others are smaller and are coupled closely to the building zone they serve. The latter will be the focus of this thesis. Before reviewing modern TES systems, it is wise to mention briefly some history of how thermal storage has been used before even it had a name.

In ancient times, man built shelter for protection against wind, sun and rain. Over the years, construction techniques improved and building materials became more diversified and specialized. It is well known that buildings from Ancient Rome had advanced plumbing systems even for today's

standards. They had running water. Some buildings would have cavities under their floors where heated water would circulate thus providing radiant heating to the space above. The floors were made of marble and would store the heat. Another example are buildings made of stone. Although stone is a poor insulator, it offers excellent thermal inertia. The enclosure of these buildings would absorb the daytime sun, keeping the interior cool, and, towards the night, would slowly radiate the stored heat to the inside. The stone enclosure acts as a TES system absorbing heat when it is harmful and releasing it when it is vital. Another historical marvel is the Mesa Verde community located in Montezuma County, Colorado. The city was constructed into a mountain using adobe starting circa 600 AD. Interestingly, the city and its living spaces were built in a way that it would be shaded from the high altitude summer sun, but the low altitude winter sun would enter; thus making Mesa Verde one of the earliest passive solar communities in North America (Straube, 2006; US National Park Service, 2015). The adobe, acting like a TES system, would reduce daily temperature fluctuations. There are numerous historical examples from around the globe of peoples harnessing their environment to their advantage to improve their comfort.

Coming now to more recent times, one of the earlier modern patents we were able to find that harvests solar energy in a controlled manner was granted to Edward S. Morse in 1881 for his "Warming and Ventilating Apartments by the Sun's Rays". (U.S. Patent No. 246,626) (Morse, 1881) (See Figure 2.1) The patent depicted a zigzagged glass arrangement (a) in front of a blackened surface

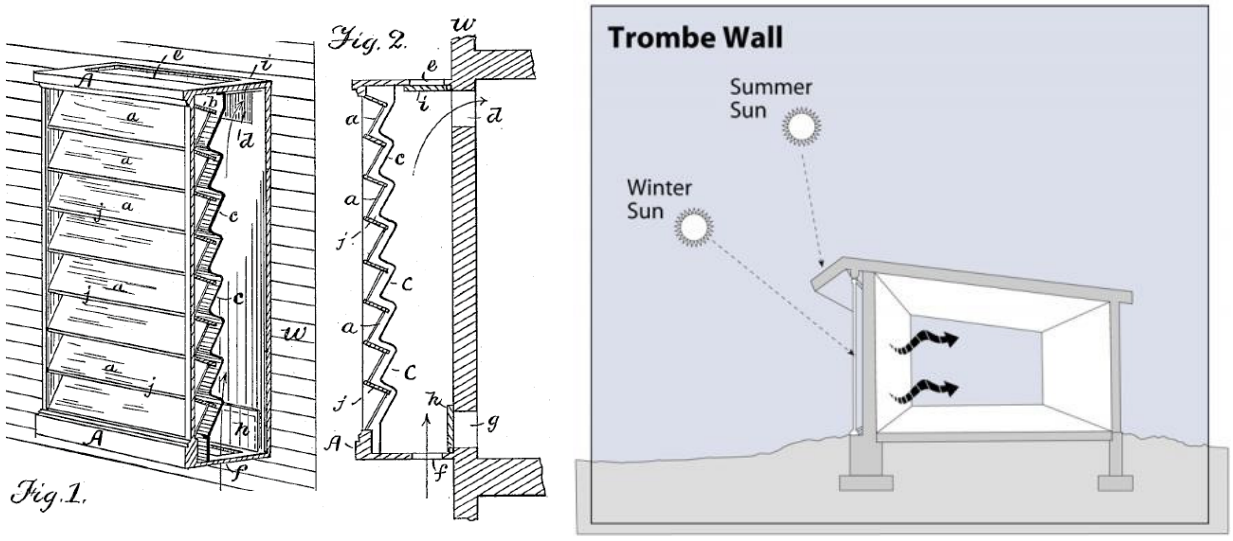

Figure 2.1: (Left) Diagram of Morse's invention (Morse, 1881) (Right) Trombe wall (Energy.Gov, 2013)

(c). There is a buffer zone behind this black surface where air circulates. The solar radiation would be transmitted through the glass and hit the black surface; the air within the cavity would heat up; and apertures at the top (d) and bottom (g) of the arrangement would allow air from the gap to circulate into or out of the living space. An opening at the very bottom (f) would allow fresh air to be preheated, or, finally, an opening at the top (e) would allow exhaust air to be rejected. All air circulation is solar buoyancy driven. Having the absorbing surfaces tilted maximizes their exposure to the sun.

This invention was in a way the predecessor of the Trombe wall (Trombe *et al.*, 1977; Energy.Gov, 2013) (See Figure 2.1). The difference between the two is that the blackened surface behind the window is here made of a heavy material like concrete, bricks, rammed earth or stone. The sun would hit the wall causing it to warm up – or charge – and it would release the heat slowly throughout the day when the sun may have set. Similar openings would allow the cavity to communicate with the house and with the environment. The glass in front of the Trombe wall allows short-wave solar radiation to enter but traps long-wave infrared radiation from the massive wall from exiting. More advanced Trombe walls would have fan-assisted circulation and motorized insulated blinds to better control the charging and discharging of the mass.

Nowadays, with the advancement of fenestration technology: double- or triple-glazed, low-emissivity (low-e or low-ε) coatings and the use of noble gases as cavity films; window systems have become less of an energy sink and now contribute in building energy efficiency measures. Trombe walls have fallen out of fashion since with these new windows, the building's massive floors and walls could be better utilized as solar heat sinks. And let us not forget that putting a massive wall behind a window will block all views to the exterior.

Athienitis (1997) suggests that "the thermal mass should be distributed on an interior building surface directly illuminated with transmitted solar radiation". The thermal mass must be sized in such a way as to minimize thermal fluctuations. In the article, he simulates an electric floor radiant system, but the heating source may just as well be air-driven or hydronic. He advises that the controls should be based on the operative room temperature since this temperature better represents occupants' thermal perception. He recommends the radiant heating be lowered at night in anticipation of the solar gains in the next morning, otherwise if a constant temperature setpoint is employed at night, the floor will remain warm and overheating would result during the day. The thermal mass should be sized correctly and this depends if a radiant heating system is used or not. Finally, he prescribes that half a

day weather prediction would be desirable for optimal control of floor heating with significant thermal mass. By using the building's thermal mass to store heat or cooling and coupling it to the zone, thermal fluctuations can be reduced, occupant comfort can be improved and there will not be a need for auxiliary storage devices in the mechanical room.

Zmeureanu and Fazio (1988) have studied a hollow core concrete floor system for passive cooling. They have modelled, using a Crank-Nicholson finite difference approach (Refer to Section 2.4.1 and Appendix A.1 for more details about this method), the building's concrete slab with channels where night-time cool air can circulate and precool the concrete. This cooled slab could be used during the day to offset chiller operation. In their conclusion, they report that an important reduction of the cooling load is achieved compared to a conventional design, there is an improvement in thermal comfort, there is a significant energy savings and they recommend, most importantly, that "[the] hollow core slab system should be integrated with a predictive control system to assess the ventilation rate at night based on [weather forecasts] for the next day".

Many other studies on hollow core slabs show similar results. Corgnati and Kindinis (2007) report on average a 1 °C reduction in operative temperature by using a hollow core ventilation system over a traditional system in Milan, Italy; both utilizing night-time free cooling. The ThermoDeck™ system developed in Sweden in the late 1970s uses interconnected hollow-core slabs where each circuit becomes a thermal bank (Winwood, Benstead and Edwards, 1997). As of June 2007, 380 institutional, commercial, and educational buildings have employed this system successfully (Termodeck, 2007). Studies on this system showed a reduction in diurnal temperature fluctuations where more passes in the slab increased thermal stability (Barton, Beggs and Sleigh, 2002).

Henze, Felsmann, Kalz and Herkel (2008) have simulated and compared the performance of a thermo-active building system (TABS) to a conventional all-air (VAV) system in a continental climate. They found the peak energy use to be similar – this may possibly be due to a control issue. The controls did not use future information to better ready the TABS for the forecasted occupancy or weather. Overall, they found the TABS system to consume 20% less primary energy that the VAV system, and would provide more comfortable conditions based on the Fanger's predicted mean vote metric. Finally, they prescribe that a TABS system utilizing low-exergy heating and cooling sources need to be carefully coordinated and controlled with the HVAC system.

In order to design TES systems to have greater effectiveness, it is recommended that the designer analyse the process using 2nd Law methods by minimising the thermodynamic irreversibilities – or maximising exergy – of the system (Dincer, 2002). Simply put, for a storage system to be effective, the quality of the source of energy used to charge the TES should be close to the quality of energy discharged. For more details, please consult Bejan (1980) & Krane (1987).

Ideally, the sensible TES system should be an integral part of the building's structure. Adding a TES system to an existing building will add a structural burden which may not have been originally considered. Lighter alternatives must be considered since reinforcing a building cannot be cost-effective.

2.3 Phase-Change Materials

A phase-change material (PCM) is a material that offers high storage density in a narrow temperature range in the form of latent heat. There exist many types of PCMs (Figure 2.2) and their applications are innumerable. Common applications include (Zalba *et al.*, 2003):

- Thermal storage of solar energy;
- Solar power plants;
- Passive storage in bioclimatic building/architecture (HDPE + paraffin);
- Cooling: use of off-peak rates and reduction of installed power, ice-bank;
- Heating and sanitary hot water: using off-peak rate and adapting unloading curves;
- Safety: temperature maintenance in rooms with computers or electrical appliances;
- Thermal protection of electronic devices (integrated into the appliance);
- Thermal protection of food: transport, hotel trade, ice-cream; special transport boxes;
- Food agroindustry, wine, milk products (absorbing peaks in demand), greenhouses;
- Medical applications: transport of blood, operating tables, hot–cold therapies;
- Cooling of engines (electric and combustion);
- Thermal protection of batteries in electric vehicles;
- Thermal comfort in vehicles;
- Softening of exothermic temperature peaks in chemical reactions;

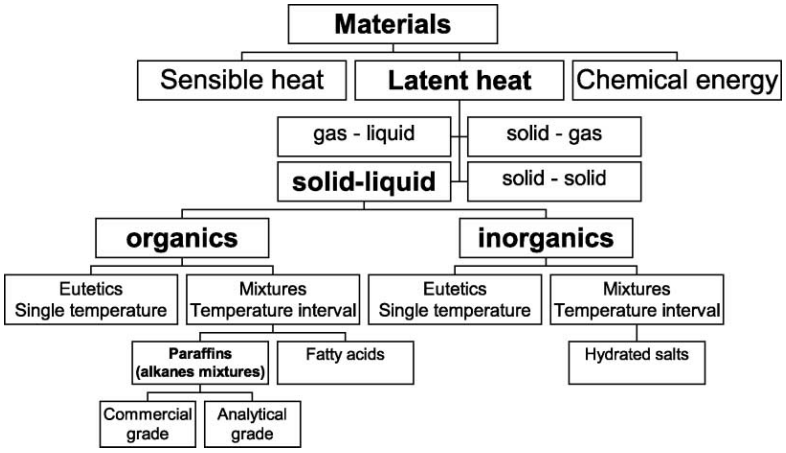

Figure 2.2: Diagram of PCM types. (Zalba *et al.*, 2003)

- Spacecraft thermal systems; and,
- PCM-embedded textiles used for spacesuits, high-performance clothing and furniture.

Schröder and Gawron (1981) list the desirable properties of a PCM:

1. High value of the heat of fusion and specific heat per unit volume and weight;
2. Melting point which matches the application;
3. Low vapour pressure (<1 bar) at the operational temperature;
4. Chemical stability and non-corrosiveness;
5. Not be hazardous, highly inflammable or poisonous;
6. Have a reproducible crystallisation without degradation;
7. Have a small sub-cooling degree and high rate of crystal growth;
8. Have a small volume variation during solidification;
9. High thermal conductivity; and,
10. Should be of abundant supply and at a low cost.

Another point to add, complementary to point "7", would be for a PCM to have minimal hysteresis between melting and freezing. Hysteresis is when there is a temperature difference between the peak melting and freezing temperatures. Sub-cooling is a phenomenon where the PCM is cooled below its freezing point yet remains liquid. For crystallization to occur, the molecules need a nucleating site; as soon as one is formed, due to some disturbance, the liquid will start freezing immediately. This effect, can in certain cases be exploited as a long-term storage strategy. Desgroseillers' (2013) work is

on improving the yield and controllability of long-term PCM storage devices. Similar work is also being conducted at the Technical University of Denmark (Streicher, 2008).

The two common types of PCM are organic and inorganic. Each have advantages and limitations. Organics, such a fatty acids and waxes, are non-corrosive, exhibit low sub-cooling, are chemically and thermally stable – will not degrade after periodic cycling; however, they have lower latent capacity, a low thermal conductivity and are inflammable. Inorganics, such as hydrated salts, have a great phase change enthalpy; however, they exhibit sub-cooling, phase separation, phase segregation, and are corrosive. (Zalba *et al.*, 2003) To combat the shortcomings, there have been made many advances in the field:

- Fire-retardants are added to paraffin PCMs, which consequently lower the thermal capacity;
- Nucleating agents are added to inorganic PCMs to reduce the sub-cooling effect;
- The use of metal fins, plates, honeycomb structures or Lessing rings to improve conductivity (Kenisarin and Mahkamov, 2007);
- Embedding PCM into a matrix of expanded graphite, in this application, the effective conductivity has increased from 0.2 $W \cdot m^{-1} \cdot K^{-1}$ to (25 to 30) $W \cdot m^{-1} \cdot K^{-1}$, whereas the thermal capacity decreases by an *acceptable* 20% (Kenisarin and Mahkamov, 2007); and,
- Special stainless steel or polymer containers to hold the corrosive salts (Kenisarin and Mahkamov, 2007).

There is an abundance of scholarly articles on phase-change materials because of the many application possibilities and the many different types in existence. There is also a lot of research being done in the private sector, but their findings remain secret. Some researchers are distributing their findings in the form of creating modules (Types) in TRNSYS, adding functionality to EnergyPlus or ESP-r, or through standalone software either as freeware or with commercial intent. There are Tasks mandated by the International Energy Agency (IEA) that study and develop PCMs. IEA's Energy Technology Network Annex 23 "Applying energy storage in ultra-low energy buildings" directed by Dr. F. Haghighat of Concordia University and IEA's Solar Heating and Cooling programme Task 32 "Advanced storage concepts for solar and low energy buildings" subtask C directed by Dr. W. Streicher are two that deal with PCM specifically.

In the Annex 23 Final Report (Haghighat, 2013b), a collection of articles is presented in 13 chapters describing extensively the fundamentals of energy storage, phase-change materials and their applications accompanied by their modelling methodologies and validation process. Lastly, demonstrative case studies are evaluated and the barriers to wider PCM adoption are discussed. In an accompanying report (Haghighat, 2013a), application best practices are detailed. This report aims to bridge the knowledge gap for architects, engineers and contractors considering PCMs to increase the thermal mass of a building by providing the basics, the required design tools and the limitations to consider. The applications include the integration of PCM in the building enclosure, in heat exchangers and in hot water tanks.

Dr. D. Feldman from the Centre for Building Studies at Concordia University has studied phase-change materials extensively. Hawes (1991) worked with him on the development of a method to impregnate concrete using various techniques and with various PCMs. Their performance, reliability, durability and fire safety were assessed. Hawes projects substantial HVAC energy savings, reduction of the mechanical room and an increase in HVAC efficiencies.

The objective here is not to repeat the work, but to extract information about applications of PCM-TES systems coupled directly to a thermal zone. Long-term seasonal storage, or centralized storage (whole building or community scale) will not be reviewed.

2.3.1 Characterisation

In order to use a PCM, it must first be characterised. There exist different techniques suitable for differed applications. The more popular being differential scanning calorimetry (DSC) and the T-history method. Newer techniques are being developed that are more appropriate for PCMs in building applications.

2.3.1.1 DSC Method

The DSC is a standard measurement method for thermal analysis. A small sample in the range of (10 to 50) µl and a reference – typically water – are simultaneously subjected to a temperature profile. The profile could either be a heating or cooling rate ($K \cdot min^{-1}$) or could have a stepped ramp. The amount

of heat absorbed or discharged in the sample is compared to the reference and through comparison the specific heat of the PCM can be calculated as a function of temperature. (Günther *et al.*, 2009)

First, the miniscule size of the sample may not be representative of the PCM in a system. The growth of crystals in inorganic PCMs depend on the size of the sample since there will be more nucleating sites in larger volumes; DSC measurements will erroneously show pronounced sub-cooling effects. For PCMs containing additives or are heterogeneous, small samples may have a disproportionate amount of a certain additive. The sample temperature is read from a sensor placed on the surface of the crucible, which results in an overestimation in heating mode. Organic PCMs have low conductivity and will result in a strong temperature gradient. (Günther *et al.*, 2009) If the heating rate would be gentle enough as to have a negligible temperature gradient {$Bi < 0.1$}, then the DSC method would be applicable for homogenous materials. Gentle heating rates, however, will yield very small temperature variations and, depending of the sensor used, could return noisy results.

2.3.1.2 T-history Method

The T-history method is similar to the DSC method but for larger samples and is more suitable for heterogeneous materials. The crucibles would contain 20 ml of sample material (Günther *et al.*, 2009). Care must again be taken to ensure that no temperature gradients form within the sample. As of this writing, no T-history test equipment is commercially available. Measurements must be done using standard laboratory equipment.

2.3.1.3 Recent Methods

Cabeza, Barreneche, Martorell, et al. (2014) have written about their experimental setups to characterize PCMs for different applications. Since larger scale models will not certainly behave like the small sample used in a DSC test, it is necessary to perform scaled tests. "At Franhofer ISE in Germany, a plate test apparatus was developed to test construction materials with PCM in large scale samples (50 x 50 cm^2 up to 30 cm thick) in different ways: heat transfer coefficient; enthalpy temperature curve; and dynamic behaviour of a construction at various conditions." This apparatus would be able to test a sample $1.5 \cdot 10^9$ times more voluminous that the DSC and would reflect the behaviour of the PCM in full-scale applications.

A new testing standard has been developed in 2013 and updated in 2014: "ASTM C1784-13 *Standard Test method for Using a Heat Flow Meter Apparatus for Measuring Thermal Storage Properties of Phase Change Materials and Products.*" (ASTM C1784-14, 2014; Kośny, 2015, sec. 4.6) It consists of using a conventional heat flux meter apparatus similarly as how a step mode DSC test is performed. A larger sample size can be inserted in the heat flux meter.

2.4 Modelling Approaches

On one end, models can be wholly described based on physics (Newton's Law of Cooling, Fourier's Law of Heat Conduction, etc.). This is called white-box, clear-box or First Principles based modelling. On the other end, models can be built purely based on statistical and learnt techniques. The inputs are related to outputs. Whether if the connections physically make sense is of no importance. This is called black-box or First Principles Free modelling and is usually done using machine learning and statistical methods (system identification, pattern recognition, autoregressive models, adaptive neural networks, etc.). In between the two, we find different shades of grey-box models. Grey-box modelling is when the model contains a mix of physics and numerical functions, e.g.: a convective heat transfer correlation is a grey-box model since it's fundamentally based on particle momentum equations, but experimental data is used to obtain empirical equations.

2.4.1 Physics-Based Models

Fourier's Law of Heat Conduction is approximated following a finite difference method (FDM) in the time domain or solved with conduction transfer functions (CTF) in the frequency domain. Frequency domain analysis is a method in studying the thermal response of the zone by applying a Fourier transformation on the time domain problem (Athienitis, Sullivan and Hollands, 1987). Unlike the finite difference method, the frequency domain method does not discretize walls into many layers, but requires a certain number of harmonics to adequately simulate the building behaviour. However, it is unnecessary to consider high order harmonics since the building's thermal inertia behaves like a low-pass filter. (Chen, Athienitis and Galal, 2014).

Different schemes are used to solve an FDM problem: fully explicit, fully implicit and the Crank-Nicholson method. The first two are 1st order approximations in respect to time, whereas the latter is

in the 2nd order. The explicit method relies on past temperatures to compute the next timestep. The implicit method solves all the temperature equations simultaneously. Finally, the Crank-Nicholson method is, in a way, the average of the two. In order to have converging results and numerical stability for the explicit and Crank-Nicholson methods, the timestep must be chosen carefully according to the stability criterion. There is no such limitation for the implicit method. In terms of computational burden, inverting a matrix for the implicit method has a complexity of at most $O(n^3)$, whereas simply computing equations in the explicit method, the complexity is at most $O(n^2)$ (Cook, 2010). For a small problem of about 10 000 nodes, the computational time required for inverting a matrix will be non-significant for modern computers. Additionally, in building physics, these matrices will be likely block diagonal: a shape that can be solved more effectively than $O(n^3)$. A detailed derivation of the finite difference method is found in Appendix A.1. For phase-change materials, however, the numerical accuracy of the implicit method is not always guaranteed for larger time steps due to a large change in the material enthalpy or specific heat.

In some cases, air flow and buoyancy effects are modelled using Navier-Stokes equations through computational fluid dynamic (CFD) methods. For simple geometries, the added complexity is not justifiable. (Al-Saadi and Zhai, 2013)

2.4.2 Black-Box Models

In a built environment, it is very often difficult to obtain a full description of the building: construction material characteristics, enclosure details, infiltration rates, occupancy and equipment schedules, etc. However, a correlation between, say, the exterior temperature and interior temperature can be established by using data logged by the building automation system (BAS). This correlation can later be used to predict the interior temperature based on exterior conditions.

Allard's thesis (2013) focuses on such a technique applied to a building-integrated hollow-core concrete TES system. The TES system was connected to a BIPV/T system on the roof and the preheated air would be drawn into the slab. Allard was able to correlate meteorological data to sensor data to predict the state of the TES system. The numerical model was then used to develop improvements to the BIPV/T system. The TES and BIPV/T systems were part of the ÉcoTerra™ house located in Eastman, Québec. The house is part of CMHC's EQuilibrium™ housing initiative. It consumes 10% the average energy of typical houses built in Canada.

Learnt models could be valuable as they can be developed quickly. Care must be taken to select parameters that influence the output, e.g.: the exterior temperature will unlikely influence the interior temperature of a well-insulated and air-tight building, and should not be included in the model. A limitation of numerical models: these models are trained and tested on historical data; if an infrequent or *freak* event were to occur, these models would break down. On the other hand, physics-based models would be able to yield more confident results. Additionally, physics-based models can be used to study design alternatives or post-retrofit performance expectations.

2.4.3 Phase-Change Material Models

After having obtained the enthalpy-temperature and conductivity-temperature characterization data using the DSC method or through other techniques described in Section 2.3.1, a mathematical model can be constructed. Since these properties vary with temperature, a linear model cannot be used.

One of the earliest computer programs involving latent heat was developed by Dr. C. O. Pederson and has 44 lines of code (1972). Modern simulation software are more complex but the underlying physics remains unchanged – EnergyPlus has more than 600 000 lines of code. EnergyPlus has a validated phase-change module where the user would input the enthalpy values for different temperatures (Tabares-Velasco, Christensen and Bianchi, 2012). The program would then interpolate between those values iteratively at each simulation timestep. The program accepts one enthalpy curve per material and so hysteresis cannot be considered (US DOE, 2014).

Using lookup tables is not computationally efficient. Another approach would be to represent the curve with a mathematical function. Athienitis (1997) has approximated the specific heat curve by a triangle. Chandrasekharan, et al. (2013) have implemented Egolf and Manz' (1994) equations into a custom version of EnergyPlus. The simplified method describes the enthalpy-temperature curve using 6 parameters: peak phase change temperature, latent heat, and, the specific heat and temperature range before and after the peak phase-change. This method is simple, quick and the manufacturers need only give 6 values per curve. One shortcoming in this method is that the enthalpy curve consists of two curves joint together at the peak phase change temperature. At this point, there is a kink, and so the specific heat {≡ dh/dT} will be discontinuous. We propose another approach based on a skewed normal distribution requiring 5 parameters in Section 4.2.1.

Modelling the thermal behaviour of PCMs is different than modelling sensible storage systems due to the strong non-linearity in enthalpy and conductivity when undergoing a phase transition. The heat capacity method of modelling is used in this thesis. It is intuitive, easy to program and suitable for gradual phase change; however, it can be computationally inefficient. It consists of gradually varying the specific heat of the material as a function of its temperature. The method accounts for both sensible and latent heat. Other main methods include: the enthalpy method, the temperature transforming method and the heat source method. (Al-Saadi and Zhai, 2013) The enthalpy method calculates the change in energy using the difference in enthalpy between the previous and current timesteps. If the change in temperature is small, numerical errors could result since: $\{\Delta h/\Delta T \approx 0/0\}$. The heat capacity method uses the specific heat – which is derived from the enthalpy curve – of the material at either the previous or current timestep temperature. For a slow system with gradual phase change, the difference between the two specific heat values will be minor $\{C_p(T^t) \approx C_p(T^{t-1})\}$. Alternatively, a temporal average of the specific heats $\{C_p^t = ½\cdot[C_p(T^t) + C_p(T^{t-1})]\}$ can be used.

Barbour and Hittle (2006) have developed a technique to model PCMs with conduction transfer functions (CTF). The methodology consists of generating transfer functions for the regions where the material undergoes a phase-change. The simulation software would then switch between the multiple sets of CTFs based on the PCM temperature. The method was shown to be within 20% of the range of conditions encountered in simulation programs. It can potentially be implemented into EnergyPlus since the software uses CTF by default. The CTF method is typically quicker in computation time compared to the finite difference approach.

Bastani (2014; Bastani, Haghighat and Kozinski, 2014; Bastani and Haghighat, 2015) has developed a framework to design wall assemblies containing PCM using a dimensionless number approach. Using this simplified method which uses tables and Heisler charts, the designer can quickly assess the potential of introducing PCM in a certain type of building given its material properties and weather conditions. The aim is to maximize the effectiveness of the PCM by assuring the material fully cycles diurnally. Such an approach can be expanded in a future work to help design active PCM systems as well.

2.4.3.1 Hysteresis

Hysteresis is the phenomenon where the material freezing and melting temperatures differ. All PCMs have a certain degree of hysteresis and for the model to be accurate, it needs to consider this effect. If the material begins to be heated when fully frozen until it is fully melted, then the heating curve should be used. When it is then cooled until it is fully melted, the cooling curve is used. The heating and melting curves outside the transition zone are the same (sensible heat only) and so switching between the curves is straightforward. However, if the material is partially melted and then cooled, switching directly to the cooling curve will lead to a violation in the energy balance. Bony and Citherlet (2007) suggest how to modify the enthalpy curve: "[during] a heating or cooling step inside the phase change zone, the slope of [the] transition is the same as the solid phase one in the bottom part of the phase change. It is also identical to the slope of the liquid phase in the superior part of the phase change." (See Figure 2.3 & Figure 4.4)

Delcroix (2015) has shown that the transition curves are different in the heating and cooling cases. (See Figure 2.4) He suspects the trajectory depends on, not only at what temperature the process was interrupted, but also on the rate of heating and cooling. The enthalpy path was obtained by inverse modelling, where the enthalpy curve was modified until the temperature profiles of the experiment and model matched. Delcroix showed that during an interrupted cooling case, the path followed Bony

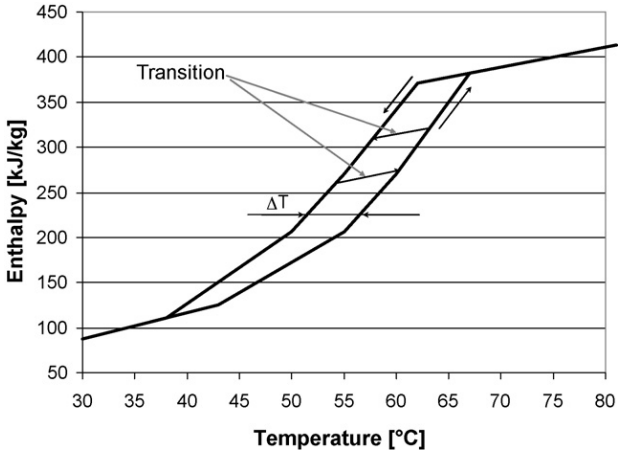

Figure 2.3: Enthalpy temperature curve showing the transition path for partial charge/discharge processes. The slope of the transition line is that of the sensible portion at the end of the phase transition. (Bony and Citherlet, 2007)

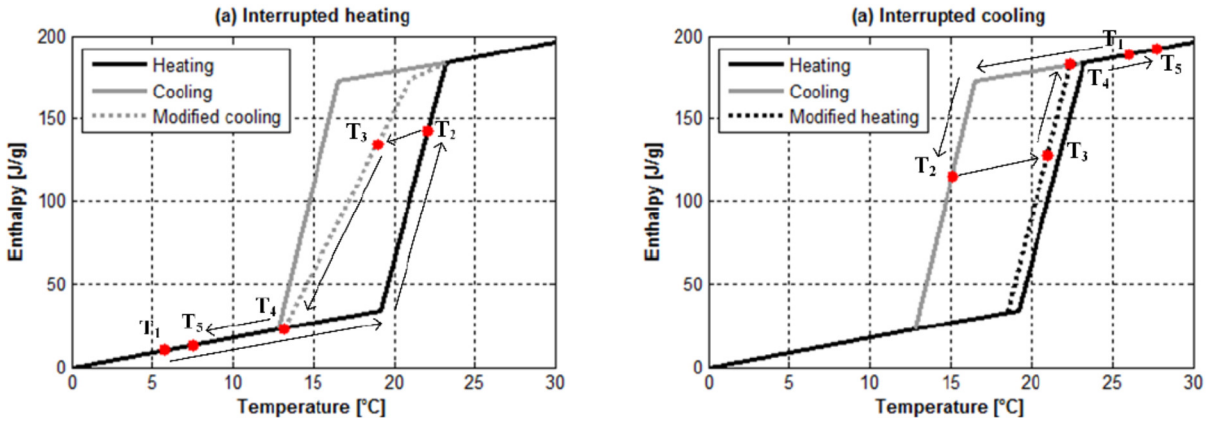

Figure 2.4: Enthalpy temperature curve showing the transition path for partial (left) discharge and (right) charge processes. (Delcroix, Kummert and Daoud, 2015)

and Citherlet's description, but with a slight difference. The interrupted heating case did not agree. More research is needed to fully understand the process.

In the case where the PCM will be actively and on demand used for peak load reduction or demand side management, the behaviour of the PCM within the first 10-30 minutes of use must be well understood. The rate of heat or cooling extraction delivered is very important. If the material's behaviour is not well programmed in the controller, then the peak cannot be reduced as planned and it may even become necessary to ramp up the HVAC system to compensate, thus nullifying the benefits of a PCM-TES system. And so, although the hysteresis effect may not certainly yield a large impact on a yearly simulation due to the averaging of the effects, it will indubitably affect the short-term dynamics of a building with a PCM-TES seeking to reduce its peak energy demand.

2.5 PCM-TES Systems

There exists a myriad of PCM-TES configurations intended for building integration (Kenisarin and Mahkamov, 2007):

- Heat storage tanks where the PCM is contained in spherical capsules, cylinders, finned tubes, coils, with or without heat transfer enhancements, such as, graphite matrices, carbon fibers or brushes, aluminum fillings or Lessing rings.

- Stand-alone PCM systems where the material is stored in pouches, micro-encapsulated or impregnated into building elements like gypsum, concrete or clay tiles, or macro-encapsulated into a shape-stabilized panels.
- The heat transfer fluid could be water, air or a glycol solution for ice banks.
- For heat, the source could be solar either by direct gains, or through solar collectors possibly assisted by heat pumps; heat from the boiler or from the condenser side of the chiller; or, from internal gains.
- For cooling, the source could be night-time outside air, HVAC air supply or from a heat pump/chiller.
- An interesting application is using PCM as part of the fenestration system. Transparent insulation materials are filled with inorganic PCM that are clear when liquid and diffusing when solid. (Manz *et al.*, 1997) The concept has now spun off into a company called GLASSX in Switzerland.

Barnard (2007) reports that the coefficient of performance for the mechanical ventilation system (cooling delivered/fan energy) is around 25 for a local system and down to 3 for a centralised system. In order to minimize heat losses and minimize the length of installed ducting or piping, the PCM-TES should be as close to the zone it serves as possible. Here, the cooling is provided by night-time ventilation and explains the high performance values. He has demonstrated an active system in London where the building mass and added pouches filled with salt-hydrate PCM in the ceiling space are used to store cooling. The system costs between 25 to 50% of a conventional system depending on the configuration and "the use of night cooling in a hybrid solution with mechanical refrigeration has enabled the size of the central air handling unit / refrigeration plant and distribution system to be halved", so additional cost savings can be envisioned.

Childs and Stovall (2012) have studied the technical potential of using a PCM in the building enclosure, more specifically, mixed in with the cellulose insulation. The system behaves passively since it's basically a building component. They conclude that the overall cooling electricity consumption needed to meet the annual cooling load does not differ compared to a building without PCM, however the peak energy demand has been reduced. Having a lower peak demand results in cost savings in locales where electricity follows a time-of-use scheme or where the supplier charges power demand as well as energy consumption.

Zhou et al. (2008) have used a shape-stabilized PCM panel (80% paraffin to 20% high-density polyethylene (HDPE)). For their passive system, they recommend the PCM panel to have at least 90 $kJ \cdot kg^{-1}$ of latent heat with the peak melting temperature (1 to 3) °C above the average room temperature. In their study, they conclude that the addition of these panels create a zone response similar to a building with more thermal mass. Thermal comfort improvements are also noted.

Charvát et al. (2014) have developed a model of a PCM-TES used for solar air systems which was then validated with experimental results. The model was assembled into a TRNSYS Type. Their experiment consists of a TES unit containing 100 aluminum panels filled with a paraffin-based PCM (Rubitherm RT47) arranged in layers with channels in between to circulate air. Material characterization data is presented from different sources and there are discrepancies due to the testing methods. The panels are modelled as a 1-D heat transfer problem since the panels are relatively thin compared to the width and thickness. The PCM is modeled using the effective heat capacity method where the heat capacity is represented by a Gaussian function. Partial charge/discharge processes are not analysed.

El-Sawi (2013; El-Sawi, Haghighat and Akbari, 2013) studied the performance of a PCM-TES system that consist of through-finned containers filled with PCM surrounded by an air channel. Air circulating in the channel would transfer energy to the fins which in turn transferred the heat deep into the PCM. He developed and validated a 3-dimensional mathematical model. The model was extended to study the effect of system geometry, charging/discharging times and mass flow rates on the system performance. However, in order to simplify the model and improve simulation times, he trained an artificial neural network to relate the outlet air temperature of the system with its input. This simplified model was used to study the energy reduction potential of the system and the impact on occupant comfort.

The PCM used in this thesis is the DuPont™ Energain© (referred to as DuPont Energain onward); it is a shape-stabilized 60%wt microencapsulated paraffin within an ethylene copolymer. The panel thickness was first optimized by Kuznik et al. (2008). They found the optimal thickness to be 10 mm for a 24 h cycle, but a 5 mm thickness would provide 70% of the enhancements and covering twice the surface area with PCM would be more beneficial. Next, a scaled test cell was built and tested for a passive application. (Kuznik and Virgone, 2008) After which, a full-scale test room was built and tested in an environmental chamber. (Kuznik and Virgone, 2009) Here, they studied a configuration

with and without PCM on its interior surface. They conclude that the PCM reduces overheating thus enhancing thermal comfort. Natural convection of the room side is improved and thermal stratification is reduced. As a final passive experiment, they have retrofitted a room in an office building with the panels on the walls/ceiling and monitored the operative temperature for about a year. (Kuznik, Virgone and Johannes, 2011) An adjacent room was left as-is and served as a reference. A reduction of (2 to 3) °C on the operative temperature was achieved compared to the case without PCM. They conclude that the addition of PCM panels are beneficial to buildings with low thermal mass. Lastly, their team has studied an active application for the panels. (Arzamendia Lopez *et al.*, 2013) The experiment consists of a number of PCM panels with an air channel between the layers. The modeling assumes a 2-D heat transfer, neglects environmental losses due to thick insulation, neglects radiative heat transfer due to symmetry and the equations are solved explicitly. As future work, they will define the optimal control strategy of the storage unit and evaluate the performance of the system in a building. Partial charge/discharge scenarios are not analysed.

Dolado et al. (2011a, 2011b, 2012) have done similar work by having designed, built and tested a full-scale PCM to air heat exchanger. The organic PCM are contained in metallic panels. Many of these panels with air channels in between them make up the PCM-TES. Although their application is to lower the peak demand of an electrical equipment room, the design and analysis principles are applicable for zones occupied by people. The PCM is characterized using an improved T-history method which showed good agreement with the full-scale setup. Mismatching the

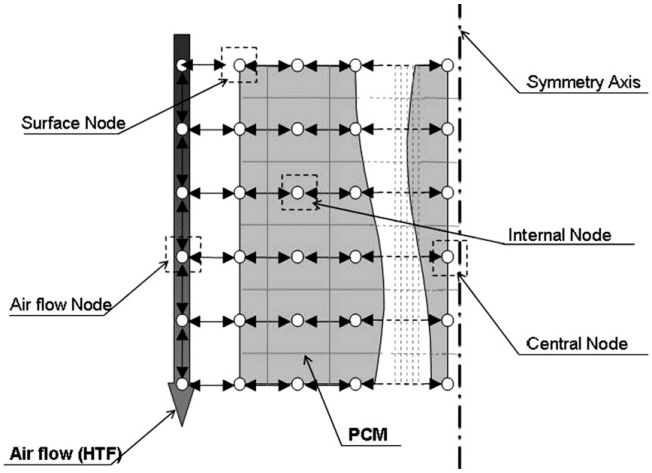

Figure 2.5: 1-D horizontal thermal network connected to the 1-D vertical air flow node. (Dolado *et al.*, 2011a)

temperature-enthalpy values by 1°C could lead to relative errors of up to 20% in the TES power curve and 14% in the time required for full melting. There is an emphasis on acquiring correct characterization data. The modelling methodology is based on a 1-D finite difference approach where the PCM control volumes are connected to the air control volume (See Figure 2.5). This assumption is valid for thickness to width ratios of more than 10. A 5 min simulation timestep is suggested. The hysteresis phenomenon is considered using (Bony and Citherlet, 2007). Results showed that a PCM with lower thermal conductivity but in a well-designed system can yield higher cooling power and can be used for free-cooling. Having a lower thermal conductivity, the stored heat will not leak as quickly; however, if significant cooling is required, the fans will need to be run at higher speeds. They conclude that improving the thermal conductivity of the PCM led to minor improvements since the bottleneck was on the air side. Finally, they conclude that it is unnecessary to modify PCM properties since application needs can be obtained by a suitable design and operating conditions (airflow, surface rugosity, PCM slab thickness, PCM system length, air gap size); this could lead to the possibility of using lower cost and lower grade PCMs.

2.5.1 Challenges

A challenge when using PCMs in building application comes from a discord between the manufacturers' material scientists and the application engineers. Manufacturer data is limited for design purposes, and so engineers are inclined to characterize the material themselves (Zalba *et al.*, 2003). The analysis instrumentation and equipment is complex. As mentioned earlier, the rate of heating or cooling in a DSC test influences the results. The temperature oscillations in a building are mild, e.g.: if the temperature in a room increases from 20 °C to 28 °C in 4 hours, that would yield a rate of 0.03 $K \cdot min^{-1}$, whereas DSC tests are performed typically in the range of (0.5 to 2.0) $K \cdot min^{-1}$.

Kenisarin and Mahkamov (2007) cast doubt on the reliability of the thermo-physical property data and suggest it be verified by an independent institution. Without reliable data, PCM-TES systems cannot be designed properly or perform as expected. Without any information on the cost of PCMs, proper return-on-investment projections cannot be made. They draw the following conclusions:

1. DSC measurements are quick but will result in significant discrepancies when the material is used in a larger application. The accuracy of DSC tests are not very high. They propose to

have a standard set of pure PCM substances that would be used to calibrate instrumentation equipment.

2. There is no national or international standard to test thermal energy storage productions and no national or international scientific center to certify PCM properties. There is no standard for quality assurance.
3. Commercially available PCM products do not offer heat transfer enhancement capabilities. The ones that have, like the metal fins or graphite composites, remain in the academic and research realm.
4. The cost of PCM is quite high and so are restricted to research or demonstration projects. For large-scale applications, prices should be in the 1 USD·kg^{-1} range. This target can be reached if technical grade materials are used with minimal processing. Research should then focus on using low-grade TES materials.
5. Chemical stability remains an issue with repeated cycling, even in stable organic substances as fatty acids.

Kuznik, David, Johannes, et al. (2011) have tabulated the number of publications dealing with PCM and have shown that there has been a strong rise in interest since 2003. Phase-change materials have been studied extensively for more than 30 years, and even now, modelling latent heat TES systems remains a challenge (Zalba *et al.*, 2003).

Phase-change materials have not been widely adopted in office and commercial buildings due to the lack of rigorous control strategies and the lack of a systematic integration between design and operation of buildings with PCMs. (Athienitis and O'Brien, 2015) Consideration in the controls is necessary to ensure the material undergoes a phase change and its latent capacity is fully utilized.

2.6 Model-Based Controls

Unlike the conventional PID control or rule-based controls, which are reactive, model-based controls (MBC) or model-based predictive controls (MPC) is a predictive control algorithm (See Figure 2.6). It makes use of future information to minimize the operating costs of a building.

Model-based controls were applied in the oil and petrochemical industries as early as the 1950s (Qin and Badgwell, 2003; Lee, 2011). Until the mid-70s, massive mainframe computers were required

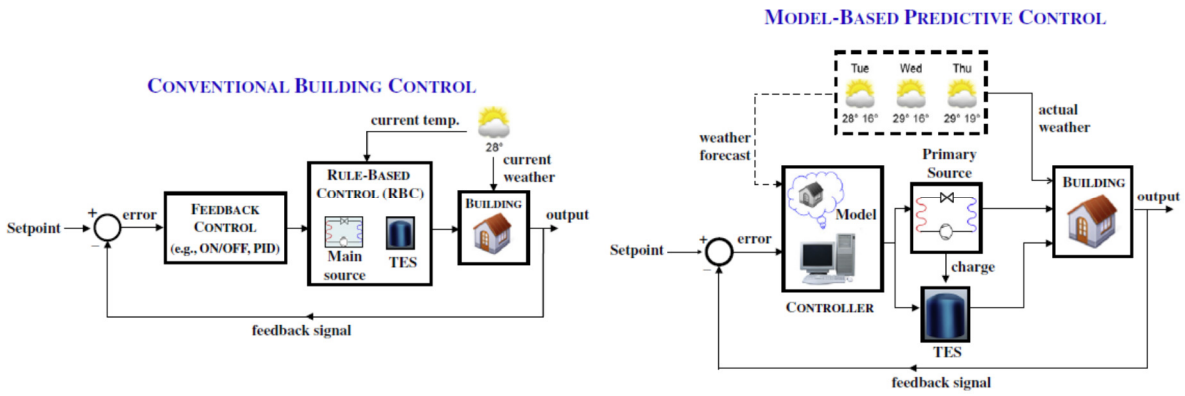

Figure 2.6: (Left) Conventional building controls; (Right) Model-based predictive controls (Candanedo, Dehkordi and Stylianou, 2013)

to compute the process settings. Since, the arrival of cheaper, more reliable and powerful microprocessors greatly aided the development and implementation of MPC. Through time, process stability was addressed by developing robust MPC and, later, nonlinear MPC. By the end of the 90s, with the improvement of the optimization algorithms and processing power, MPC has matured to a technology used in various fields, such as: medicine (real-time insulin regulation), finance (revenue management, product pricing, credit assessment), buildings (maximize comfort, reduce power demand and energy use), among countless examples. The control industry sometimes refers it as *real-time embedded optimization* with solving times in the milli- to microseconds. (Boyd, 2007)

2.6.1 MPC in Buildings

The earliest noted application of MPC as supervisory control for a building was from 1988. (Coffey *et al.*, 2010) However, due to computational requirements, it did not receive much attention until the 2000s.

MPC is a dynamic optimization problem where the objective function J, typically an operating cost, is minimized over a control horizon. (Athienitis and O'Brien, 2015, chap. 6.3) Applied to buildings, the cost can be the sum of the power demand and power consumption for the equipment in the building, i.e. HVAC system, domestic hot water, lighting, equipment, appliances, etc. The constraints typically include temperature range restrictions for occupant comfort or safety reasons, equipment capacity limitations, cycling limitations among many. The control variables are what can be manipulated in order to improve the building performance. The constraints can be softened into

penalties on the objective function where violations result in a worsened objective value instead of an infeasible solution.

There are different types of models, going from a physics or first-principals based model, to a gray-box model and to a black-box or learned models. Different research groups have focused on different approaches.

The Swiss OptiControl team (Oldewurtel *et al.*, 2012; Lehmann *et al.*, 2013) have developed a detailed RC-model. The nonlinearities were linearized within the operating range. They used a stochastic MPC strategy to take into account the uncertainty due to weather variability. The objective function was to minimize energy consumption while limiting the number of thermal comfort violations. They report that stochastic MPC outperforms current control practices.

Hovgaard et al. (2012) have applied a nonconvex MPC strategy for commercial refrigeration units. The systems were modelled using heat balance equations without linearization. The nonconvexity was treated by solving a sequential convex optimization problem. A 30% cost savings would be achieved in a time-of-use priced electricity locality.

Henze et al. (2010) have studied near-optimal control strategies for various types of commercial buildings in four climate zones offering different electrical tariffs. They conclude that the cost savings are very sensitive to the utility electrical rates. The effect of internal gains are more influential on the outcome than the weather.

Coffey et al. (2010) have augmented GenOpt to be able to handle MPC. GenOpt is "an optimization program that can minimize a cost function evaluated by an external simulation program, such as EnergyPlus, TRNSYS, [etc.]". (LBNL, 2011) They have added an optimization layer, called SimCon, where an MPC algorithm already available or user-defined can be used to find the near-optimal control parameters. The program can generate output files that can be read by the building energy management system (BEMS). The optimization problem is, however, relatively slow since the underlying equations within the external simulation software is not available to GenOpt directly. It cannot analytically derive gradients or parse the problem into sub-regions, which would dramatically improve computational efficiency.

Keeping to packaged building simulation software, a technique to speed up the optimization part required for MPC consists of simplifying the model using system identification (SI) (Ljung, 1999). The method consists of relating controllable inputs to outputs of interest, essentially, transforming the detailed modelled to a simple black-box model. The simplified model would then be used in the MPC optimization algorithm. Candanedo et al. (2013) has used this technique to study the near-optimal use of an ice storage bank for a medium office building. Ma et al. (2012) have extended the method by applying SI at every simulation timestep. Essentially, SI would be applied to the EnergyPlus model, then, the MPC algorithm would determine the near-optimal control parameters. The parameters would be applied to the original EnergyPlus model to verify the result, after which the process would be repeated. They calculated around 25% of cost savings compared to common controls. May-Ostendorp et al. (2011) applied MPC to an EnergyPlus model as-is. Although the computational time was long, their objective was to then extract simplified control rules that can be implemented in the BEMS today.

MPC highly depends on the accuracy of the forecasts. Occupants' behaviour remains the biggest uncertainty. (Gunay *et al.*, 2014) Erickson et al. (2011) have created agent based models to simulate occupants. The models would be refined over time with the addition data. A better prediction of where occupants will be and what they will do will yield a better control of the HVAC system and result in increased comfort and productivity.

2.7 Conclusion

This section presented works about thermal energy storage systems with or without phase-change materials and briefly introduced model-based controls.

The main points from the literature review can be summarized:

- TES systems, when properly utilized, can lower peak energy demand while improving occupants' comfort.
- PCM offers thermal mass equivalent to heavier materials but with minimal weight. Thus, the use of PCM has the ability to potentially decouple the concept of effective thermal mass from actual physical weight.

- Research is needed in PCM characterization; standards and testing methods more suitable for building applications must be drafted; 3rd party testing and certification is crucial.
- The behaviour of PCM in the mushy region, when interrupting the heating or cooling process, requires more research.
- Ease of modelling can come by simplified PCM characterization inputting. This will also aid computational times.
- The PCM panels can be adequately modelled 1-dimensionally if they are relatively thin: the level of modelling detail should be adjusted depending on the study's objectives.
- For MPC to be effective, the underlying models need to be simple and fast for the algorithm to converge to a solution. The models can either be simple in themselves or simplified for a given simulation timestep. The optimal or near-optimal values would then be sent to the BAS.
- Simplified models are easier to interpret and calibrate in an installed system since they contain fewer parameters to adjust. The parameters can be learned in real time (online calibration) with data from the BAS. The disrepencies can be due to construction, installation or system tolerances.

Having worked through the literature and gotten insight as to how the PCM-TES should be used and modelled, the following chapter focuses on the experimental aspect of this thesis. The experiment will then serve to validate the modelling of Chapters 4 & 5.

Chapter 3

Experimental Evaluation of an Active PCM-TES Integrated into a Wall

3.1 Experiment Description

The experiment and the experimental results are presented here in greater detail. The various hypotheses are explained and analysed.

A full scale isolated single air channel active PCM-TES is built and tested (See Figure 1.1, Figure 1.3 & Figure 3.1). The experiment is conducted in the Paul Fazio Concordia University Solar Simulator and Environmental Chamber (SSEC) research facility (Montreal, Canada). DuPont Energain, a shape-stabilized 60%wt microencapsulated paraffin within an ethylene based copolymer (Kuznik, Virgone and Noel, 2008; Kuznik and Virgone, 2009; DuPont, 2011) is used as the PCM. (See Table 3.1 for specifications) The PCM is laminated on both sides with a 100 μm aluminum sheet. Paraffin is one of the most common organic PCMs, is inexpensive, thermally stable and demonstrates very little sub cooling (Zalba *et al.*, 2003; Charvát, Klimeš and Ostrý, 2014). Its melting range is close to room temperature, which is normally set to around 21°C.

Table 3.1: PCM panel technical specifications

	Manufacturer's data	Kuznik et al. (2008)	Kuznik & Virgone (2009)
Mass, kg	5.39		
Dimensions, mm x mm	1000 x 1198		
Thickness, mm	5.2		
Density, $kg \cdot m^{-3}$	855.5	1019	≈ 900
Heating & cooling rate, $K \cdot min^{-1}$	1.	2.	0.05
T melting, °C	21.7	≈ 22	
T melting, peak, °C		22.2	22.3
T freezing, peak, °C			17.8
Latent heat, melting, $J \cdot kg^{-1}$	> 70 000		72 400
Latent heat, freezing, $J \cdot kg^{-1}$			71 000
C_p sensible, $J \cdot kg^{-1} \cdot K^{-1}$	2333		2400
C_p melting, peak, $J \cdot kg^{-1} \cdot K^{-1}$		15 200	13 400
C_p freezing, peak, $J \cdot kg^{-1} \cdot K^{-1}$			12 900
Conductivity, solid, $W \cdot m^{-1} \cdot K^{-1}$	0.18	0.22	*0.18 **
Conductivity, liquid, $W \cdot m^{-1} \cdot K^{-1}$	0.14	0.18	*0.22 **

* Not consistent with the authors' previous study, values likely inverted inadvertently

20 shape-stabilized PCM panels are used: 4 covering the surface on 5 layers in depth. There is a 30 mm [1¼ in.] air channel between the 2nd and 3rd layers. (See Figure 3.1 & Figure 3.2) The system offers 2.66 kWh of thermal storage (79% latent) between 18 to 26°C which is at the limits of thermal comfort. The front of the PCM wall is insulated with 38 mm [1½ in.] of rigid insulation, and the back with 25 mm [1 in.] of rigid insulation and 100 mm [4 in.] of fiberglass insulation as part of a studded wall.

Type T thermocouples (± 0.5 °C) are placed in 9 locations transversely in the PCM-TES to determine the through temperature distribution. The right side (See Figure 3.1 & Figure 3.3) of the wall is split into 6 vertical sections along the height (air stream). The left side has only thermocouples in the center of the PCM panels. The assumption here is that the behaviour of the left and right sides should be similar due to symmetry. The thermocouples on the left are used for verification. On the bottom section of the right side, extra thermocouples were placed around the edges of the panels to check if there were any edge effects. In total, around 120 thermocouples were installed.

On the air stream side, cool or warm air is supplied by the environmental chamber. It enters by the inlet plenum of the PCM-TES and exits through the outlet plenum where it is directed towards a calibrated orifice flow meter (± 2%, as per the manufacturer's specifications). 1/10 DIN RTDs (± 0.06 °C) are installed to accurately measure the inlet and outlet air temperatures. Type T thermocouples are placed at the inlet, middle and outlet of the air channel as well.

Simply consulting Table 3.1, a few discrepancies can be observed. First, there is a disagreement in the material density values. It is possible that one party measured strictly the PCM substance within the panel and another density measurement can be for the panels including the aluminum lamination. The peak melting specific heat is significantly different for both Kuznik measurements, i.e.: 15 200 v. 13 400 $J \cdot kg^{-1} \cdot K^{-1}$, possibly due to differing heating rates of their respective DSC tests. Thus emphasizing the need for independent characterization as suggested by Kenisarin and Mahkamov (2007).

The test room containing the PCM-TES is moved to the lab where the air is maintained at 21°C, the chamber temperature is lowered to 10°C. An inlet and outlet plenum is installed in the test room to assure uniform airflow.

At the beginning of the experiment, the PCM-TES is heated (charged) by supplying 28°C air at a rate of 400 $kg \cdot s^{-1}$ [93 $L \cdot s^{-1}$ or 200 CFM, 1.3 $m \cdot s^{-1}$ or 4.3 fps average speed] until steady state is

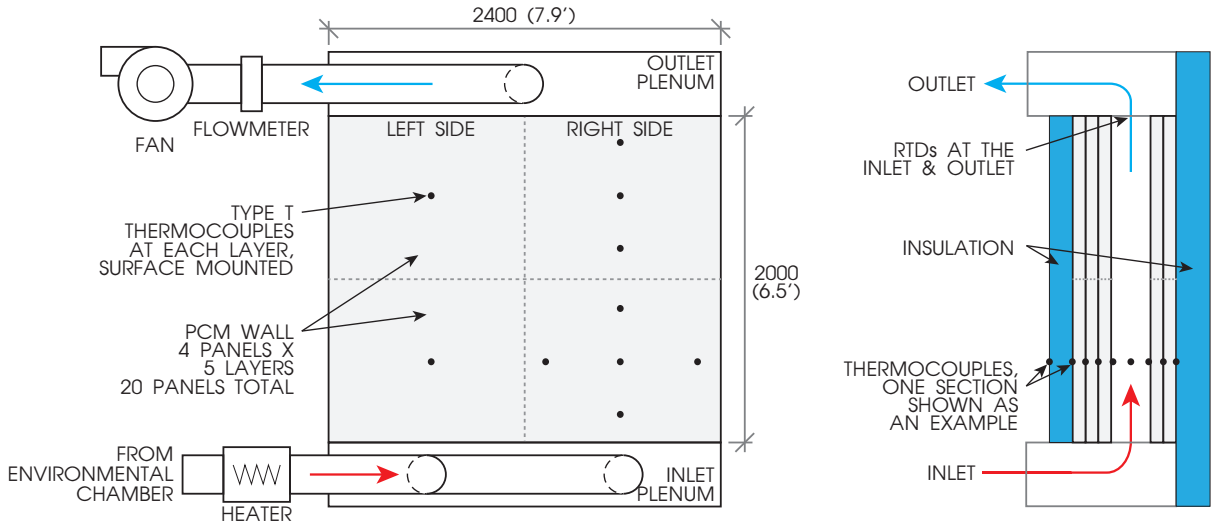

Figure 3.1: (Left) Schematic of the PCM-TES experiment. (Right) Cross-section of the wall.

Figure 3.2: Thermocouple nomenclature along the transverse direction. Also see Figure 3.3. E.g.: Thermocouple "2bD" measures the air stream temperature located at the center of the bottom panel on the right side of the PCM-TES.

attained. Next, the heater is turned off and cold air from the chamber at around 13°C [55°F] is supplied, again, until steady state is attained. 13°C [55°F] is the typical supply air temperature of HVAC systems in North America. This process is run twice to verify repeatability. The flow rate is chosen since it would provide a good convection heat transfer rate with minimal pressure losses. The temperatures are read every 30 seconds and the average is recorded minutely.

Next, heating (charging) and cooling (discharging) is performed for two other mass flow rates, 300 & 500 $kg \cdot s^{-1}$ [70 & 115 $L \cdot s^{-1}$ or 150 & 245 CFM, 0.97 & 1.6 $m \cdot s^{-1}$ or 3.2 & 5.3 fps average speed].

Finally, two interrupted heating and cooling tests are performed. During the interrupted heating run, the PCM-TES is pre-cooled. Warm air is supplied until the deepest thermocouple (node A, See Figure 3.2) reaches 21°C, after which, cold air is supplied to discharge the system. During the interrupted cooling run, the PCM-TES is pre-heated. Cold air is now supplied until node A reaches 20°C. Then, warm air is supplied to charge back the system.

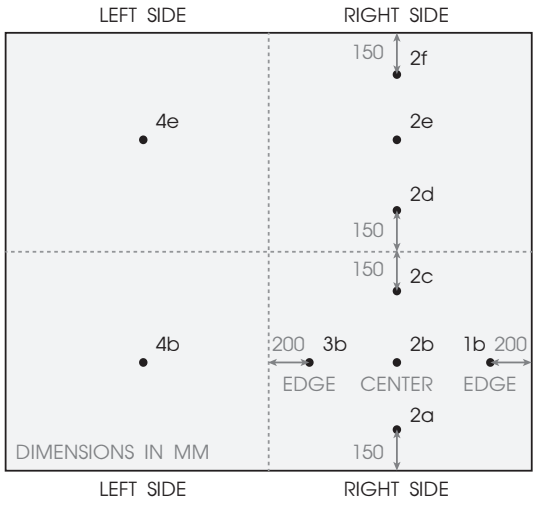

Figure 3.3: Thermocouple nomenclature along the width and height

By running tests with different flowrates, the objective is to study its effect on the heating and cooling times. The interrupted cases would serve to analyse the behaviour of the PCM-TES in the mushy zone: to test if it verifies Bony and Citherlet's suggested behavioural path. (See Section 2.4.3.1)

3.2 Results and Analysis

For this experiment, to test the uniformity of flow across the width of the PCM-TES and thus the symmetry assumption, the correlation of the right and left sides of the PCM-TES (See Figure 3.3) are

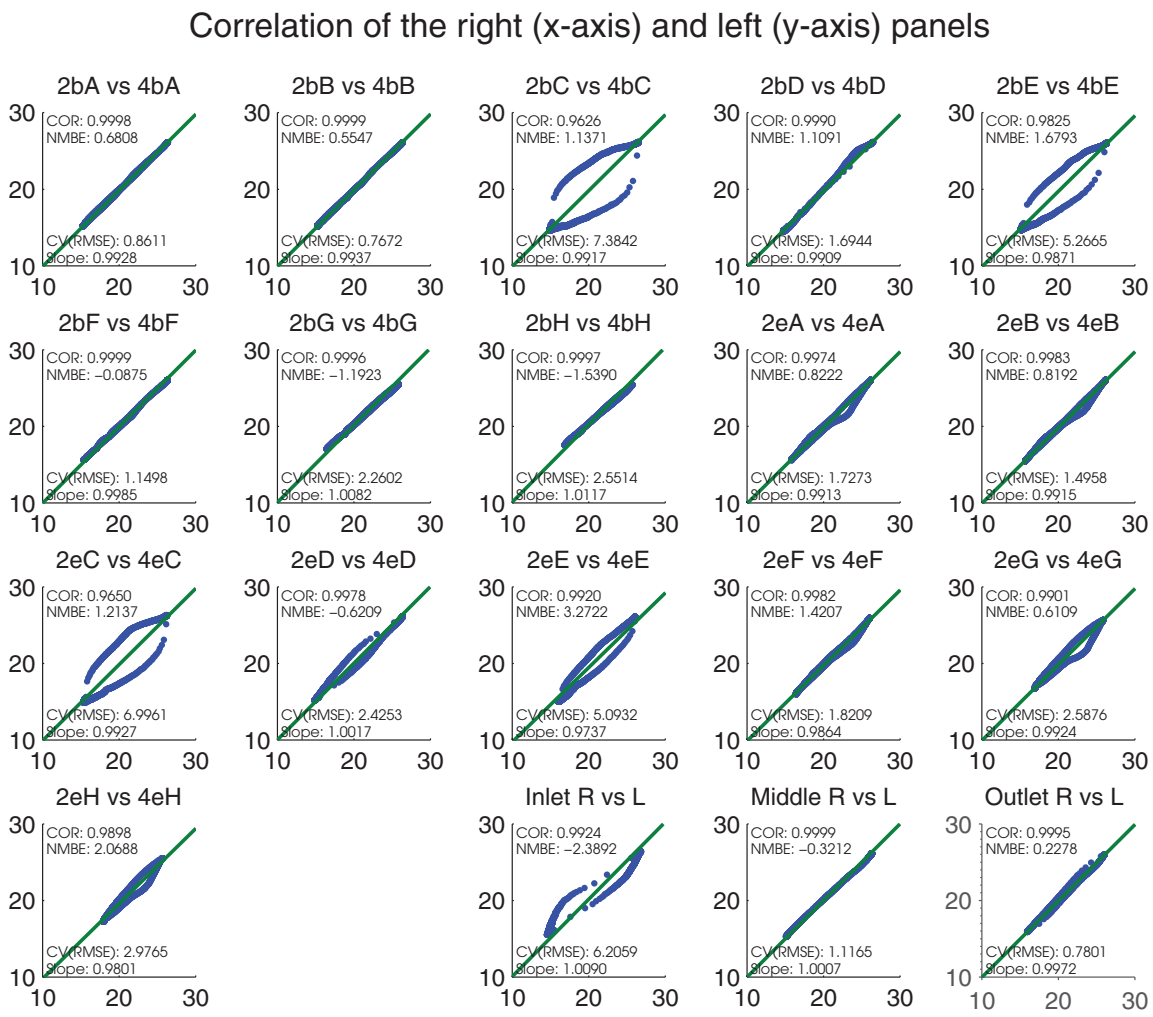

Figure 3.4: Correlation analysis between the right (x-axis) and left (y-axis) sides of the PCM-TES. The blue points are given per timestep and are temperatures (in °C). Various metrics are computed: correlation (COR), normalized mean bias error (NMBE), coefficient of variation of the root mean square error (CV(RMSE)), and the slope (Slope) of the best-fit line (green line) passing through the origin.

plotted for a full heating followed by a cooling sequence. Similarly, the correlation between the bottom right panel edges to its center is analysed to assess if any edge effects are present.

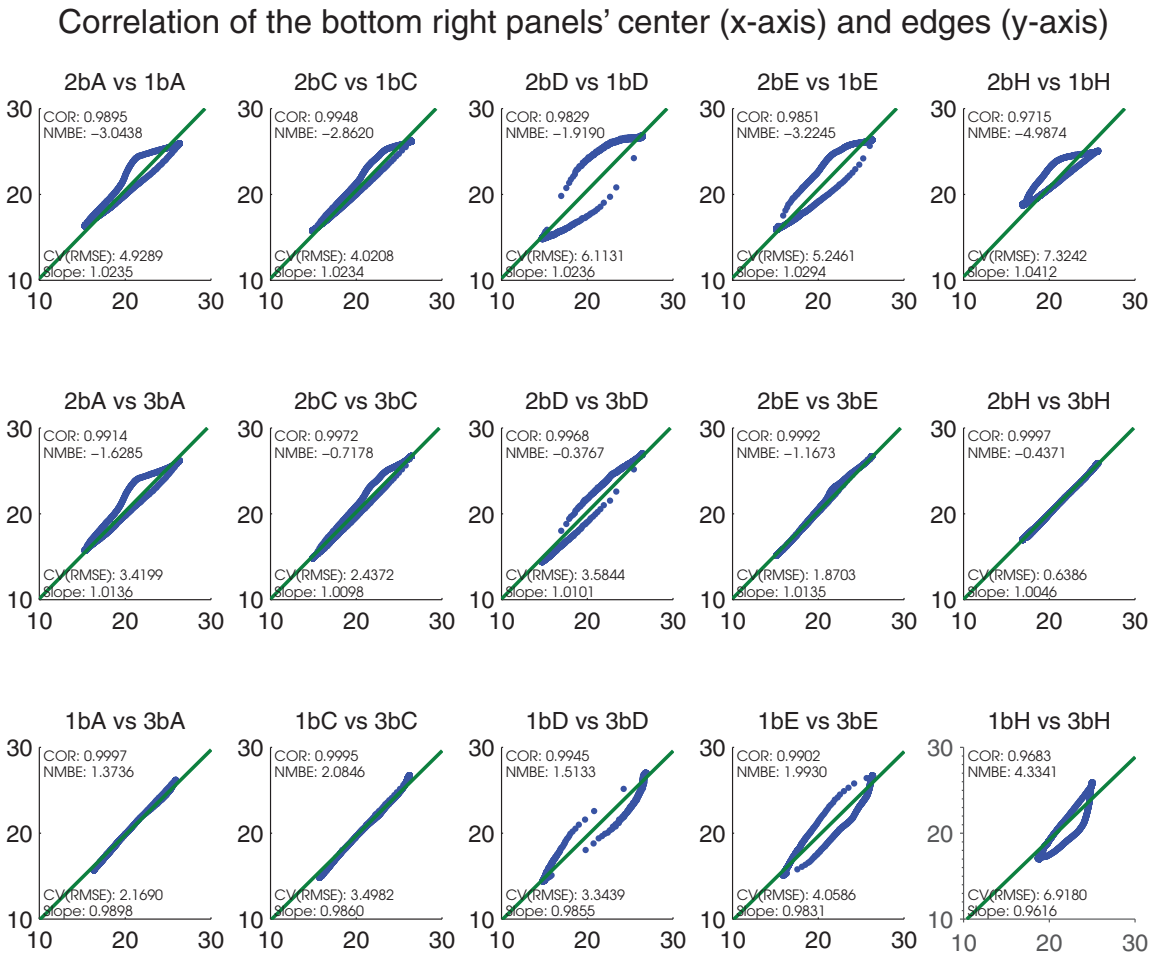

Figure 3.5: Correlation analysis between the center (x-axis) and edges (y-axis) of the bottom right section of the PCM-TES. The blue points are given per timestep and are temperatures (in °C). Various metrics are computed: correlation (COR), normalized mean bias error (NMBE), coefficient of variation of the root mean square error (CV(RMSE)), and the slope (Slope) of the best-fit line (green line) passing through the origin.

Looking at the above figures, for most pairs of values, the symmetry assumption holds, i.e.: at a given timestep, both pairs show similar temperatures. There are some surface mounted thermocouple pairs that do not agree as well. These were thermocouples installed on the surface of the PCM panels in the air cavity. It's quite possible that a thermocouple from the pair got unstuck and was measuring the air temperature, whereas the other was still attached to the surface. Otherwise, although great care has been put to make sure the inlet airflow is even – by having installed baffles – the airflow may very well be not perfectly distributed on both sides of the PCM-TES.

Nonetheless, for the vast majority of the data sets, left vs. right and center vs. edges, the assumption of uniform air distribution and, consequently, uniform temperature along the width holds.

3.2.1 Heating of the PCM-TES (Charging)

Showing all the data over time may be cumbersome since there are around 120 installed thermocouples. The nodes in the traverse plane are averaged and plotted instead. Additionally, the deepest layer (node A) is plotted to better assess the state of the PCM-TES. (See Figure 3.6) Comparing the two 400 $kg \cdot h^{-1}$ runs, the curves look similar. The experiment seems to be repeatable. Comparing the cases, the speed of charging is proportional to the flowrate. Looking now simply at node A, when the PCM reaches around 21°C, a kink is present. At this temperature, the PCM is considered to be fully melted and any additional heat contributes to sensible gains only.

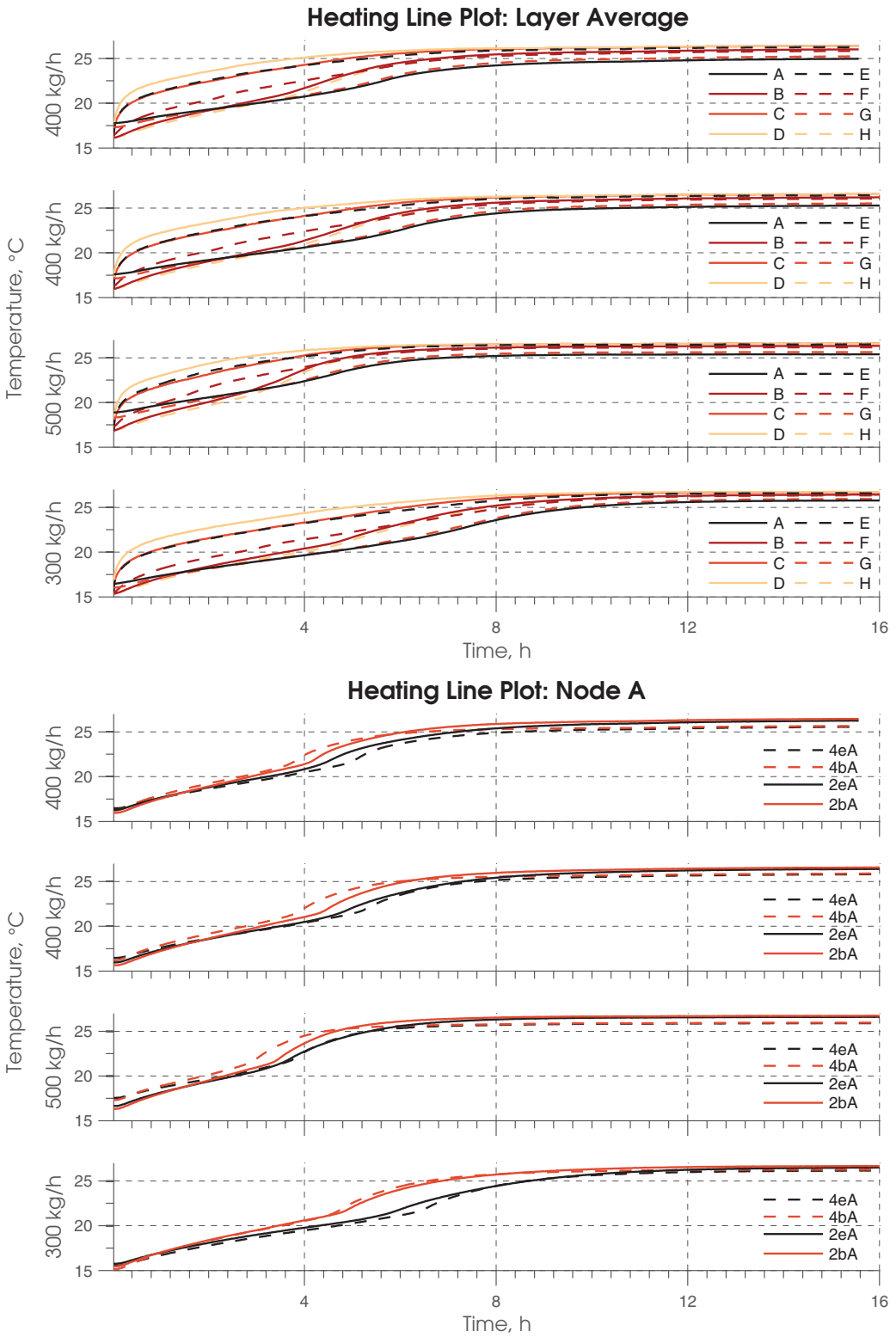

Figure 3.6: Heating (charging) of the PCM-TES: (Top) Averaged thermocouple data; (Bottom) Node A at the center of the panels.

A second way to visualize all the data is to plot a heat map. (See Figure 3.7) Here, all the thermocouple temperatures are shown for a specific time for the right side centerline of the PCM-TES. Air enters from the bottom at node 2aD and exits at the top at node 2fD. Node A is at the back of the wall. By the 8th hour of charging, all the nodal temperatures are stabilized.

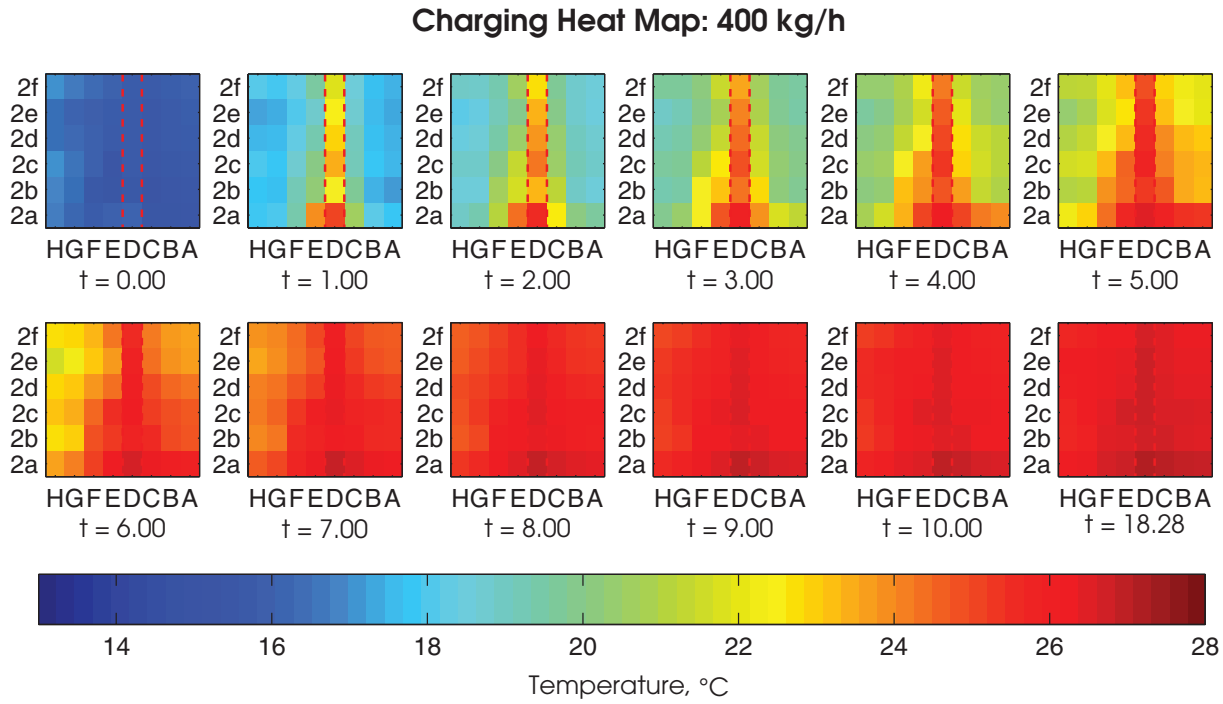

Figure 3.7: Spatial and temporal temperature heat map of the heating (charging) of the PCM-TES. The squares replicate a side view of the system similar to the illustration in Figure 3.1.Right. Time t is in hours.

Another way to determine when charging has ended is to look at the air inlet and outlet temperatures. (See Figure 3.8) For an ideal system with no thermal losses, charging is completed when there is no difference between the inlet and outlet air temperatures. In a real system, there will always be a slight difference. Comparing the different flowrates, it can be seen that the 300 $kg \cdot h^{-1}$ case yields the largest temperature differential between inlet and outlet initially.

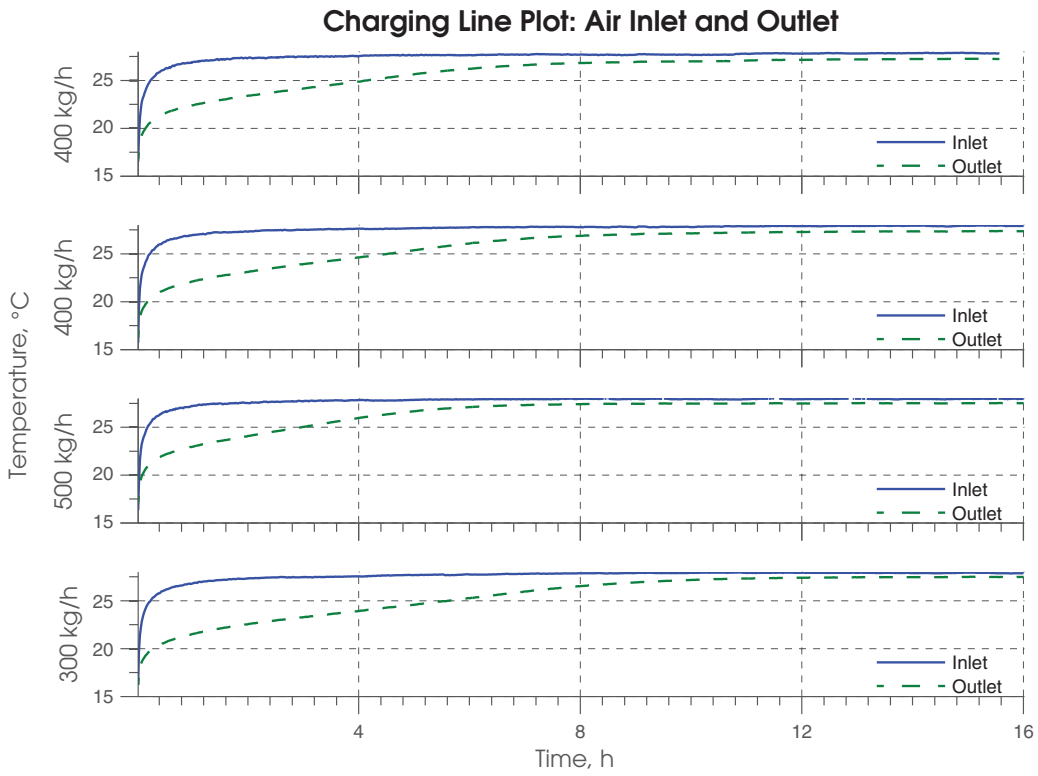

Figure 3.8: Heating (charging) air inlet and outlet temperatures.

Figure 3.9 shows the temperature gradient along the airflow path on the PCM surfaces for the heating process. This serves to see the behaviour of the PCM-TES along the airflow path direction.

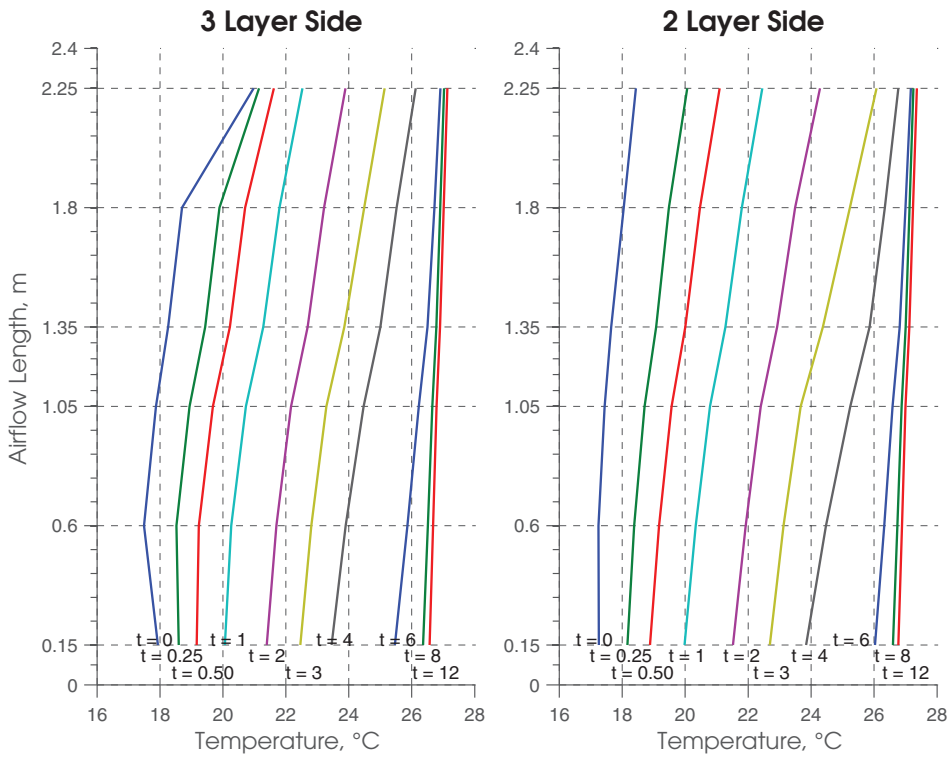

Figure 3.9: Temperature gradient along the airflow path on the PCM surface per time t in hours. (Left) Temperature of the PCM surface of the front 3-layer side [namely, nodes 2aE, 2bE, 2cE, 2dE, 2eE and 2fE] (Right) Temperature of the PCM surface of the back 2-layer side [namely, nodes 2aC, 2bC, 2cC, 2dC, 2eC and 2fC]

3.2.2 Cooling of the PCM-TES (Discharging)

Similarly, we can draw the same charts for the cooling process. Focusing on the node A chart, at around 19°C, the curves reach a plateau. After this point, the PCM is considered to be fully frozen. It is also noticeable that some of the curves increase in temperature after dropping below this temperature. There is a slight sub-cooling effect, independent of flowrate. However, not in every layer; only layers experiencing a high rate of heat flow show sub-cooling. As shown by Delcroix et al. (2015), the enthalpy-temperature correlation depends on the rate of heat transfer. This is further demonstrated in Figure 3.11.

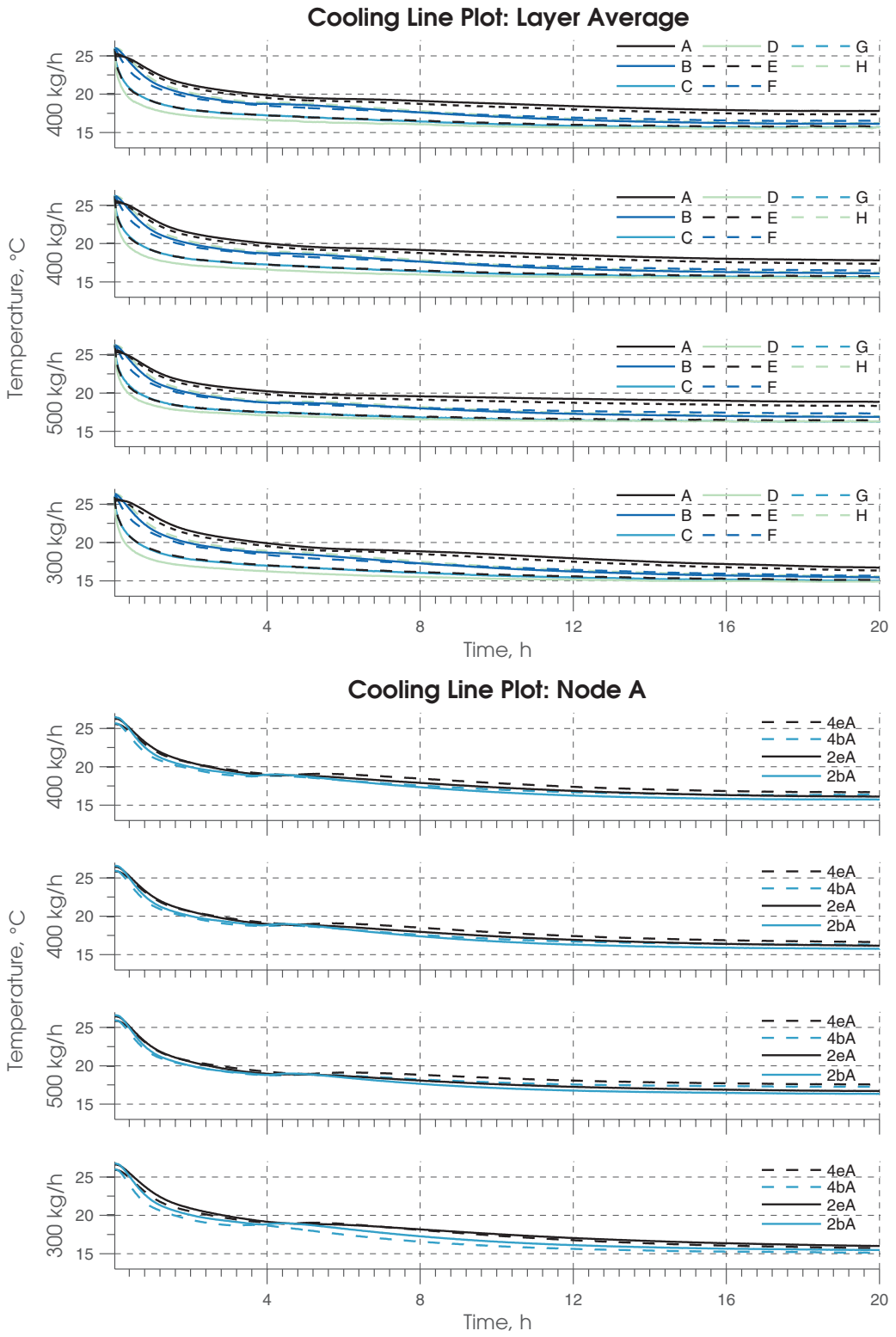

Figure 3.10: Cooling (discharging) of the PCM-TES: (Top) Averaged thermocouple data; (Bottom) Node A at the center of the panels.

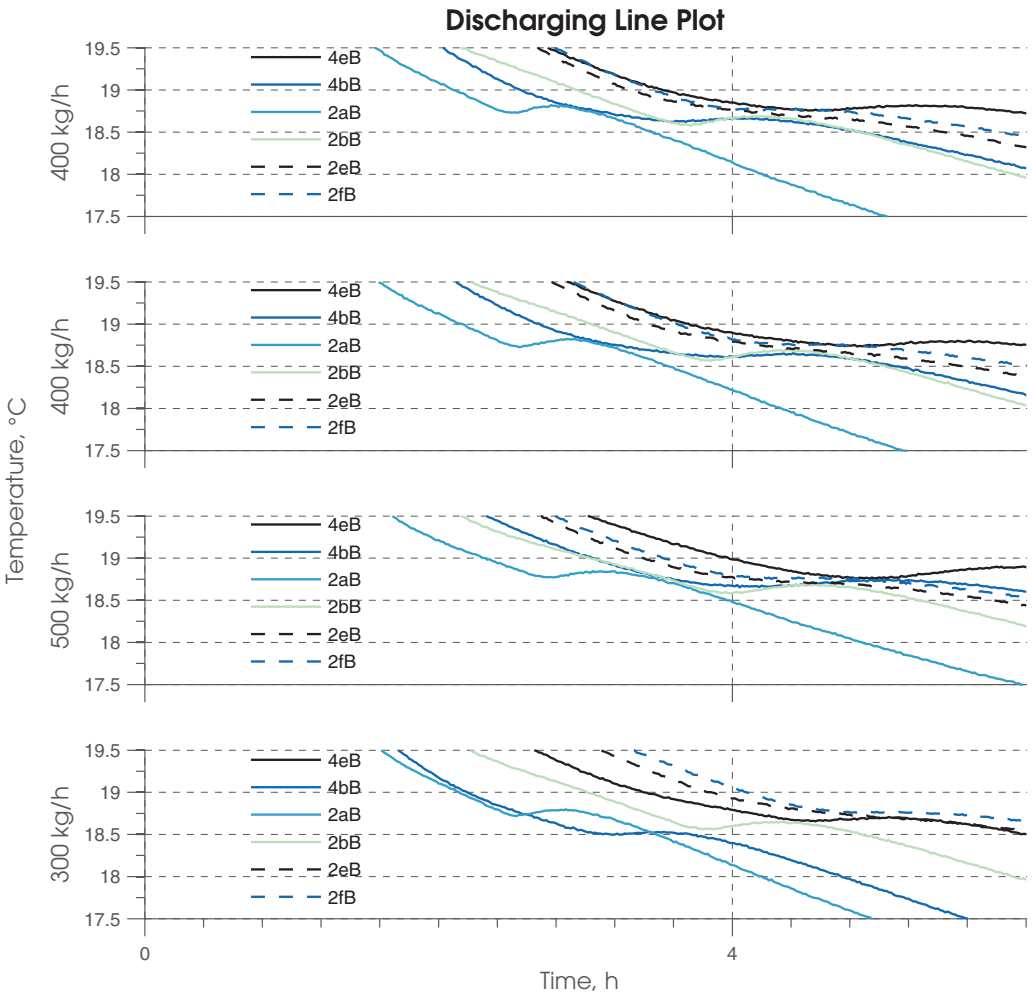

Figure 3.11: Nodes with most pronounced sub-cooling

Looking at the cooling (discharging) heat map (Figure 3.12), unlike the heating (charging) case, the temperature profile is never uniform. Even with insulation on the front of the wall, there are thermal losses.

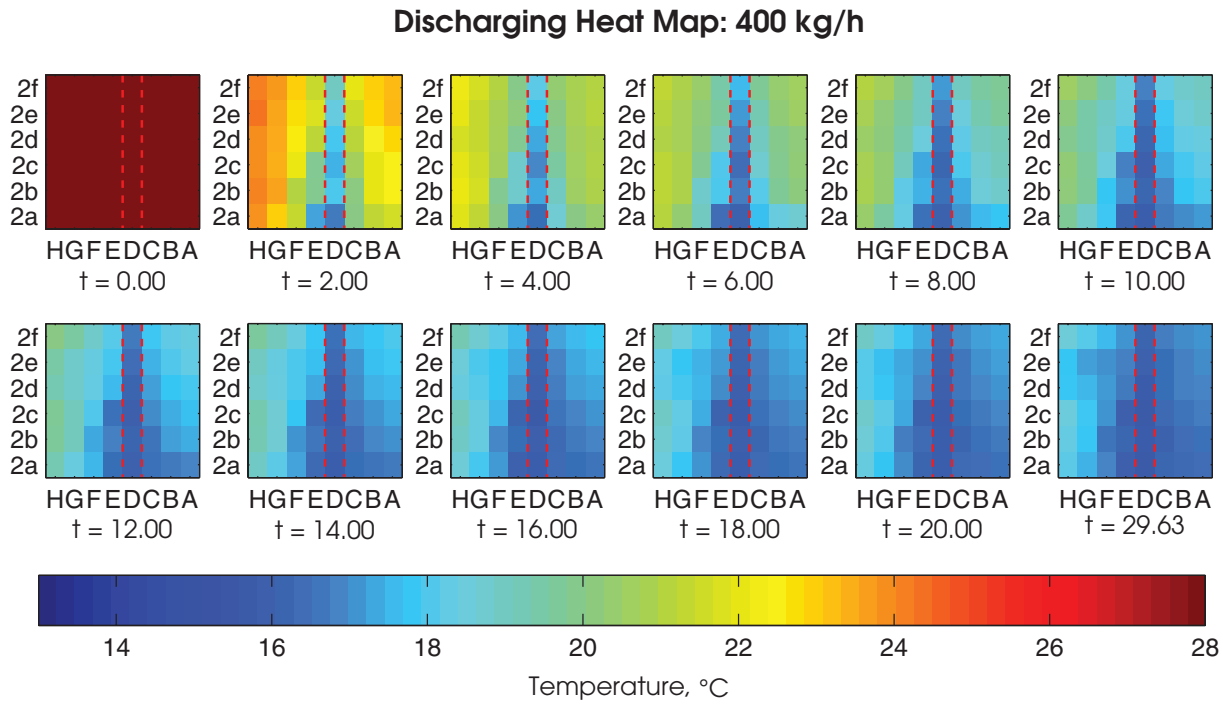

Figure 3.12: Spatial and temporal temperature heat map of the cooling (discharging) of the PCM-TES. The squares replicate a side view of the system similar to the illustration in Figure 3.1.Right. Time t is in hours.

Finally, the air stream temperatures are plotted:

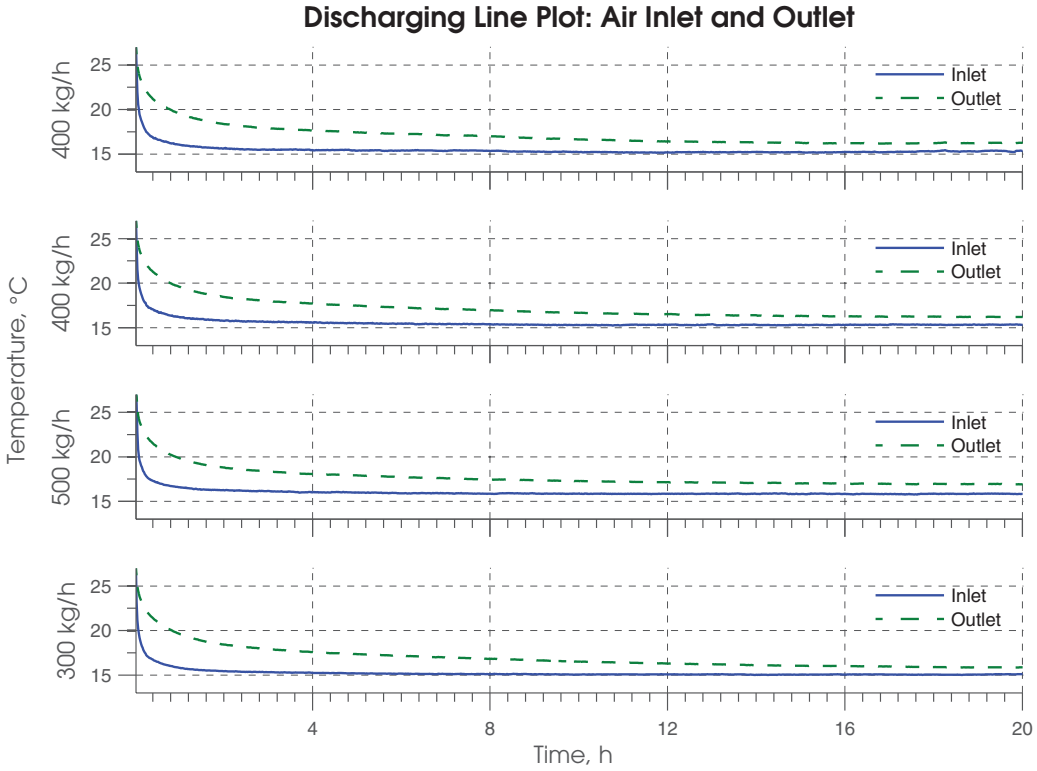

Figure 3.13: Discharging air inlet and outlet temperatures.

With the described conditions and setup, the system charges to 70% of the final steady-state value in 3.8 hours (1.76 kWh) and to 90% in 6.9 hours (2.26 kWh) when the mass flow rate is set to 400 $kg \cdot s^{-1}$ [93 $L \cdot s^{-1}$]. The PCM-TES discharges 70% in 6.0 hours and 90% in 9.7 hours. Having multiple channels, different flow rates and different configurations, these charging/discharging times can be tweaked to better match the load profile of the room: design and operation go hand in hand. (See Section 5.2)

3.2.3 Interrupted Heating and Cooling

A set of interrupted (partial) heating and cooling tests were performed. For the interrupted heating case, a phase-change can be observed. However, for the interrupted cooling case, there is no phase-change occurring even when the PCM temperature is lowered to 20°C, 1 degree lower than the specified melting temperature. In a building, in order to freeze this PCM, its temperature must be lowered below 18-19°C. If the freezing temperature is not specified, the designer will be ill informed

about how to specify the HVAC control sequence to ensure that the PCM is fully pre-cooled for the following day.

Looking at Figure 3.14, the temperature curves for the interrupted heating case seem almost linear. In a pure sensible heat gain scenario, the curves would be exponential. Looking at node A, there is never a clear kink, which implies that the charging process was interrupted at that layer. After stopping the flow of warm air, the discharging also follows a linear profile.

The bottom two curves, the interrupted cooling case, shows mostly a sensible behaviour: exponential decay. The peak freezing temperature is not reached for node A. The other nodes seem to have reached a plateau around the 2 hour mark. Then, heating is once again supplied. The curves follow an exponential profile implying that only a minor phase change had occurred.

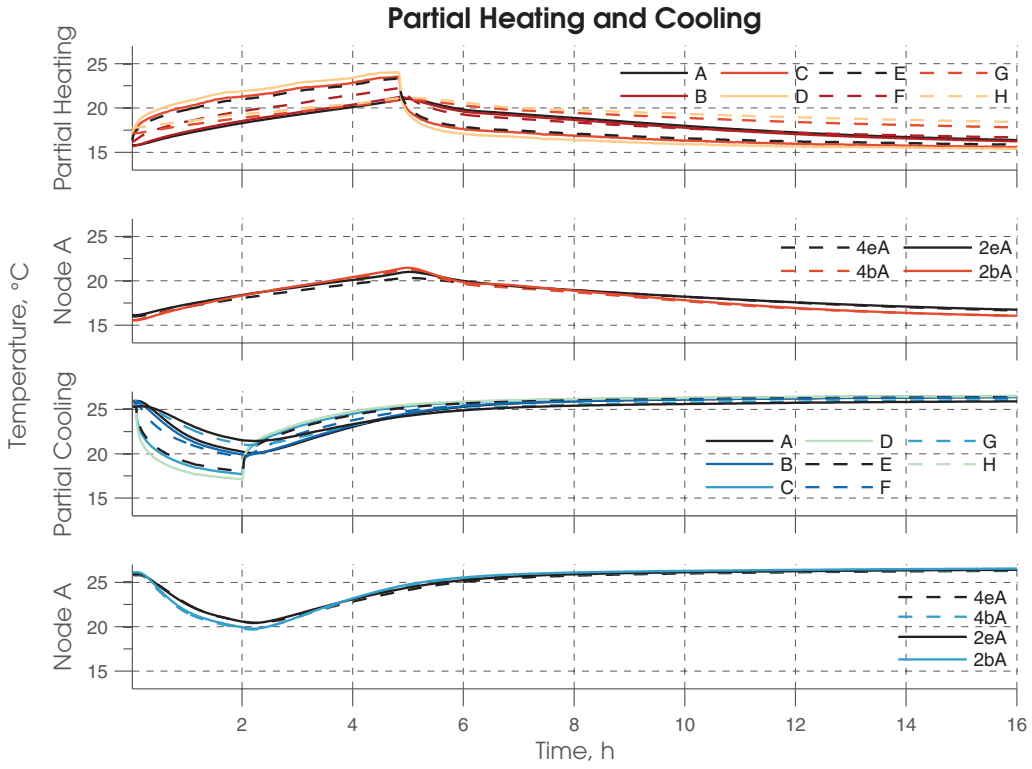

Figure 3.14: Interrupted (partial) heating and cooling curve plots.

From the above result, it is clear that many cases need to be studied to obtain enough data to fully understand the behaviour of the PCM when the heat flow is interrupted. The rate of heating/cooling, the airflow rate, the type and characteristics of the PCM will all likely influence the results. Currently, there is a lack of sufficient information on this phenomenon available and more work is needed in

this area. For a PCM-TES to be utilized for peak load reduction, the immediate behaviour of the system must be well understood.

3.3 Energy Balance Uncertainty Analysis

For any experiment, the instruments thus the measurements contain uncertainties. An uncertainty analysis must be performed to quantify the impact of these uncertainties over the performance of the PCM-TES system. The measurements are performed using Type T thermocouples (± 0.5 °C), 1/10 DIN RTDs (± 0.06 °C, within measurement range) and a calibrated orifice flowmeter (± 2%, as per the manufacturer's specifications). An uncertainty analysis of the energy balance of the air stream is completed as per the JCGM 101:2008 Guidelines §7 based on the Monte Carlo method (BIPM, 2008). The script is included in Appendix A.3.

The energy balance of the air stream is calculated:

$$E = \dot{m}_{air} \cdot C_{p,air} \cdot \Delta t \cdot \sum_{n=1}^{t} \left(T^{n}_{air,outlet} - T^{n}_{air,inlet} \right) \tag{3.1}$$

where

E, cumulative energy balance, from timestep *1* to *t*, J;

$\dot{m}_{air}$, air mass flow rate, $kg \cdot s^{-1}$;

$C_{p,air}$, specific heat of air, $J \cdot K^{-1}$; and,

Δt, timestep, s.

The uncertainties in the instrument measurements follow a Gaussian probability distribution. The plus-minus values above are given for the 95% coverage interval which corresponds to $\{1.96 \cdot \sigma\}$ on the Gaussian curve. In just this section, σ is the probability standard deviation. In order to run the Monte Carlo method, a randomized Gaussian noise is added to each measurement with its mean centered at the measurement value and with its standard deviation equal to $\{U_{uncertainty,\ \pm value}/1.96\}$. The energy balance is recalculated successively until its mean value and standard deviation converge. For this study, the energy balance for both processes was calculated 1 million times and the results are plotted:

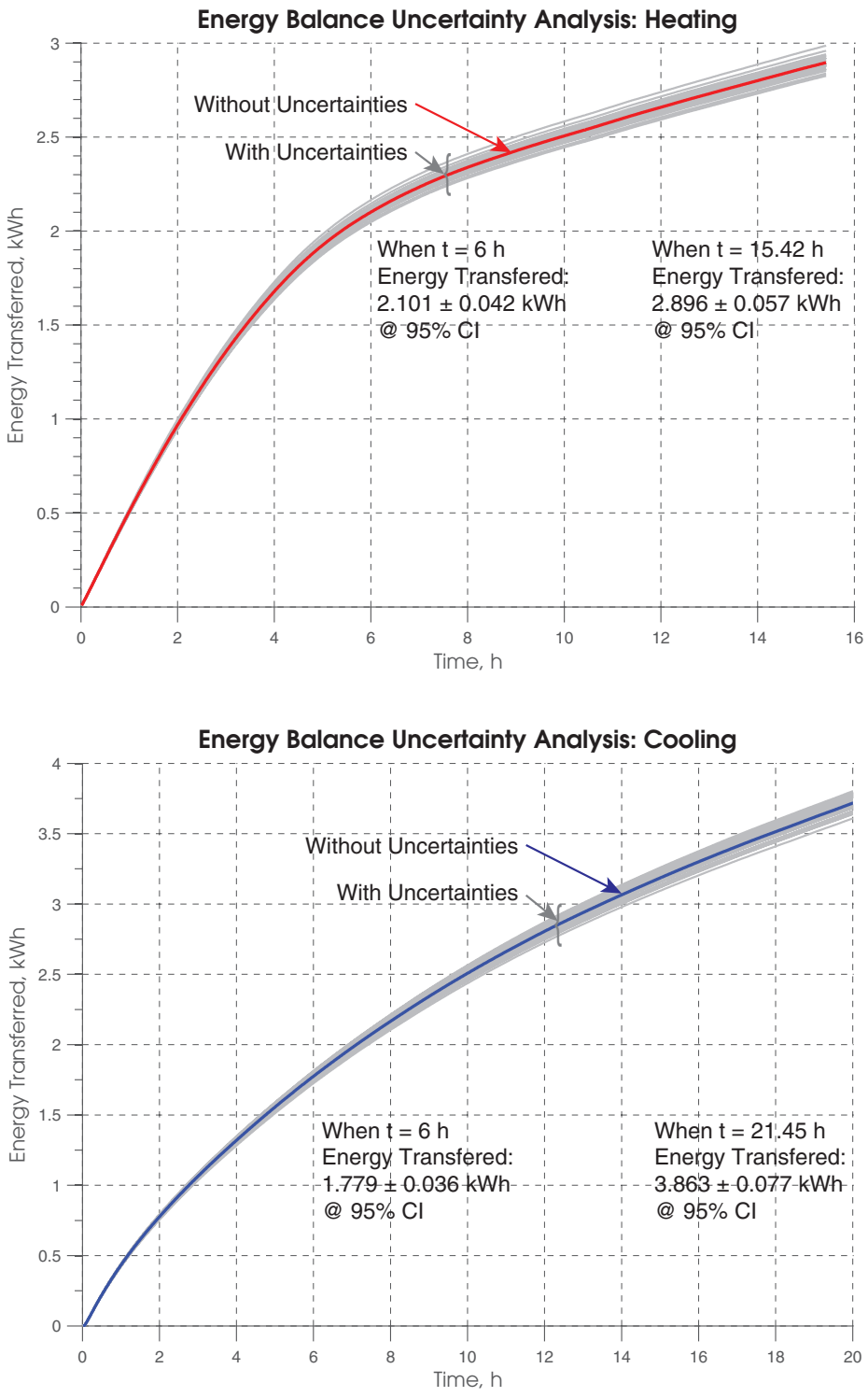

Figure 3.15: Uncertainty analysis in the air stream energy balance for (top) the heating and (bottom) the cooling processes. The uncertainties are given at t=6 hours and at the end of the process (varies). Only a few curves with uncertainties are shown as an example.

As it can be seen from Figure 3.15, the uncertainty in the energy balance increases with time since it represents the integration of power over time: the uncertainties are accumulated. The 6 hour uncertainty is shown since it would represent the realistic upper-limit use of the PCM-TES in a building.

3.4 Conclusion

This section presented the experiment and the experimental results. The experiment consisted of a PCM-TES system where the circulation of air within the system is controlled. Thermocouples, RTDs and a flowmeter are used to measure various aspects of the experiment.

For the first part of the experiment, the PCM-TES was fully charged (heated) and discharged (cooled) at three different flowrates; the rate of heat transfer proportional to the flowrate as shown by the time necessary to complete the process.

An interrupted charge/discharge case was presented at the end. However, diversified interrupted runs must be performed with various heating/cooling rates, airflow rates, etc. to obtain better insight on the performance of the PCM-TES. This is of great importance especially if the PCM-TES will be utilized for peak load reduction where the short-term behaviour of the system is critical, i.e. will the system be able to effectively release its stored energy in such a way as to reduce the peak load?

The following chapter covers the numerical modeling of the PCM-TES system.

Chapter 4

Active PCM-TES Modelling Methodology

This section covers the numerical modeling of the PCM-TES. It starts by introducing the thermal network and heat transfer equations. Simplified parametric equations are developed for the PCM's specific heat and conductivity.

4.1 Thermal Network

The PCM-TES is modeled by a thermal network (Figure 4.1). Within the storage medium control volume heat transfer is governed by conduction. Unlike a sensible material, like concrete, the specific heat and conductivity of a phase-change (latent) material varies with temperature. Within the air

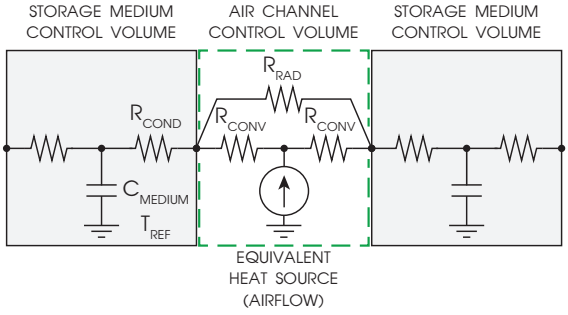

Figure 4.1: Basic thermal network of an active TES, 1-dimensional section

channel control volume, air will either gain or lose its energy to the storage medium surface through convection. The heat exchanged by the air stream is modelled by an equivalent heat source. The exposed surfaces on the sides will exchange heat through radiation. Within a 1-dimensional section, the nodal temperatures are assumed to not vary neither by with height nor width.

4.2 Storage Medium Control Volume

Heat conduction through the medium is governed by Fourier's Law of heat conduction. Starting with an energy conservation equation (Dolado *et al.*, 2012):

$$\rho \cdot \frac{\partial h}{\partial t} + \nabla (-k(T) \cdot \nabla T) = 0 \tag{4.1}$$

Since the specific heat and conductivity of the material vary with temperature (non-linear system), a closed form solution can seldom be obtained and a finite difference approach is necessary:

$$\sum_j \left[U_{ij}^{t+1} \left(T_j^{t+1} - T_i^{t+1} \right) \right] - \frac{C(T)_i^t}{\Delta t} T_i^{t+1} + \dot{Q}_i^{t+1} = -\frac{C(T)_i^t}{\Delta t} T_i^t \tag{4.2}$$

where

T_i^t, temperature at the current node *i*, at timestep *t*, °C;

U_{ij}, conductance between nodes *i* and *j* and is equal to $2 \cdot A \cdot k(T) \cdot dx^{-1}$ for conductance, $h_{conv} \cdot A$ for convection or $h_{rad} \cdot A$ for radiation, $W \cdot K^{-1}$;

$C(T)_i^t$, capacitance of node *i* as a function of its temperature at the current timestep *t* and is equal to $\varrho \cdot A \cdot dx \cdot C_p(T)$, $C_p(T)$ is constant for a building material not undergoing a phase-change, $J \cdot K^{-1}$;

$\dot{Q}_i$, heat flow into the node, W; and,

Δt, timestep, s.

Generalizing for a system, the equation can be written in a matrix form:

$$\begin{bmatrix} (\sum_N U_{1N} + \sum_M U_{1M} + \frac{C_1}{\Delta t}) & -U_{12} & \cdots & -U_{1N} \\ -U_{21} & (\sum_N U_{2N} + \sum_M U_{2M} + \frac{C_2}{\Delta t}) & \cdots & -U_{2N} \\ \vdots & \vdots & \ddots & \vdots \\ -U_{N1} & -U_{N2} & \cdots & (\sum_N U_{NN} + \sum_M U_{NM} + \frac{C_N}{\Delta t}) \end{bmatrix} \begin{Bmatrix} T_1 \\ T_2 \\ \vdots \\ T_N \end{Bmatrix}^{t+1} = \begin{Bmatrix} \dot{Q}_1 + \sum_M U_{1M} T_M + \frac{C_1}{\Delta t} T_1^t \\ \dot{Q}_2 + \sum_M U_{2M} T_M + \frac{C_2}{\Delta t} T_2^t \\ \vdots \\ \dot{Q}_N + \sum_M U_{NM} T_M + \frac{C_N}{\Delta t} T_N^t \end{Bmatrix} \tag{4.3}$$

where

N, is the number of thermal nodes; and,

M, is the number of thermal nodes with specified temperatures.

The equation shown more compactly, and finally solved for the temperature vector:

$$[U]_{N\times N}\{T\}_N^{t+1} = \{Q\}_N^{t+1} \tag{4.4}$$

$$\{T\}_N^{t+1} = [U]_{NxN}^{-1}\{Q\}_N^{t+1} \tag{4.5}$$

For a linear system, the U-matrix is symmetrical and never singular. For nodes with negligible thermal capacitance, the value of C can be set to zero.

For the derivation of the finite difference method, please consult Appendix A.1. For this study, the implicit scheme was used. For commentary on the different schemes, i.e.: implicit v. explicit, please consult Section 2.4.1.

4.2.1 Specific Heat

A sensible thermal storage material such as concrete or bricks have a specific heat and conductivity that is, for engineering purposes, constant. PCMs, however, have a specific heat and conductivity that varies greatly in the temperature range around which the phase transition occurs. Also, there is usually a shift between the peak temperature at which melting occurs and at which freezing occurs, which is called *hysteresis*.

As explained in Section 2.3.1, there are various methods to obtain the effective heat capacity as a function of temperature of a PCM. DuPont Energain panels are used in the case study. (See Table 3.1 for specifications) The shape-stabilized panels consist of a paraffin wax (60%wt) suspended in an ethylene-based polymer. Kuznik, Virgone and Noel (2008) have characterized the material using the DSC method with a heating and cooling rate approaching rates commonly found in buildings – 0.05 $K \cdot min^{-1}$. These set of curves can be implemented as lookup tables in the numerical simulation, but this approach would result in longer simulation times. A continuous curve based on a skewed normal distribution requiring 5 parameters is proposed (Equation (4.6)). The curve would be applicable for PCMs with limited sub-cooling, such as organic materials (Zalba *et al.*, 2003). It offers a simplified method to input characterization data and improves simulation time.

$$C_p(T) = \Delta h \cdot \frac{1}{\sqrt{2\pi}} \cdot \exp\left(\frac{-(T - T_c)^2}{2 \cdot \omega^2}\right) \cdot \left[1 + erf\left(\frac{skew \cdot (T - T_c)}{\sqrt{2} \cdot \omega}\right)\right] + C_{p,\ average} \tag{4.6}$$

where

Δh, enthalpy of fusion, $J \cdot kg^{-1}$;

T_c, approximate temperature of peak phase change, °C;

ω, temperature range of phase change;

$skew$, *skewness* factor; and,

$C_{p,\ average}$, average specific heat of PCM in the sensible range, $J \cdot kg^{-1} \cdot K^{-1}$.

The error function is given by:

$$erf(x) = \frac{2}{\sqrt{\pi}} \cdot \int_0^x \exp(-t^2)\ dt \tag{4.7}$$

Having determined the 5 parameters which best fit the data (Table 4.1), we can draw the $C_p(T)$ curves:

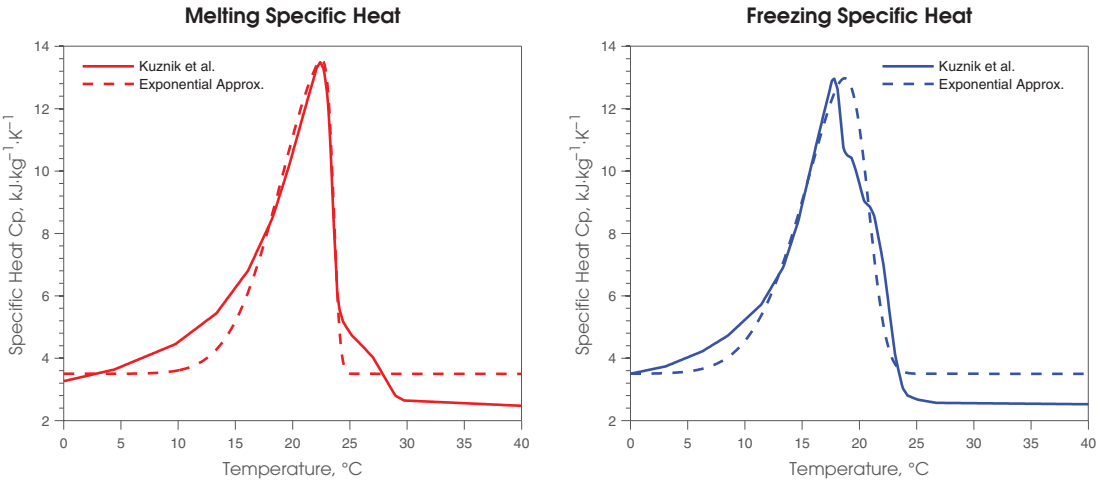

Figure 4.2: (Left) Melting and (Right) Freezing specific heat curves showing characterization data from Kuznik et al. and the approximation

Table 4.1: Specific heat equation input values

Parameters	Melting	Freezing
Δh, kJ·kg^{-1}	13 100	12 600
T_c, °C	23.6	20.8
ω, °C	4.5	4.7
skew	-10	-4
$C_{p,\,average}$, kJ·kg^{-1}	3500	3500

4.2.2 Conductivity

As for the conductivity of the material, Equation (4.8) can be used to represent the gradual shift.

$$k(T) = k_{solid} + \frac{k_{liquid} - k_{solid}}{2} \cdot \left[1 - erf\left(slope \cdot (T - T_k)\right)\right] \tag{4.8}$$

where

k_{solid}, conductivity of the solid phase, W·m^{-1}·K^{-1};

k_{liquid}, conductivity of the liquid phase, W·m^{-1}·K^{-1};

slope, slope of the transition between phases; and,

T_k, approximate temperature of peak phase change, value can differ from T_c, °C.

Having determined the 4 parameters which best fit the data around the operating range of the PCM-TES, we can draw the k(T) curves.

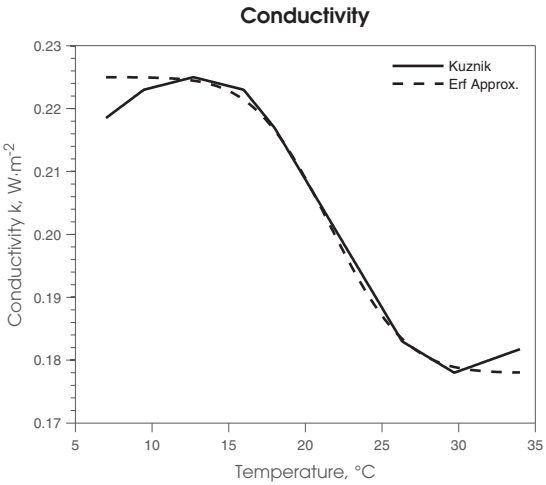

Figure 4.3: Conductivity curve showing characterization data from Kuznik et al. and the approximation

4.2.3 Hysteresis

The hysteresis phenomenon was introduced in Section 2.4.3.1. There, Figure 2.3 shows the transition path on the enthalpy-temperature curve. Here, Figure 4.4 shows the same procedure adapted for the specific heat-temperature curves. Programming this behaviour is challenging and is not the integral process.It is unclear as to how the transition should occur for materials with differing melting and freezing enthalpy profiles/shapes. The method should be as such so that at the end of an interrupted cycle (returning to the original state/temperature), the energy balance must not be violated. As mentioned in Section 2.4.3.1, further work is necessary.

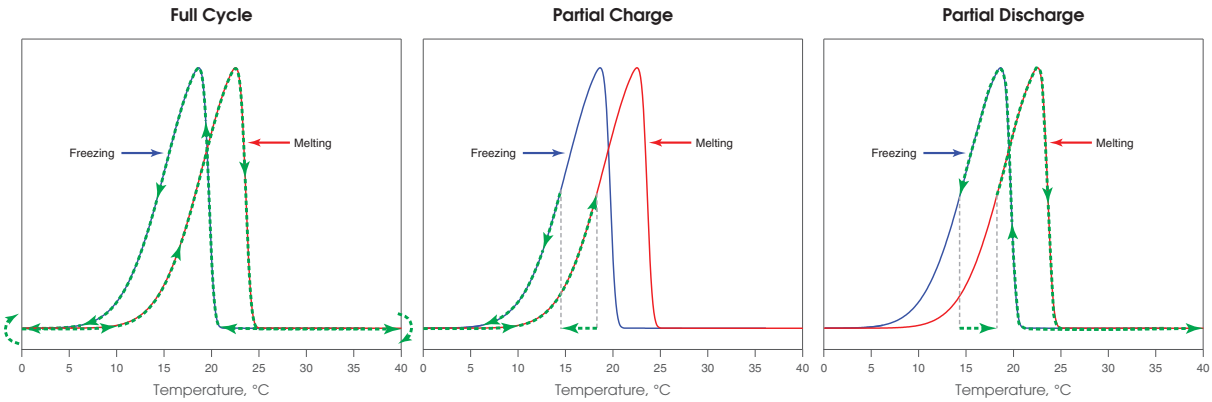

Figure 4.4: Specific heat curves showing the process path. (Left) For a full cycle, the switch from melting to freezing specific heat curve is straightforward since both lines coincide. (Center) For a partial charge, the process begins on the melting specific heat curve; when discharging begins, the sensible specific heat is taken until it reaches the temperature where the freezing specific heat is equal to the melting one when discharging begun. (Right) The partial discharge follows a similar process as the partial charge.

4.2.4 Additional Assumptions

The PCM used in this study is shape-stabilized. Even in the liquid state, the paraffin cannot flow. The copolymer matrix holds the paraffin in place like gelatin holds water in a well-known colourful treat. Because the liquid paraffin does not move, the effects of buoyancy within the PCM is negligible. Secondly, the ethylene-based matrix is a porous structure. As the paraffin melts, it occupies the voids. Therefore, the density of the board would remain practically unchanged.

4.3 Air Channel Control Volume

The heat transferred to and from the storage medium comes from the circulating fluid. Figure 4.5 illustrates an elemental slice of the air channel. Air enters, heat is transferred from the storage medium surfaces by convection, the temperature of air changes per travelled distance, until it exits. For the air channel control volume, it is assumed that the temperature of the PCM surfaces are uniform within that control volume and that the front and back surfaces have the same dimensions.

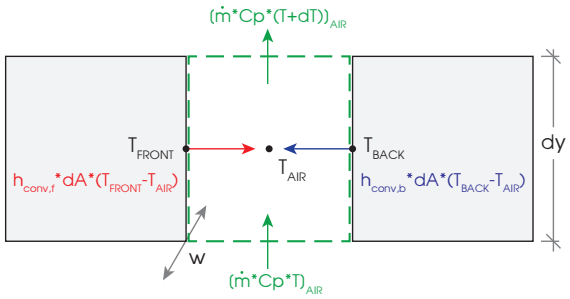

Figure 4.5: Air channel finite volume

Starting from the heat balance differential equation:

$$(\dot{m}\cdot C_p\cdot dT)_{air} = w\cdot dy\cdot\left(h_{conv,\,front}\cdot\left(T_{front}-T_{air}\right)+h_{conv,\,back}\cdot\left(T_{back}-T_{air}\right)\right) \tag{4.9}$$

where

w, width of the air control volume, m;

$\dot{m}_{air}$, air mass flow rate, $kg\cdot s^{-1}$;

A_{PCM}, total PCM surface area in contact with the air stream, m^2; and,

$T_{surface}$, average temperature of the front and back PCM surfaces, °C.

Solving for the air temperature, as a function of distance travelled, for the case where the convection coefficients are distinct:

$$T_{air}(y) = H+\exp\left(\frac{-(h_{conv,\,front}+h_{conv,\,back})\cdot w\cdot y}{\dot{m}_{air}\cdot C_{p,air}}\right)\cdot\left(T_{air,\,inlet}-H\right) \tag{4.10}$$

$$H=\frac{h_{conv,\,front}\cdot T_{front}+h_{conv,\,back}\cdot T_{back}}{h_{conv,\,front}+h_{conv,\,back}} \tag{4.11}$$

For the case where the coefficients are equal, the equation can be simplified:

$$T_{air}(y) = \frac{T_{front}+T_{back}}{2}+\exp\left(\frac{-2\cdot h_{conv}\cdot w\cdot y}{\dot{m}_{air}\cdot C_{p,air}}\right)\cdot\left(T_{air,\,inlet}-\frac{T_{front}+T_{back}}{2}\right) \tag{4.12}$$

The first term in the previous equation on the right hand side is simply the average temperature of the front and back surfaces, let's call it $T_{surface}$. And finally, solving for the outlet temperature, or when y equals to the total height of the air channel:

$$T_{air,outlet} = T_{surface} + \exp\left(\frac{-2 \cdot h_{conv} \cdot A_{surface}}{\dot{m}_{air} \cdot C_{p,air}}\right) \cdot \left(T_{air,inlet} - T_{surface}\right) \tag{4.13}$$

$$A_{PCM} = 2 \cdot A_{surface} \tag{4.14}$$

Rearranging the variables,

$$T_{air,outlet} = T_{air,inlet} \cdot \exp\left(\frac{-h_{conv} \cdot A_{PCM}}{\dot{m}_{air} \cdot C_{p,air}}\right) + T_{surface} \cdot \left[1 - \exp\left(\frac{-h_{conv} \cdot A_{PCM}}{\dot{m}_{air} \cdot C_{p,air}}\right)\right] \tag{4.15}$$

The outlet temperature is used to compute the equivalent heat source at the air node of a given section along the height.

$$\dot{Q}^{t}_{equivsource} = \dot{m}_{air} \cdot C_{p,air} \cdot (T^{t}_{air,outlet} - T^{t}_{air,inlet}) \tag{4.16}$$

4.3.1 Convective Heat Transfer Coefficient within the Air Channel

The convective heat transfer coefficient within the air channel depends on diverse factors: geometry, airflow rate, fluid and surface temperatures, intended application, etc. Candanedo (2010, sec. 3.3.6) has tabulated a list of empirical equations for this coefficient. Although his application is for a BIPV/T system, the flow within the PCM-TES is comparable. From the many equations, experimentally, it was found that the corrected Martinelli equation was most applicable for the system being studied and is reproduced:

$$Nu_{Martinelli} = \frac{\mathrm{Re}\,\mathrm{Pr}\sqrt{f/2}}{\left(\frac{T_w - T_b}{T_w - T_p}\right)\cdot 5\cdot\left(\left(\mathrm{Pr} + \ln(1+5\,\mathrm{Pr}) + 0.5N_{DR}\ln\left(\frac{\mathrm{Re}}{60}\sqrt{\frac{f}{2}}\right)\right)\right)} \tag{4.17}$$

where

T_w, average temperature of the channel wall surface, K;

T_b, bulk air temperature, K;

T_p, temperature at the center of the pipe, K; and,

N_{DR}, diffusivity ratio, between 0.70 and 0.98 for air, (See Martinelli 1947).

And since,

$$Nu = \frac{h_{conv}\cdot L}{k_{air}} \tag{4.18}$$

The convective heat transfer coefficient for various flowrates and channel widths can be graphed; and, similarly, a correlation between mass flow rate and channel width to obtain a certain convective heat transfer coefficient can be formulated.

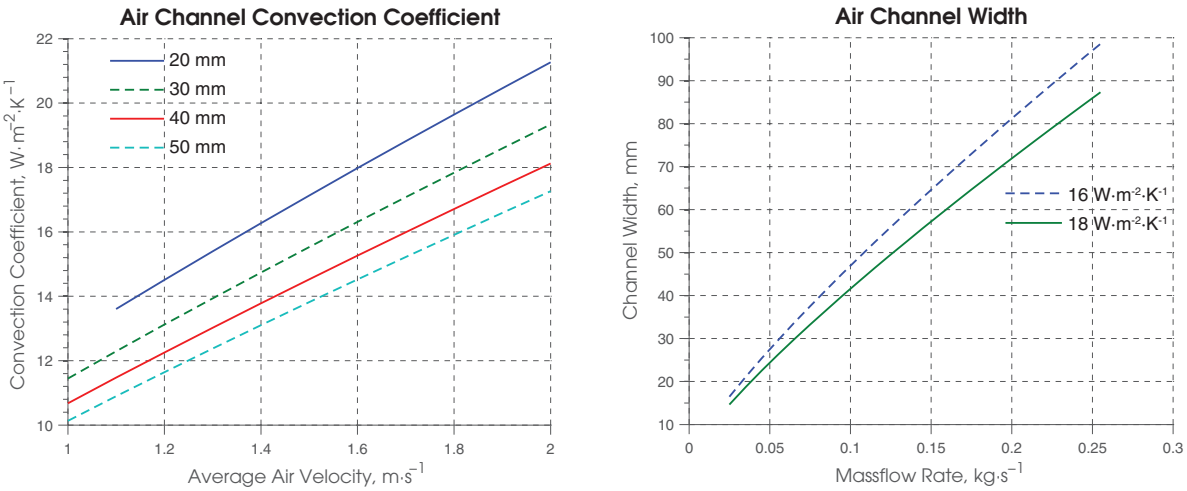

Figure 4.6: (Left) Convection coefficient within the air channel for various flowrates and channel widths; based on Equation (4.17), (Right) Channel width required to obtain a convection rate as a function of mass flow rate.

Narrowing the width or increasing the flowrate augments the convective heat transfer rate. However, more energy will be required by the fan which is required to draw air through the PCM-TES system.

4.3.2 Radiation

To calculate the radiation exchange, since the surfaces are not ideal blackbodies {ε ≠ 1}, there needs to be a surface resistance added:

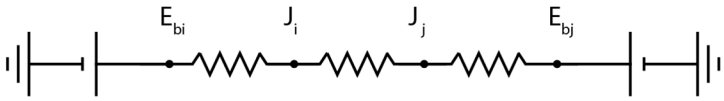

Figure 4.7: Radiation thermal network

Therefore, the total resistance between two surfaces that see each other is:

$$R_{ij,rad} = \frac{1-\varepsilon_i}{A_i\varepsilon_i} + \frac{1}{A_i F_{i\to j}} + \frac{1-\varepsilon_j}{A_j\varepsilon_j} = \frac{1-\varepsilon_i}{A_i\varepsilon_i} + \frac{1}{A_j F_{j\to i}} + \frac{1-\varepsilon_j}{A_j\varepsilon_j} \tag{4.19}$$

And the corresponding conductance due to radiation between the surfaces:

$$U_{ij,\,radiation} = \frac{\sigma(T_j^4 - T_i^4)}{R_{ij,rad}\,(T_j - T_i)} \tag{4.20}$$

Within the air channel, the view factor between the panels facing each other approaches 1. For this case, the conductance due to radiation is simplified to:

$$U_{ij,\,radiation,\,parallel\,plates} = \frac{A_i\sigma(T_j^2 + T_i^2)(T_j + T_i)}{\frac{1}{\varepsilon_i} + \frac{1}{\varepsilon_j} - 1} \tag{4.21}$$

4.4 Friction Losses and Fan Power

A fan is required to draw air through the PCM-TES system. To estimate the required fan power, first, the friction losses are calculated. Losses through the system vary according to the Darcy-Weisbach equation (ASHRAE, 2009):

$$\Delta p = f \frac{L_{rough}}{D_h} \frac{\rho v^2}{2} \tag{4.22}$$

where

Δp, pressure drop in pipe or duct, Pa;

f, friction factor;

L_{rough}, absolute roughness, m;

D_h, hydraulic diameter, {defined as: 4*cross_sectional_area*wetted_perimeter^{-1}}, m;

ρ, fluid density, kg·m^{-3}; and,

v, average fluid velocity, m·s^{-1}.

For flow in the laminar range {Re<2300}, the following friction factor equation is used (Candanedo, 2010):

$$f_{laminar} = \frac{64}{\mathrm{Re}} \tag{4.23}$$

Candanedo (2010, sec. 3.7.1) has used the Blasius relationship to obtain the friction factor for his BIPV/T system in the turbulent range {Re>4000}. Although the Blasius relationship is developed for smooth pipes, it is often used due to its simplicity:

$$f_{Blasius} = \frac{0.3164}{\mathrm{Re}^{0.25}} \tag{4.24}$$

Alternatively, the Colebrook-White equation (Colebrook and White, 1937) can be used to obtain the friction factor in the turbulent range:

$$\frac{1}{\sqrt{f}} = -2\log_{10}\left(\frac{L_{rough}}{3.7D_h} + \frac{2.51}{\mathrm{Re}\sqrt{f}}\right) \tag{4.25}$$

Additionally to friction losses, other miscellaneous losses due to the entrance and exit effect must be considered:

$$\Delta p_{total} = \Delta p + \sum K \cdot \frac{\rho v^2}{2} \tag{4.26}$$

where

K, hydraulic loss coefficients; typically 0.5 for the entrance and 1.0 for the exit.

Finally, the fan power required:

$$P_{fan} = \frac{(A \cdot v) \cdot \Delta p_{total}}{\eta_{fan}} \tag{4.27}$$

where

P_{fan}, fan power required, W;

A, cross sectional area of fluid flow, m^2; and,

η_{fan}, combined fan and motor efficiency, %.

For the PCM-TES system, the pressure requirements are estimated for a 1 m unit wide system with various air channel widths, overall heights and air velocities. The Colebrook-White equation is used to calculate the friction factor. Combined fan and motor efficiency is assumed to be 40%. Entrance and exit effects are taken into account while effects such as ducting and flow diverting/adding transitions are not considered.

The convective heat transfer coefficient is a strong function of average air velocity (and Reynolds number) in the channel. Using an average velocity higher than about 2 $m \cdot s^{-1}$ results in high friction losses without achieving higher charging/discharging rates due to the relatively low thermal conductivity of the PCM panels. For velocities less than 2 $m \cdot s^{-1}$, the fan energy consumption is negligible compared to the heat stored.

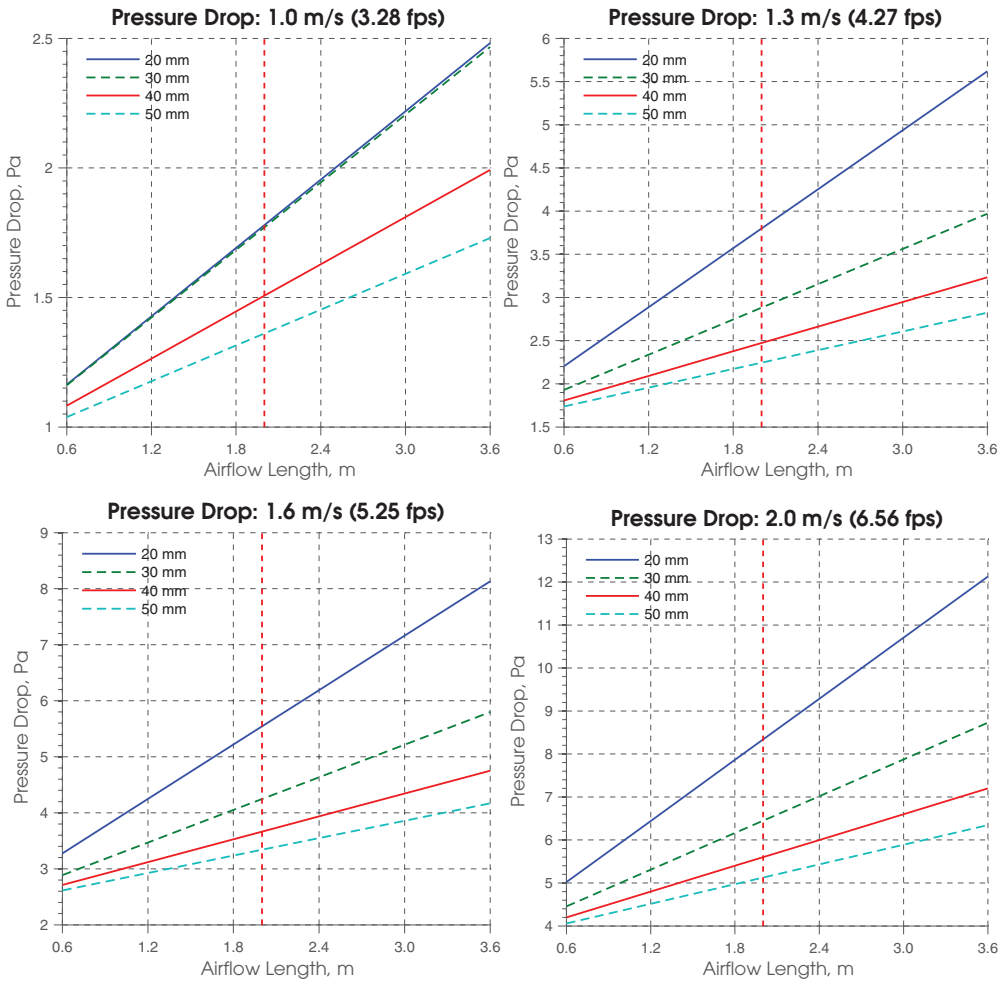

Figure 4.8: Pressure drop for a smooth 1 m unit wide PCM-TES system with various channel widths, airflow lengths and air velocities.

4.5 Conclusion

This section presented the numerical modeling of the PCM-TES. The heat transfer equations were described for conduction in the storage material, and for convection and radiation in the air channel. Simplified parametric equations were developed for the PCM's specific heat and conductivity. Finally, friction loss and fan power equations were described.

The formulations in this chapter are used to construct the single-channel PCM-TES model in the following chapter. The experimental measurements will be used for validation. Finally, this model will be simplified to study the effect of model resolution on its behavioural accuracy.

Next, multi-channel systems will be analysed to study the effect of channel width and air velocity on the rate of charging/discharging. Various lengths are also studied.

Chapter 5

Modelling of Active PCM-TES Systems for Control Applications

In this chapter, the modelling methodology described previously will be used to construct the single-channel PCM-TES model. The experimental measurements will be used for validation. Finally, the effect of model resolution on the accuracy of its thermal behaviour will be analysed.

In the second part of this chapter, the single-channel system will be expanded to multi-channel systems. Multi-channel systems will be analysed to study the effect of channel width and air velocity on the rate of charging/discharging. Identical systems installed in series will be used to study various overall lengths and storage capacities.

In the last part, a multi-channel PCM-TES system is inserted into a simple office to study its impact on the heating peak load reduction during the morning start-up.

5.1 Single-Channel PCM-TES

The motivation for this work is to develop practical simplified models that can be used for control applications and model-based control. This requires adequate modeling of the energy charge and

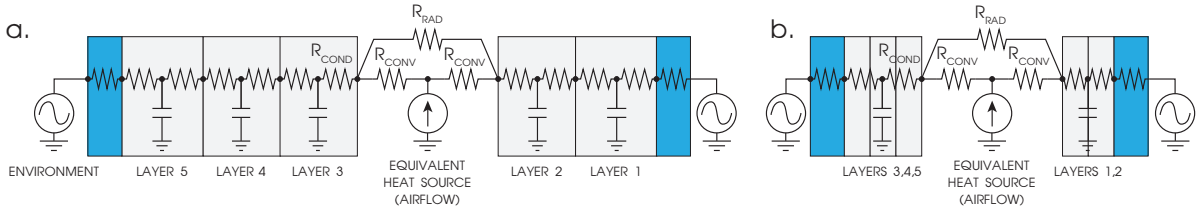

Figure 5.1: Thermal network of the (a) detailed 5-capacitance vertical section, and (b) simplified 2-capacitance section

discharge process, i.e. how much thermal energy is stored/discharge and over how much time. In the previous chapter, the thermal nodes and the means of heat transfer are described. Here, we apply those equations to construct the thermal networks of the isolated single-channel PCM-TES system.

Three models are considered with different numbers of control volumes (CV) (Figure 5.1 & Figure 5.2). The detailed model has a node for each thermocouple used in the experiment. This allows a direct comparison between simulation and measurement. Next, the objective is to simplify the model without sacrificing its ability to predict the amount of energy stored/discharged in the PCM-TES system. The approach consists of reducing the number of thermal capacitances as well as the number of vertical sections by aggregating them. Here are the 3 models under consideration:

a. Detailed model consisting of 6 vertical sections of 5 solid CV and 1 air CV for a total of 36 CV; 30th order – 30 capacitances. Each PCM layer is modelled individually.
b. Simplified model consisting of 2 vertical sections of 2 solid CV and 1 air CV for a total of 6 CV; 4th order – 4 capacitances. The PCM layers are aggregated.

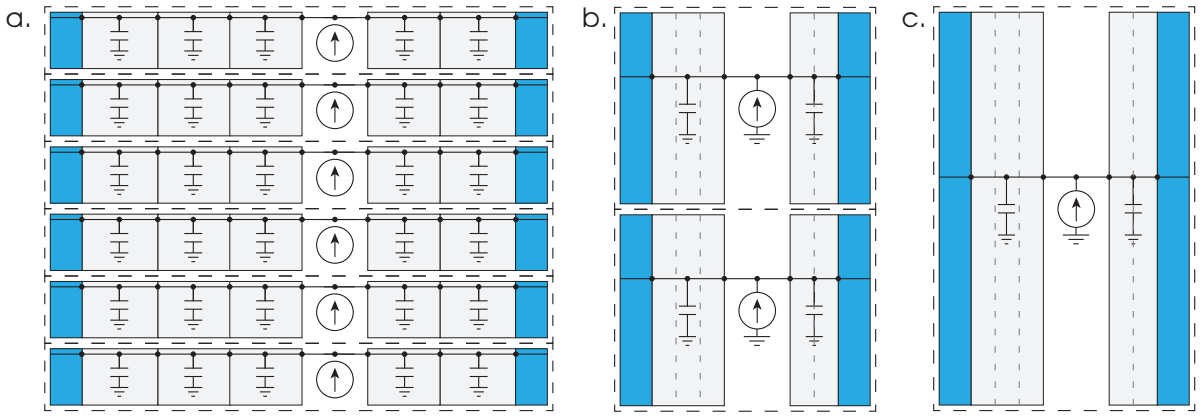

Figure 5.2: (a) 6 section, 5 capacitance per section, 30th order model (b) 2 section, 2 capacitance per section, 4th order model (c) 1 section, 2 capacitance per section, 2nd order model.

c. Simplified model consisting of 1 vertical section of 2 solid CV and 1 air CV for a total of 3 CV; 2nd order – 2 capacitances. The PCM layers are aggregated.

Along the height, the PCM-TES is split into vertical sections and connected at the air nodes. The air outlet of one becomes the air inlet of the following. The PCM panels are relatively thin compared to the total height – a ratio of around 150 to 1. Thus, the heat transfer through the PCM between vertical sections is minimal compared to the heat transfer in the transversal direction, therefore the thermal network behaves 1-dimensionally. The assumption holds for a height to thickness ratio of at least 10 to 1. (Dolado *et al.*, 2011b) The simulation timestep is set to 1 minute to assure numerical stability.

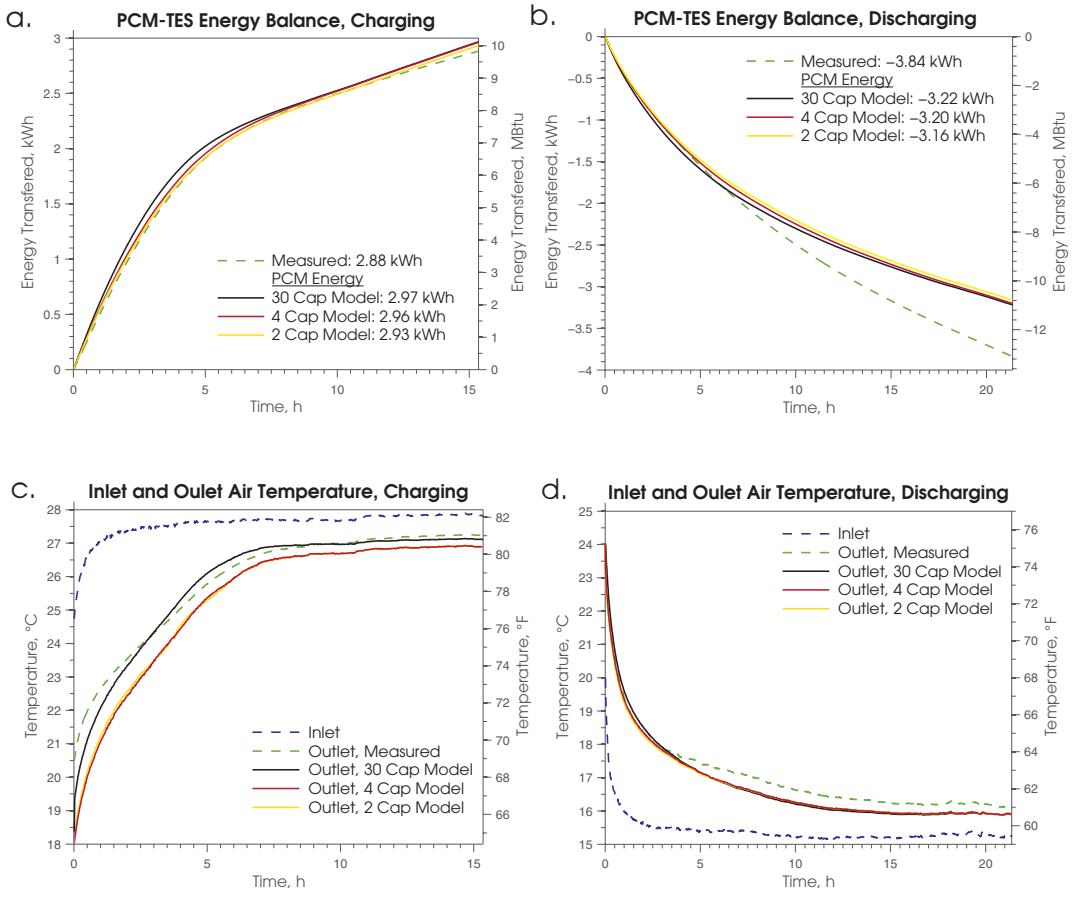

Figure 5.3: PCM-TES energy balance for (a) charging and (b) discharging. The measured energy is calculated using the measured temperature difference of the air stream inlet and outlet from the experiment. Inlet and outlet air stream temperatures for (c) charging and (d) discharging. The inlet air is directly from the experiment.

In order to run the simulation, first the 30-capacitance model is used. All nodes are initialized to the corresponding experimental values. Then, only the experimental inlet air temperature is input into the simulation. To compare model to experiment, most importantly, the energy balance between stored energy in the PCM and the energy transferred by the air stream should agree. The former is calculated using the energy balance at the nodes with capacitance. The latter is calculated using both measured inlet and outlet air temperatures. Although some disrepencies exist in the agreement between thermal nodes with experimental data, on the system level, the amounts of energy transferred match well. Results are shown in Figure 5.3. Between the measurements and model, there is a 3.1% difference in the charging energy balance after around 15 hours, and a 16.1% difference in the discharging balance after around 22 hours. In practice, however, the practical time frame for charging or discharging would be at most 6 hours. For this period of time, between the measurements and model, there is a 3.7% difference in the charging energy balance, and a 0.3% difference in discharging – coincidently, the measurement and simulated data for the discharging case cross at around 6 hours and, therefore, this reported error is an underestimation. The energy balance uncertainty due to instrumentation uncertainty at 6 hours is ± 2.0% for either charging or discharging (See Section 3.3).

For the vertical section least fitting with the experimental data, a temperature fit having a NMBE of 4.74 and CV(RMSE) of 5.79 is calculated for the charging case; and, a NMBE of 4.18 and CV(RMSE) of 4.27 for the discharging case – consult the Appendix A.2 for NMBE and CV(RMSE) definitions. The 95% quartile of the temperature difference between simulation and experiment is 2.1°C, and the 75% quartile is 1.1°C for charging; and, 1.0°C for the 95% quartile and 0.4°C for the 75% quartile for discharging.

Table 5.1: Simulation time in seconds

	Heating Process	Cooling Process
30^{th} order, lookup tables for both C_p and k values	78.6	89.5
30^{th} order, equations for both C_p and k values	17.0	15.2
4^{th} order, equations for both C_p and k values	4.5	4.8
4^{th} order, equation for C_p value, constant k value	4.0	3.3
2^{nd} order, equations for both C_p and k values	1.9	2.3
2^{nd} order, equation for C_p value, constant k value	1.5	2.0

The outlet air stream temperature is also important since the air will be directed into the room. For the charging case, the fit results in a NMBE of 0.18 and CV(RMSE) of 1.15. For the discharging case, the fit results in a NMBE of 1.57 and CV(RMSE) of 1.99. Although the PCM is organic, there is some sub-cooling around 18 to 19°C during discharging (See Section 3.2.2).

To simplify the thermal model, the front 3 capacitances are lumped together as well as the back 2. Furthermore, the vertical discretization is reduced to 2 and 1 sections along the height. All other material properties and parameters are unchanged. When comparing the reduced order models to the detailed version, the energy balance representing the level of charge and the outlet air temperatures are of primary interest. The agreement of the 4th order and 2nd order models to the 30th order model are satisfactory with a maximum error of 1.9% in the energy balance at the end of the cycle. Between the 2nd order model and the experiment, there is a 1.7% error in the energy balance during charging and 4.1% during discharging after 6 hours. Temperature gradients exist in the transverse direction, this variation however is not very significant. A lumped-capacitance model will average the 2/3 capacitances from the detailed model and is why the outlet air temperature is under predicted during the charging process. The reduced order models are sufficient for control-oriented purposes. In an actual application, the parameters of the simplified model would be modified or learnt in real time to match installed PCM-TES to the model. Simplified models have less parameters to adjust; these can include: the C_p-temperature correlation, added resistance due to contact resistance and edge effects, container U-value or losses to the environment, actual fan power consumption, and air channel convective heat transfer coefficient. The structure of the model being set, adjusting its parameters is not difficult. With additional work, the model could be further fine-tuned.

Table 5.1 shows the times required to run the simulations. It can be seen that moving from a lookup table to an equation for the specific heat and conductivity values, the simulation time for the 30th order model decreased by 78 to 83%. If a piecewise linear correlation is used instead of Equation 4.6, similar performances can be obtained, however, a physically meaningful equation can give designers better intuition on the behaviour of the PCMs. Different materials can be examined by comparing their parameters. Simplifying further, a 4th order model offers a 68 to 74% decrease in simulation time compared to the 30th order equation-based characterization model. Finally, the 2nd order model offers the quickest solving times. Shorter simulation times will ensure the convergence

of the MPC optimization algorithm. The simulations were run using the solvers built-in MATLAB on a 2.8 GHz hexa-core consumer desktop computer.

5.1.1 Conclusion

The detailed 30th order model is shown to predict the overall behaviour of the PCM-TES. Simplified 2nd and 4th order models are shown to predict the energy storage of the PCM-TES and its air outlet temperature. The latter configurations are accurate for practical control-oriented models. A simplified model is easier to interpret, calibrate, program and would result is faster computational times.

5.2 Multi-Channel PCM-TES

Having developed and validated a model of a single channel PCM-TES system, the methodology will be used to explore multiple channel systems. The objective here is to compare systems with varying numbers of equally distributed air channels (increasing the amount of PCM surface exposed) and of varying overall lengths. The ideal system would charge/discharge quickly and offer a larger temperature differential initially. Such a system would allow the reduction and shifting of the peak heating and/or cooling demand of a building.

Multi-channel active panel systems will be analyzed comparatively using the control volume methodology described in the previous section. The systems consist of 12 DuPont Energain PCM panels with 1, 2, 3 or 6 equally distributed air channels (Figure 5.4). Identical 1.2 m systems are put in series to obtain a total length of 1.2, 2.4 or 3.6 m, offering 2.15, 4.30 and 6.45 kWh of energy storage within the analysis temperature range. For comparative purposes, the width of the channels and air velocity are chosen in order to maintain both a constant convective heat transfer coefficient and a

Table 5.2: Multi-channel PCM-TES air channel parameters

# Channels (#)	Mass Flow ($kg \cdot s^{-1} \cdot channel^{-1}$)	Average Velocity ($m \cdot s^{-1}$)	Air Channel Width (mm)
1	0.1667	2.23	62
2	0.0833	1.93	36
3	0.0556	1.75	26
6	0.0278	1.47	16

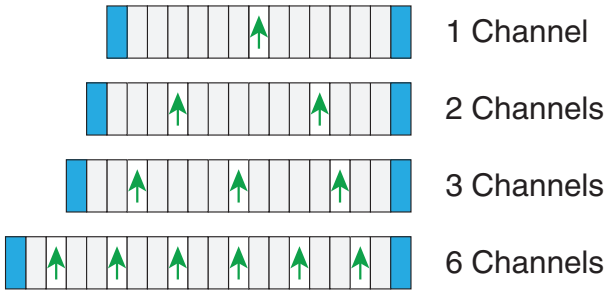

Figure 5.4: Isolated single/multiple channel systems: (Top) Single channel system; (Other three) Two, three and six channel systems.

constant total mass flow rate across the different systems. The boundaries (surface area of the edge panels) are insulated and exposed to air at room temperature. The simulation parameters are presented in Table 5.2 and Table 5.3.

5.2.1 Results

A comparative analysis between two sets of simulations is presented. The first set – called "Input Hot Air" – consists of the active PCM-TES initially at the cold air temperature after which hot air is introduced until steady state is attained. This case would represent a TES system pre-cooled and would be used to reduce the peak cooling demand. Similarly, the second set – called "Input Cold Air" – consists of the active PCM-TES initially at the hot air temperature after which cold air is introduced.

Table 5.3: Multi-channel simulation parameters

Mass flow, $kg \cdot h^{-1}$	600
PCM-TES width, m	1
PCM density, $kg \cdot m^{-3}$	850
Insulation RSI-value, $m^2 \cdot K \cdot W^{-1}$	2
Convective heat transfer coefficient, air channel, $W \cdot m^{-2} \cdot K^{-1}$	18
Film coefficient, environment, $W \cdot m^{-2} \cdot K^{-1}$	5
Environment temperature, °C	22
Cold air temperature, °C	10
Hot air temperature, °C	28
Simulation time step, s	30

A TES charged with heat would be used to reduce the peak heating demand. The temperature range chosen allows the TES system to be fully melted or solidified within this process.

The TES may be cooled using night-time free-cooling or through the use of the HVAC system. The TES may be charged with heat using solar gains, internal loads or, again, through the HVAC system.

As expected, the charge/discharge time is inversely proportional to the number of channels or to the amount of PCM surface exposed (See Figure 5.5). The single channel system would take more than half a day to charge in both heating and cooling modes, and would not be useful for fast peak reduction measures. The energy stored in the TES would be best utilized in a 6 channel system for faster and more easily controllable storage of heat/cool. Looking at the temperature differential graphs in Figure 5.6, it can be observed that a 3.6 m length system will not cool or heat the inlet air significantly more than a 2.4 m length system. However, compared to the 1.2 m system, the 2.4 m system offers a 3 to 4°C greater temperature differential between the air inlet and outlet for the first 3 hours of discharging: a 33% improvement for the 6-channel case and up to a 100% improvement for the 1-channel case.

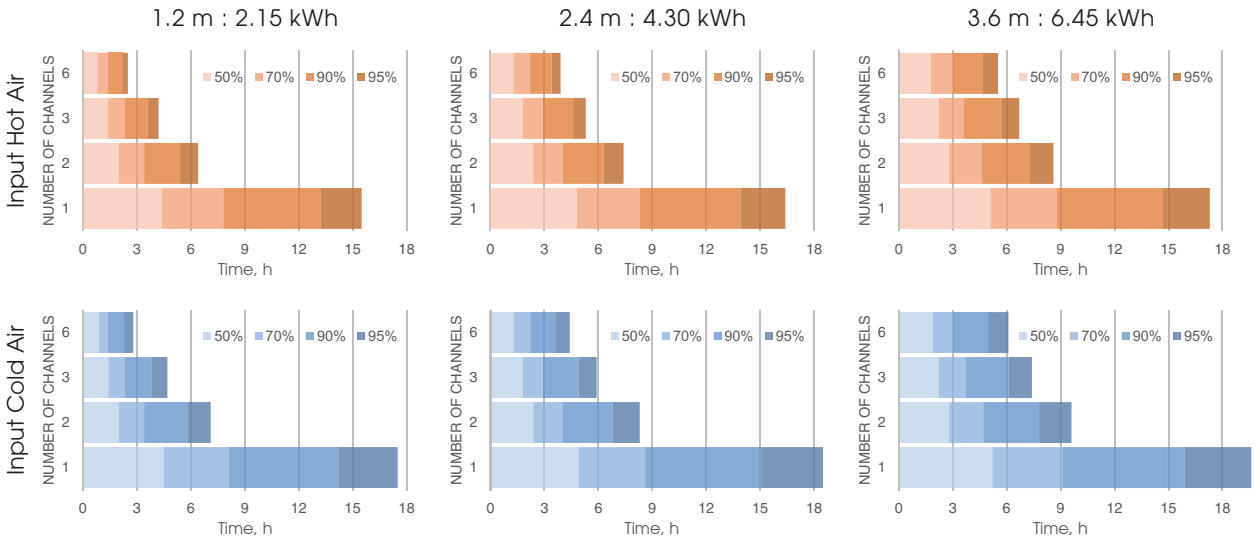

Figure 5.5: Time required to charge the TES system to a certain percentage of its steady state energy value: (top) hot air introduced in an initially cold TES system; (bottom) cold air introduced in an initially hot TES system.

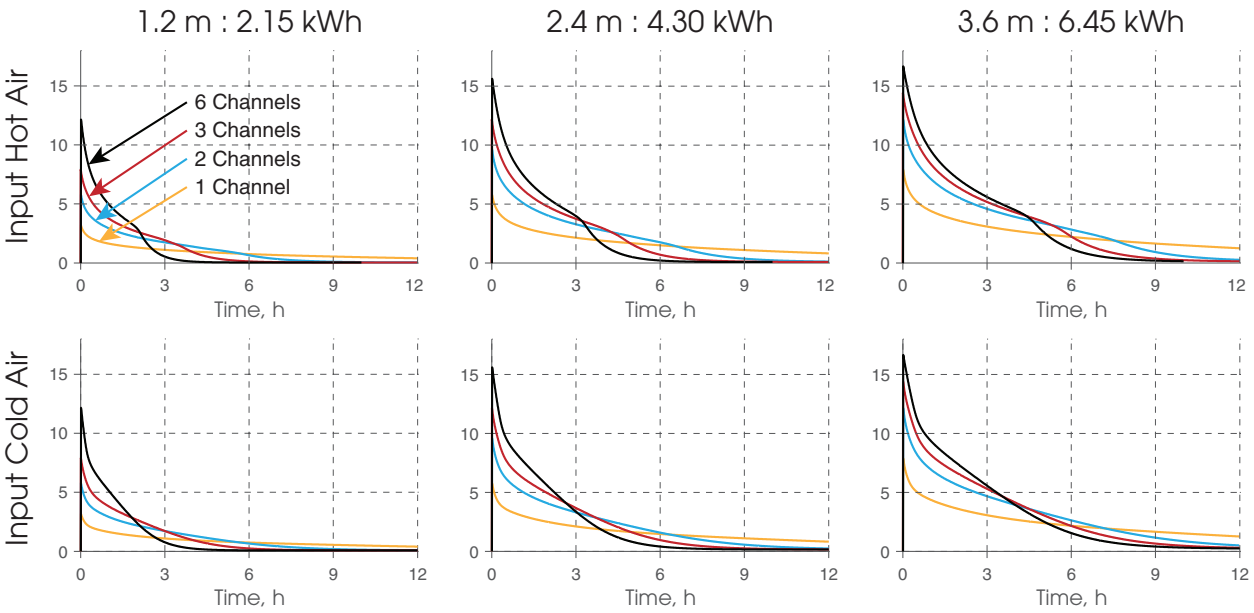

Figure 5.6: Absolute temperature differential between inlet and outlet air streams: (top) hot air introduced in an initially cold TES system; (bottom) cold air introduced in an initially hot TES system.

The 2.4 m system with 6 air channels charges to 95%, of its total capacity of 4.30 kWh, in 3.9 hours in the "Input Hot Air" mode and in 4.4 hours in the "Input Cold Air" mode. It can discharge 50% (2.15 kWh) of its capacity in 1.3 hours. Figure 5.7 shows the constituent energy balance of the system. To increase the storage capacity, installing such systems in parallel would be more beneficial than in series.

The panels are 5.2 mm thick. The 6 channel case has 2 panels inserted back-to-back within the middle part of the system. Reducing the thickness further in order to increase the exposed surface area may lead to the panels starting to flutter, eventually leading to its degradation.

Fan energy is considered, but it is shown to be negligible compared to the energy transferred into the PCM-TES system. The PCM panels used in the study consist of flat panels with a very smooth aluminum surface. The distance the air needs to travel is short and the velocities are not necessarily high. Reasons which explain the minimal pressure losses through the system.

For peak load reduction, a fast-acting system is often preferred, but for some applications, such as solar heat storage for use in the next day, slow charge/discharge may be adequate.

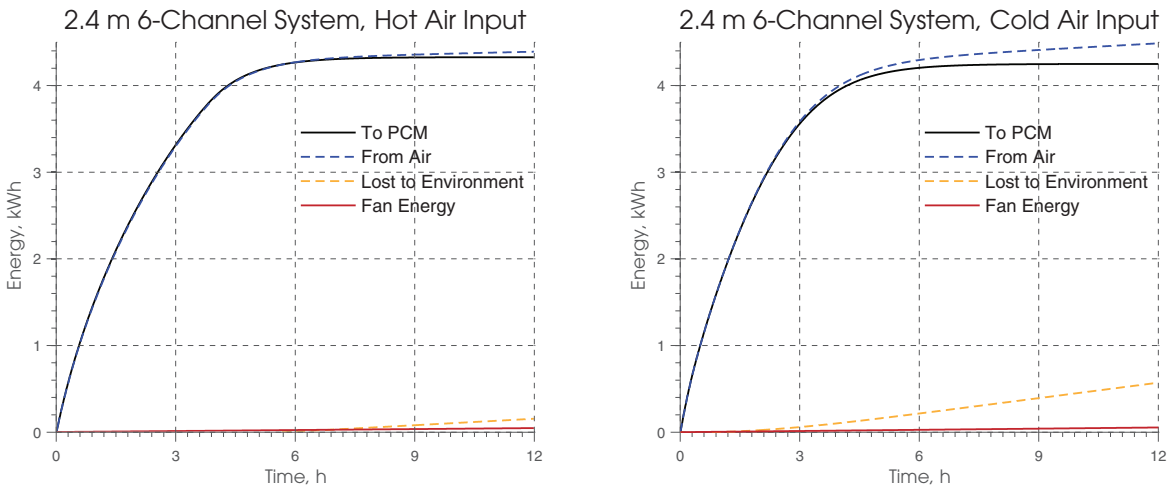

Figure 5.7: Total energy transferred in an active 2.4 m 6-channel system. "To PCM" is the energy stored in the PCM; "From Air" is the energy transferred from the air stream to the PCM; "Lost to Environment" is the energy transferred (or lost) to the environment from the insulated boundaries; "Fan Energy" is the energy required by the fan to circulate the air. (Left) hot air introduced in an initially cold system and (right) cold air introduced in an initially hot system.

5.2.2 Exposed PCM Active Systems for Wall and Ceiling Integration

One surface of the insulation can be removed from the previously described systems, exposing a PCM panel. The exposed active system can then be installed in the wall enclosure with the exposed PCM surface towards the occupied interior space. Alternatively, the exposed surface can be on the ceiling. This way, heat can be directly absorbed by the PCM material. However, this heat can be transferred to the room passively. Having an exposed surface will reduce the controllability of the system and controllability is paramount for peak load reduction strategies. For this reason, an insulated system is preferred.

5.2.3 Conclusion

Systems with varying numbers of air channels (exposed surface area to the air stream) and varying overall lengths were compared. The total mass flow rate remained constant among the cases. The channel width and air velocity were selected as such to have a constant convective heat transfer rate. The system with the most air channels (6 air channels) is found to be the one with the fastest response. Since the underlying purpose of this study is to reduce the peak demand for heating or cooling, a TES

system releasing/absorbing the most energy in a reasonably short time is favourable. Among the different overall lengths, the 2.4 m length systems offers comparable performance to the 3.6 m systems. The 2.4 m systems outperform the 1.2 m long ones by offering a 3 to 4°C greater air stream temperature differential: an improvement between 33 and 100%.

5.3 Case Study: PCM-TES for Peak Load Reduction

In this section, the above multi-channel PCM-TES system is incorporated into a simple office to study its impact on the heating load during the morning start-up. A full description of the office and its modelling considerations are expanded in Appendix A.6. The computer program is in Appendix A.7. Although this example is for a single office, a single but larger PCM-TES system can serve multiple offices with similar behaviour (e.g. south-facing office wing). The larger system can be place in the floor's mechanical room, near the air handling unit.

The room modelled is a south-facing perimeter office among self-similar offices located in Montreal, QC. A window-to-wall ratio of 40% is used. The window is double-glazed with a low-e coating. The office dimensions are 4 m (width) x 4 m (depth) x 3.2 m (height). Gypsum walls and a 50 mm concrete floor/ceiling make up the interior construction. The exterior wall is fabricated with RSI-3.0 pre-constructed panels. A series of overcast cold February days following a sinusoidal temperature profile peaking at 3:00 PM with a mean of -15°C and a ΔT of 10°C are assumed. There are no internal gains since the office is assumed to be unoccupied at all times. Full radiation exchange between the internal surfaces was considered.

Generally, during the evening, when offices are unoccupied, there is a setpoint setback where the setpoint temperature is lowered to preserve energy. The occupied setpoint is set to 21°C, and the unoccupied, 18°C. The following morning, before the occupants' arrival there is a start-up period where the temperature of the office is raised to a comfortable temperature. During this moment, the peak heating demand occurs. The size of the heater is set to 3000 W (100% efficiency) and uses a proportional control algorithm. The objective of the PCM-TES is to reduce this surge. The PCM-TES will be activated an hour before the start-up time in order to start preheating the office. Additionally, the heater output will be limited to reduce the peak demand.

The PCM-TES system is connected to the office, but it is outside the office boundaries. It consists of 2 systems in series each containing 12 panels with 6 equally distributed air channels. The total mass flow rate is set to 600 $kg \cdot h^{-1}$ with the convective heat transfer coefficient inside the channels set to 18 $W \cdot m^{-2} \cdot K^{-1}$. The PCM-TES is heated to 28°C. Charging of the system happens at a favourable time with no impact on the peak electrical demand of the building. During the morning start-up, room air is drawn into the PCM-TES, where it is heated, and discharged back into the room. Air stops being diverted into the PCM-TES when this system can no longer supply heat.

For the base scenario, heating is provided solely by the electric heater. The morning start-up time is set to 6:00 AM. The results are shown in Figure 5.8. The heating system peaks for 21 minutes. The total energy consumed by the auxiliary heater is reported on the figures.

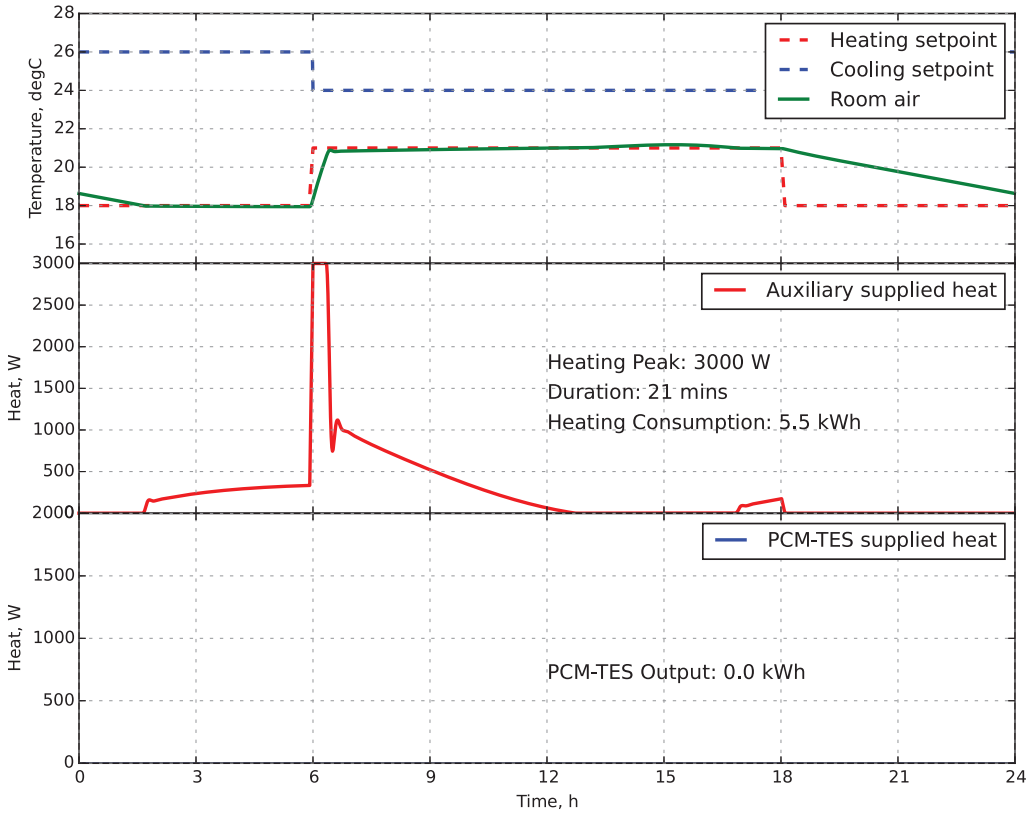

Figure 5.8: Base scenario without the PCM-TES system. (Top) Room temperature profile with the heating/cooling setpoints; (middle) auxiliary heating supplied to room air; and, (bottom) heating supplied by the PCM-TES system.

For the second scenario, the PCM-TES is activated an hour before the morning start-up time, namely, 5:00 AM. This allows the system to preheat the room air. The results are shown in Figure 5.9.

Here, the heating system peaks for 5 minutes: a 76% duration reduction. However, valuable cost savings are attributed only to peak demand reductions.

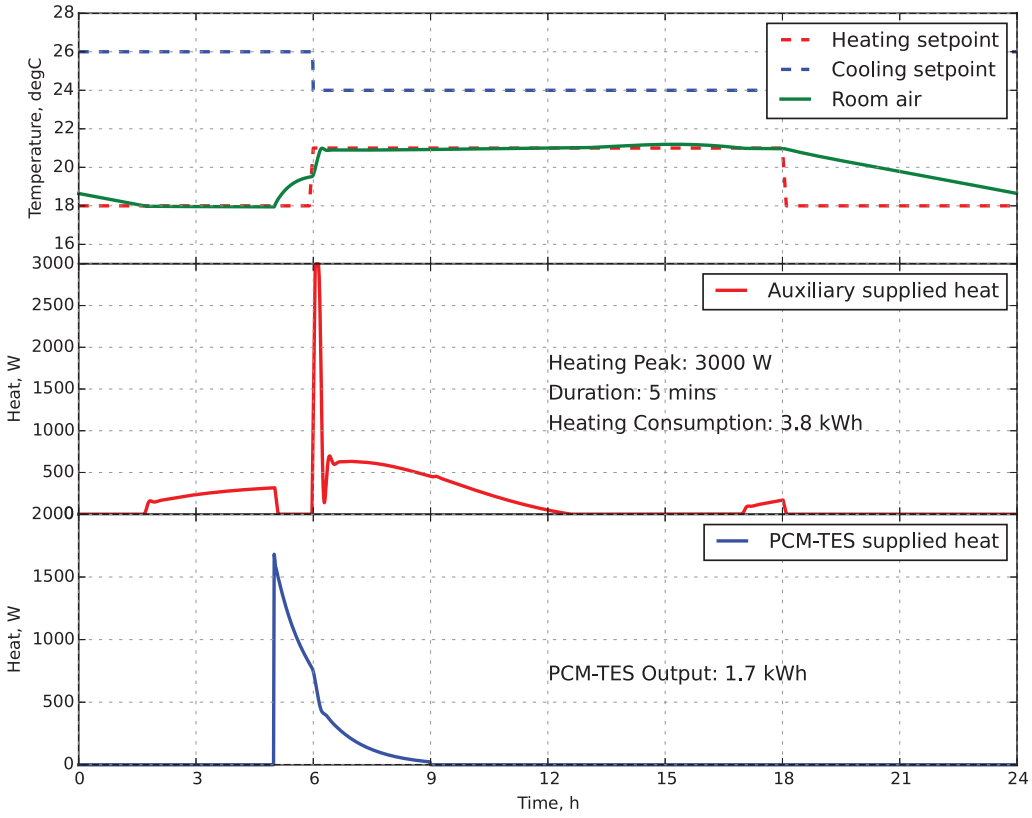

Figure 5.9: Scenario with an active PCM-TES system *on* at t=5h. (Top) Room temperature profile with the heating/cooling setpoints; (middle) auxiliary heating supplied to room air; and, (bottom) heating supplied by the PCM-TES system.

For the final scenario, the PCM-TES is activated an hour before the morning start-up and the heater output is limited to 50% of its capacity (1500 W). Results in Figure 5.10 show that the reduced capacity system is capable of timely heating the room air. The heating system peaks for 14 minutes, which is shorter than the non-PCM-TES scenario. Limiting the heater output to 33% of its capacity (1000 W) resulted in a 26 minute peak duration which is still acceptable. However, if the outside temperature was colder, a 1000 W system could be undersized.

Therefore, practically, a PCM-TES system is capable of reducing the peak electrical demand of this office by at least 50%. The reduction depends on the control algorithm used. An optimization-driven model-based control system will yield further improvements.

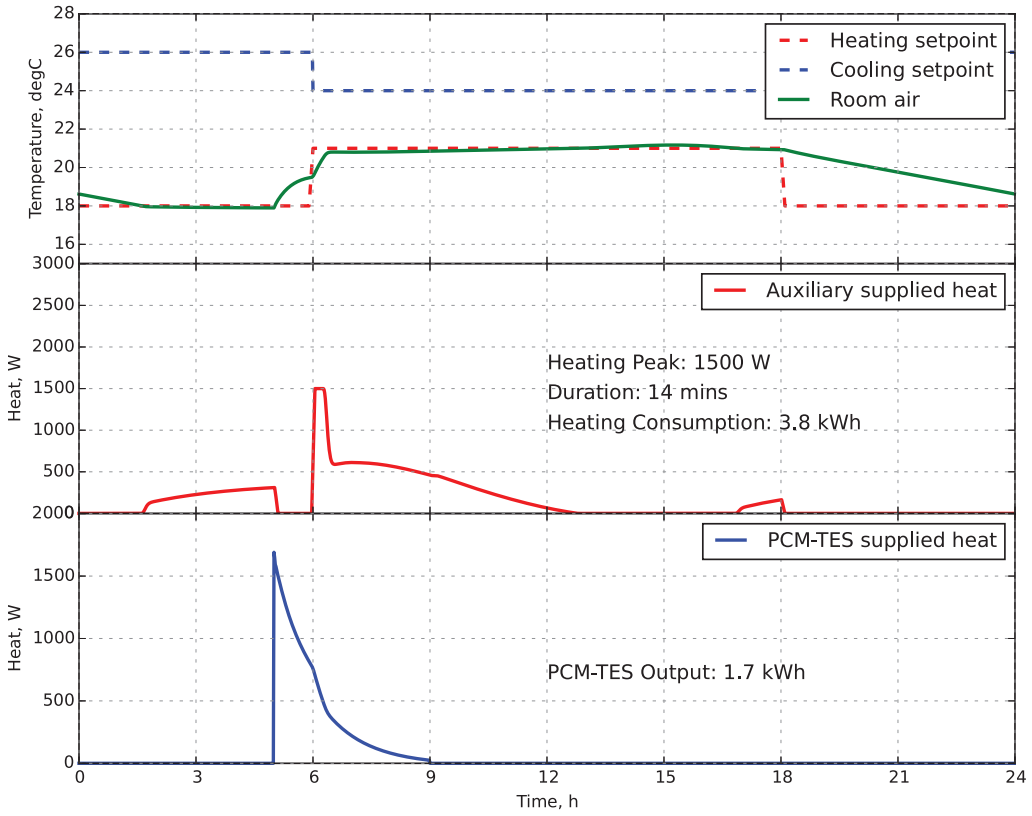

Figure 5.10: Scenario with an active PCM-TES system *on* at t=5h and a 50% limited heater. (Top) Room temperature profile with the heating/cooling setpoints; (middle) auxiliary heating supplied to room air; and, (bottom) heating supplied by the PCM-TES system.

By linking the design of the PCM-TES with the heating control sequence, it is possible to reduce the size of the specified heater during a new construction or limit the output of a heater in a retrofit project without compromising occupants' comfort. The reduction of the heater's size and the reduction of the peak electrical load will yield cost savings. Savings that can fund the purchase of the PCM-TES system. In a future study, the optimal start-up times for both PCM-TES and heater can be determined for an optimally configured PCM-TES system. The PCM-TES will be designed based on the room's operating sequence and conditions; where the operating sequence relies on the design of the PCM-TES. There is a strong link between design and operation, and both must be considered during the conception stage.

5.4 Summary

A detailed 30th order single-channel PCM-TES model was described and validated with experimental data. Simplified 2nd and 4th order models were developed and were used to assess the effect of model resolution on the thermal response accuracy. Here, the amount of energy stored in the TES and the outlet air temperature were of importance. The simplified models are able to accurately capture the dynamics of the PCM-TES and would be adequately used in a model-based control algorithm.

The models were extended to investigate the effect of increasing the number of channels (exposed surface area to the air stream) while keeping the total air mass flow rate and convective heat transfer coefficients constant. It was found that increasing the number of channels resulted in ever increasing peak power reduction, limited solely by the mechanical robustness of the panels themselves.

A simple case study demonstrated the peak load reduction potential of the multi-channel PCM-TES system. A 50% reduction was attainable compared to the base case.

Chapter 6

Conclusion

Reducing the peak energy demand in buildings minimizes the associated electricity costs and the environmental concerns of peaking power plants burning natural gas, diesel oil, or jet fuel. Traditional light commercial and residential buildings, typically wood-framed, do not possess significant thermal mass. In order to increase the thermal storage capacity, phase-change material (PCM)-based TES systems can be incorporated into buildings of any construction type. The use of PCMs has the ability to potentially decouple the concept of effective thermal mass from actual physical weight.

Active PCM-TES systems were evaluated based on experimental and numerical investigations. The PCM-TES is a system of PCM panels with a channel through which air is actively circulated along the face of the panels. This creates the possibility of a light weight building behaving like a traditional high mass building and thereby gaining the advantages commonly associated with traditional TES systems such as an ability to incorporate peak power reducing and shifting strategies without the significant weight of a tradition high mass building. For the PCM-TES to be effective (i.e. go through the phase-change in the desired time frame) advanced controls are necessary to integrate the system with the building HVAC system and to better utilize *free* sources of energy such as solar gains, internal gains and night-time free-cooling. Model-based control algorithms can effectively control the

PCM-TES for peak reducing and shifting strategies. However, the control implementation work is not part of this thesis.

A prototype PCM-TES integrated to a wall was built and tested in an environmental chamber. The experimental data was used for model validation. The models were developed using an implicit finite difference formulation with the PCM modelled using the heat capacity method. The heat capacity method consists of gradually modifying the effective specific heat of the latent material with respect to its temperature. Simplified equations are used to represent the characterization data. The model is shown to predict the dynamics of the system.

A simplified 2nd order non-linear model was able to capture the main dynamics of the detailed 30th order model satisfactorily and would be more conducive in an MPC strategy. Simplified practical models are easier to interpret, implement and calibrate since they contain fewer parameters to adjust. For an installed PCM-TES system, tuning of model parameter values can be achieved manually or automatically over time (realt time learning, online calibration) using measurements from the building automation system to compensate for installation, construction and system tolerances (e.g. as installed PCM properties, contact resistances, heat losses, fan losses, etc.). Having the structure of a physically-meaningful model set, the calibration process is not difficult.

The model was extended to investigate the effect of increasing the exposed surface area to the air stream (number of channels) while keeping the total air mass flow rate and convective heat transfer coefficients constant. For peak load reduction or shifting measures, the stored energy would best be discharged in a short period of time. Increasing the exposed area resulted in faster responding systems, limited solely by the mechanical robustness of the panels themselves. A case study was simulated to demonstrate the heating peak load reducing capabilities of the PCM-TES. A simplified 2nd order non-linear model was used to simulate the PCM-TES. Compared to the base scenario, the PCM-TES was shown to reduce the peak significantly for the simulated conditions.

However, sometimes a slower thermal response is required, such as when solar heat is used during the evening in a residential building and in this case, fewer air channels would suffice.

6.1 Contributions

In Section 5.1, the PCM-TES system was modelled in varying resolution. It was demonstrated that a simplified 2nd and 4th order model would satisfactorily capture the thermal dynamics of a PCM-TES system. The simplified model will be used in a model-based predictive control algorithm in a future work. The PCM-TES system in this study consists of 5 layers of shape-stabilized PCM with a single 30 mm air channel. The airflow path is 2 m in length and 2.4 m wide. The mass flow rate was set to 400 $kg \cdot h^{-1}$. The heating and cooling temperatures were 15 and 28 °C, respectively.

A prototype PCM-TES system integrated to a wall was designed, built, instrumented and tested in an environmental chamber. This design would serve as dispatchable storage. It can be installed near the thermal zone it serves augmenting the zone's thermal inertia and being able to reduce its peak energy demand.

An analysis was conducted on multi-channel PCM-TES systems in Section 5.2. It was shown that the number of air channels (exposed PCM surface area to the air stream) is inversely proportional to the thermal response time of the system. By having two systems in series, the initial temperature difference is comparable to having three; and is much greater than the single system. For peak energy reduction strategies, a large temperature difference is desirable. The fan energy requirement was minimal since the panel surface is flat and smooth.

Parametric equations for the specific heat and conductivity as a function of temperature was developed in Sections 4.2.1 & 4.2.2. The equations would be applicable to low sub-cooling PCM, such as organic PCM. The equations would offer a simplified method for characterization data entry and would reduce the simulation time.

6.2 Suggestions for Future Work

There are to this day many knowledge gaps in the field. There is a panoply of PCM materials and applications. There has been substantial research on the material science side of PCMs, but there is a need for systems-level research, especially since these materials are destined to be used in buildings.

Hysteresis modelling: the melting and freezing enthalpy curves generally do not coincide. As explained in Sections 2.4.3.1 & 4.2.3, for full heating/cooling cycles, the process is straightforward: take the melting enthalpy (or specific heat) curve for heating until the PCM is fully melted; then, take the freezing enthalpy curve for cooling until the PCM is fully frozen. When the process is interrupted, it is unclear on how one should proceed. In building applications, especially for passive applications, there is no guarantee that full melting or freezing can be completed every time. There will always be a situation of an interrupted process and in order to predict the behaviour of the system, a reliable hysteresis model is crucial.

With the development of ASTM C1784-13 "Standard Test method for Using a Heat Flow Meter Apparatus for Measuring Thermal Storage Properties of Phase Change Materials and Products", there is now a standard to characterize heterogeneous PCM in larger samples. Although this method is applicable for materials in building enclosures and components, it is unclear as to how a PCM would behave in direct solar radiation or exposed to other sources of intense heat flux.

Design-oriented characterization data: many manufacturer's produce PCM products. Typically, their catalogues only state the peak melting temperature and the latent heat of fusion. The materials are characterized using the DSC method at a high heating rate (around 2 °C·min^{-1}), which yields erroneous measurements. There is a lack of design-oriented characterization data. The PCMs will be used in building enclosures or in PCM-TES systems (or storage tanks). The characterization of its dynamic behaviour is required. Both melting and freezing enthalpy curves in accordance to ASTM C1784 is needed, along with the conductivity curve, material density, cost, dimensions, etc.

Benchmarks: many researchers have studied PCM. They have built their own models and they present their results in charts. For the outside reader, it is difficult to gauge the accuracy of the model. The raw data or the models are seldom available. To be able to compare various models, there needs to be a multitude of benchmarks, similar to the ANSI/ASHRAE Standard 140 "*Standard Method of Test for the Evaluation of Building Energy Analysis Computer Programs*". Various benchmarks should include one or many of the following: analytical solutions, hysteresis, sub-cooling, interrupted heating/cooling processes, sinusoidal heat flux profiles, multiple PCM layers with different properties, etc.

Availability of datalogs of installed systems: buildings utilizing PCM in their architecture and their mechanical system must be logging its performance. To better analyse the benefits of having PCM,

such data could be made publically available. The data will also serve as a case study or benchmark to test the building-level modelling procedure. The information given for installed systems is very limited offering no performance values or simply stating "the system performs as intended and reduces the energy consumption of the building" and nothing more.

Cost – quoting Arthur M. Wellington: "An engineer can do for a dollar what any fool can do for two." Without the price of PCM and its performance data, any PCM-related return on investment study will be incomplete. Generally, PCMs are quite expensive and the added costs cannot be justified given the benefits. Recently, BASF halted the production of its Micronal® microencapsulated PCM due to shunt adoption in the building industry due mostly to its high cost.

Research on low-grade PCMs originating from food industry wastes, such as saturated fatty acids, have a great potential for wide applications. If the cost can be low enough, a system can be designed to utilize its full potential. These PCM can be used in deployable shelters for rescue missions or military use. The material can also potentially be used in greenhouse/sunspace applications where the temperature is allowed to fluctuate in a larger range. Greenhouses can overheat when in full sun, even in winter when the outside temperature is extremely cold. The low-cost PCM can be used to store this excess heat and be used at night.

Photovoltaic (PV) panel pricing: with the recent trend in PV pricing, cooling load peaks can be offset with solar electricity production. For heat pumps or chillers with a coefficient of performance of 3, each kW of electricity will deliver 3 kW of cooling. It may be more cost-effective to cool the building directly than it is to store the excess heat in PCM and discharge it overnight.

Having modelled the behaviour of the PCM in interrupted processes, the MBC implementation can proceed. An HVAC controller has limited memory and storage. It is designed to be robust and to drive actuators/dampers. A controller is not intended to run complex simulation software; it was never its purpose. A regular computer on the other hand, can run all the optimization algorithms, but it can't control equipment. So, in an MPC setup, the computer (processor-based) can act as the "supervisor" while the controller is the "muscle". Simple routines (e.g. turn on the fan/heater, open the damper for free-cooling) can be programmed in the controller and the computer would decide when to run which. The algorithms running on the computer would be to minimize, for example, the peak energy demand of an office. As detailed in Section 2.6, the algorithm will look at the future load predictions and will

try to minimize the future energy requirements by pre charging the PCM-TES using either free sources (outdoor air, room air, server room air, etc.) or from the HVAC system. The algorithm uses the model of the system which also considers fan power, thermal losses, etc. in parallel with a model of the room being conditioned. This ensures a well coupled system.

References

Allard, A. (2013) *A Linear Data-Driven System Identification Methodology for an Active/Passive Solar Thermal Storage System and Application to a Solar House* (Master's thesis). Concordia University. Available at: http://spectrum.library.concordia.ca/977501/

Al-Saadi, S. N. and Zhai, Z. (2013) 'Modeling phase change materials embedded in building enclosure: A review', *Renewable and Sustainable Energy Reviews*. Elsevier, 21, pp. 659–673. doi: 10.1016/j.rser.2013.01.024.

Arteconi, A., Hewitt, N. J. and Polonara, F. (2012) 'State of the art of thermal storage for demand-side management', *Applied Energy*. Elsevier Ltd, 93, pp. 371–389. doi: 10.1016/j.apenergy.2011.12.045.

Arzamendia Lopez, J. P., Kuznik, F., Baillis, D. and Virgone, J. (2013) 'Numerical modeling and experimental validation of a PCM to air heat exchanger', *Energy and Buildings*. Elsevier B.V., 64, pp. 415–422. doi: 10.1016/j.enbuild.2013.04.017.

ASHRAE (2009) *ASHRAE Fundamentals 2009*, *Atlanta, GA: American Society of Heating, Refrigerating and Air-Conditioning Engineers*. Atlanta, GA: American Society of Heating, Refrigerating and Air-Conditioning Engineers.

ASTM C1784-14 (2014) 'Standard Test Method for Using a Heat Flow Meter Apparatus for Measuring Thermal Storage Properties of Phase Change Materials and Products.' West Conshohocken, PA: ASTM International. doi: 10.1520/C1784-14.

Athienitis, A. K. ., Stylianou, M. . and Shou, J. (1990) 'A methodology for building thermal dynamics studies and control applications', *ASHRAE Transactions (American Society of Heating, Refrigerating and Air-Conditioning Engineers)*, 96(2).

Athienitis, A. K., Liu, C., Hawes, D., Banu, D. and Feldman, D. (1997) 'Investigation of the thermal performance of a passive solar test-room with wall latent heat storage', *Building and Environment*, 32(5), pp. 405–410. doi: 10.1016/S0360-1323(97)00009-7.

Athienitis, A. K. and O'Brien, W. (eds) (2015) *Modeling, Design, and Optimization of Net-Zero Energy Buildings*. 1st edn. John Wiley & Sons. doi: 10.1002/9783433604625.

Athienitis, A. K., Sullivan, H. F. and Hollands, K. G. T. (1987) 'Discrete fourier series models for building auxiliary energy loads based on network formulation techniques', *Solar Energy*, 39(3), pp. 203–210. doi: 10.1016/S0038-092X(87)80029-4.

Barbour, J. P. and Hittle, D. C. (2006) 'Modeling Phase Change Materials With Conduction Transfer Functions for Passive Solar Applications', *Journal of Solar Energy Engineering*, 128(February), p. 58. doi: 10.1115/1.2000977.

Barnard, N. (2007) 'Hybrid Cooling Solutions: Night Cooling and Mechanical Refrigeration', *The Institute of Refrigeration*, pp. 1–8.

Barton, P., Beggs, C. B. and Sleigh, P. a. (2002) 'A theoretical study of the thermal performance of the TermoDeck hollow core slab system', *Applied Thermal Engineering*, 22, pp. 1485–1499. doi: 10.1016/S1359-4311(02)00059-5.

Bastani, A. (2014) *Developing a Framework to Design a Building Envelope Integrated with PCM* (Doctoral dissertation). Concordia University.

Bastani, A. and Haghighat, F. (2015) 'Expanding Heisler chart to characterize heat transfer phenomena in a building envelope integrated with phase change materials', *Energy and Buildings*. Elsevier B.V. doi: 10.1016/j.enbuild.2015.05.034.

Bastani, A., Haghighat, F. and Kozinski, J. (2014) 'Designing building envelope with PCM wallboards: Design tool development', *Renewable and Sustainable Energy Reviews*. Elsevier, 31(2014), pp. 554–562. doi: 10.1016/j.rser.2013.12.031.

Bejan, A. (1980) 'Second law analysis in heat transfer', *Energy*, 5, pp. 721–732.

BIPM (2008) *Evaluation of measurement data — Supplement 1 to the 'Guide to the expression of uncertainty in measurement' — Propagation of distributions using a Monte Carlo method*. Cedex, France.

Bony, J. and Citherlet, S. (2007) 'Numerical model and experimental validation of heat storage with phase change materials', *Energy and Buildings*, 39, pp. 1065–1072. doi: 10.1016/j.enbuild.2006.10.017.

Boyd, S. (2007) *EE364b Lecture 16: Model predictive control*, *Stanford University*. Available at: http://stanford.edu/class/ee364b/videos/video16.html.

Cabeza, L. F., Barreneche, C., Martorell, I., Miró, L., Sari-bey, S., Fois, M., Paksoy, H. O., Sahan, N., Weber, R., Constantinescu, M., Maria, E., Malikova, M., Krupa, I., Delgado, M., Dolado, P., Furmanski, P., Jaworski, M., Haussmann, T., Gschwander, S. and Fernández, A. I. (2014) 'Unconventional experimental technologies available for phase change materials characterization - Part 1 - Thermophysical properties', *Renewable and Sustainable Energy Reviews*. Elsevier, pp. 1–16. doi: 10.1016/j.rser.2014.07.191.

Candanedo, J. A., Allard, A. and Athienitis, A. K. (2011) 'Predictive Control of Radiant Floor Heating and Transmitted Irradiance in a Room with High Solar Gains.', *ASHRAE Transactions*, 117(2).

Candanedo, J. A., Dehkordi, V. R. and Stylianou, M. (2013) 'Model-based predictive control of an ice storage device in a building cooling system', *Applied Energy*. Elsevier Ltd, 111, pp. 1032–1045. doi: 10.1016/j.apenergy.2013.05.081.

Candanedo, L. M. I. (2010) *Modelling and evaluation of the performance of building-integrated open loop air-based photovoltaic thermal systems* (Doctoral dissertation). Concordia University. Available at: http://spectrum.library.concordia.ca/979429/

Çengel, Y. and Ghajar, A. (2010) *Heat and mass transfer: a practical approach*. 4th edn. London: McGraw-Hill Education.

Chandrasekharan, R., Lee, E. S., Fisher, D. E. and Deokar, P. S. (2013) 'An Enhanced Simulation Model for Building Envelopes with Phase Change Materials.', *ASHRAE Transactions*, 119(2).

Charvát, P., Klimeš, L. and Ostrý, M. (2014) 'Numerical and experimental investigation of a PCM-based thermal storage unit for solar air systems', *Energy and Buildings*, 68, pp. 488–497. doi: 10.1016/j.enbuild.2013.10.011.

Chen, Y., Athienitis, A. K. and Galal, K. E. (2014) 'A charging control strategy for active building-integrated thermal energy storage systems using frequency domain modeling', *Energy and Buildings*. Elsevier B.V., 84, pp. 651–661. doi: 10.1016/j.enbuild.2014.09.004.

Childs, K. and Stovall, T. (2012) 'Use of phase change material in a building wall assembly: a case study of technical potential in two climates', *2nd International High Performance Buildings Conference at Purdue*, p. 10.

Chwif, L., Paulo, S. and Paul, R. J. (2000) '2000: on Simulation Model Complexity', (Simon 1964), pp. 449–455.

CNW Telbec (2015) *Hydro-Québec | Use of Bécancour generating station during peak hours: Hydro-Québec Distribution reaches agreements with TranCanada and Gaz Métro*. Available at: http://www.newswire.ca/en/story/1533557/use-of-becancour-generating-station-during-peak-hours-hydro-quebec-distribution-reaches-agreements-with-trancanada-and-gaz-metro.

Coffey, B., Haghighat, F., Morofsky, E. and Kutrowski, E. (2010) 'A software framework for model predictive control with GenOpt', *Energy and Buildings*. Elsevier B.V., 42(7), pp. 1084–1092. doi: 10.1016/j.enbuild.2010.01.022.

Colebrook, C. F. and White, C. M. (1937) 'Experiments with Fluid Friction in Roughened Pipes', *Proceedings of the Royal Society A: Mathematical, Physical and Engineering Sciences*, 161(906), pp. 367–381. doi: 10.1098/rspa.1937.0150.

Concordia University (2011) *Concordia University launches the Solar Simulator-Environmental Chamber and NSERC Smart Net-Zero Energy Buildings Strategic Network*. Available at: http://www.concordia.ca/cunews/main/releases/2011/12/15/concordia-university-launches-the-solar-simulator-environmental-chamber-and-nserc-smart-net-zero-ene.html (Accessed: 1 April 2015).

Concordia University (2014) *Solar Buildings Research Network*. Available at: http://www.concordia.ca/encs/bcee/research/centres/solar-buildings-research-network.html (Accessed: 1 April 2015).

Cook, J. C. (2010) *Don't invert that matrix*, *Johndcook.com*. Available at: http://www.johndcook.com/blog/2010/01/19/dont-invert-that-matrix/ (Accessed: 31 July 2015).

Corgnati, S. P. and Kindinis, A. (2007) 'Thermal mass activation by hollow core slab coupled with night ventilation to reduce summer cooling loads', *Building and Environment*, 42, pp. 3285–3297. doi: 10.1016/j.buildenv.2006.08.018.

Delcroix, B., Kummert, M. and Daoud, A. (2015) 'Thermal behavior mapping of a phase change material between the heating and cooling enthalpy-temperature curves', in Centro Congressi Internazionale SRL (ed.) *6th International Building Physics Conference, IBPC 2015*. Elsevier Ltd.

Desgrosseilliers, L., Whitman, C. a., Groulx, D. and White, M. A. (2013) 'Dodecanoic acid as a promising phase-change material for thermal energy storage', *Applied Thermal Engineering*. Elsevier Ltd, 53(1), pp. 37–41. doi: 10.1016/j.applthermaleng.2012.12.031.

Dincer, I. (2002) 'On thermal energy storage systems and applications in buildings', *Energy and Buildings*, 34(September 2001), pp. 377–388. doi: 10.1016/S0378-7788(01)00126-8.

Dolado, P., Lazaro, A., Marin, J. M. and Zalba, B. (2011a) 'Characterization of melting and solidification in a real scale PCM-air heat exchanger: Experimental results and empirical model', *Renewable Energy*. Elsevier Ltd, 36(11), pp. 2906–2917. doi: 10.1016/j.renene.2011.04.008.

Dolado, P., Lazaro, A., Marin, J. M. and Zalba, B. (2011b) 'Characterization of melting and solidification in a real scale PCM-air heat exchanger: Numerical model and experimental validation', *Energy Conversion and Management*. Elsevier Ltd, 52(4), pp. 1890–1907. doi: 10.1016/j.enconman.2010.11.017.

Dolado, P., Lázaro, A., Marín, J. M. and Zalba, B. (2012) 'PCM-Air Heat Exchangers: Slab Geometry', *Heat exchangers - Basics Design Applications*.

DuPont (2011) *DuPont Energain - Energy-saving thermal mass systems - Product datasheet*. UK. Available at: http://energain.co.uk/Energain/en_GB/assets/downloads/documentation/download/Energain?_Datasheet_UK.pdf.

Egolf, P. W. and Manz, H. (1994) 'Theory and modeling of phase change materials with and without mushy regions', *International Journal of Heat and Mass Transfer*, 37(18), pp. 2917–2924. doi: 10.1016/0017-9310(94)90346-8.

El-Sawi, A. (2013) *Centralized Thermal Storage Systems Model for Buildings of the Future : Development and Validation School of Graduate Studies* (Doctoral dissertation). Concordia University.

El-Sawi, A., Haghighat, F. and Akbari, H. (2013) 'Centralized latent heat thermal energy storage system: Model development and validation', *Energy and Buildings*. Elsevier B.V., 65, pp. 260–271. doi: 10.1016/j.enbuild.2013.05.027.

Energy.Gov (2013) *Passive Solar Home Design*. Available at: http://energy.gov/energysaver/articles/passive-solar-home-design (Accessed: 1 April 2015).

Erickson, V. L., Carreira-Perpinan, M. a. and Cerpa, A. E. (2011) 'OBSERVE: Occupancy-based system for efficient reduction of HVAC energy', *Proceedings of the 10th ACM/IEEE International Conference on Information Processing in Sensor Networks*, pp. 258–269.

Gunay, H. B., Bursill, J., Huchuk, B., Brien, W. O. and Beausoleil-morrison, I. (2014) 'Shortest-prediction-horizon model-based predictive control for individual of fi ces', *Building and Environment*. Elsevier Ltd, 82, pp. 408–419. doi: 10.1016/j.buildenv.2014.09.011.

Günther, E., Hiebler, S., Mehling, H. and Redlich, R. (2009) 'Enthalpy of phase change materials as a function of temperature: Required accuracy and suitable measurement methods', *International Journal of Thermophysics*, 30, pp. 1257–1269. doi: 10.1007/s10765-009-0641-z.

Haghighat, F. (2013a) *Applying Energy Storage in Building of the Future: Best Practice for Architects and Engineers*. Montreal, Canada. Available at: www.iea-eces.org/files/a4.2.2_best_practices_annex23.pdf. doi: 10.13140/RG.2.1.4477.3282.

Haghighat, F. (2013b) *Applying Energy Storage in Ultra-Low Energy Buildings: Final Report*. Montreal, Canada. doi: 10.13140/RG.2.1.4995.4727.

Hawes, D. W. (1991) *Latent Heat Storage in Concrete* (Doctoral dissertation). Concordia University.

Henze, G. P., Felsmann, C., Kalz, D. E. and Herkel, S. (2008) 'Primary energy and comfort performance of ventilation assisted thermo-active building systems in continental climates', *Energy and Buildings*, 40, pp. 99–111. doi: 10.1016/j.enbuild.2007.01.014.

Henze, G. P., Florita, A. R., Brandemuehl, M. J., Felsmann, C. and Cheng, H. (2010) 'Advances in Near-Optimal Control of Passive Building Thermal Storage', *Journal of Solar Energy Engineering*, 132(2), p. 021009. doi: 10.1115/1.4001466.

Hovgard, T. G., Larsen, L. F. S., Jørgensen, J. B. and Boyd, S. (2012) 'Fast nonconvex model predictive control for commercial refrigeration', *IFAC Proceedings Volumes (IFAC-PapersOnline)*, 4(PART 1), pp. 514–521. doi: 10.3182/20120823-5-NL-3013.00082.

Hydro-Québec (2014) 'Annual Report 2014', pp. 1–28. doi: 10.1016/j.parkreldis.2015.02.017.

IBPSA US (2015) *Model Validation Measures - Bembook*. Available at: http://www.bembook.ibpsa.us/index.php?title=Model_Validation_Measures.

Kenisarin, M. and Mahkamov, K. (2007) 'Solar energy storage using phase change materials', *Renewable and Sustainable Energy Reviews*, 11, pp. 1913–1965. doi: 10.1016/j.rser.2006.05.005.

Koschenz, M. and Lehmann, B. (2004) 'Development of a thermally activated ceiling panel with PCM for application in lightweight and retrofitted buildings', *Energy and Buildings*, 36, pp. 567–578. doi: 10.1016/j.enbuild.2004.01.029.

Kośny, J. (2015) *PCM-Enhanced Building Components: An Application of Phase Change Materials in Building Envelopes and Internal Structures*. Springer International Publishing (Engineering Materials and Processes). doi: 10.1007/978-3-319-14286-9.

Krane, R. J. (1987) 'A Second Law analysis of the optimum design and operation of thermal energy storage systems', *International Journal of Heat and Mass Transfer*, 30(1), pp. 43–57. doi: 10.1016/0017-9310(87)90059-7.

Kuznik, F., David, D., Johannes, K. and Roux, J. J. (2011) 'A review on phase change materials integrated in building walls', *Renewable and Sustainable Energy Reviews*, 15, pp. 379–391. doi: 10.1016/j.rser.2010.08.019.

Kuznik, F. and Virgone, J. (2008) 'Experimental investigation of wallboard containing phase change material: Data for validation of numerical modeling', *Energy and Buildings*, 41, pp. 561–570. doi: 10.1016/j.enbuild.2008.11.022.

Kuznik, F. and Virgone, J. (2009) 'Experimental assessment of a phase change material for wall building use', *Applied Energy*. Elsevier Ltd, 86(10), pp. 2038–2046. doi: 10.1016/j.apenergy.2009.01.004.

Kuznik, F., Virgone, J. and Johannes, K. (2011) 'In-situ study of thermal comfort enhancement in a renovated building equipped with phase change material wallboard', *Renewable Energy*. Elsevier Ltd, 36(5), pp. 1458–1462. doi: 10.1016/j.renene.2010.11.008.

Kuznik, F., Virgone, J. and Noel, J. (2008) 'Optimization of a phase change material wallboard for building use', *Applied Thermal Engineering*, 28, pp. 1291–1298. doi: 10.1016/j.applthermaleng.2007.10.012.

LBNL (2011) *GenOpt: Generic Optimization Program*. Available at: http://simulationresearch.lbl.gov/GO/.

Lee, J. H. (2011) 'Model predictive control: Review of the three decades of development', *International Journal of Control, Automation and Systems*, 9(3), pp. 415–424. doi: 10.1007/s12555-011-0300-6.

Lehmann, B., Gyalistras, D., Gwerder, M., Wirth, K. and Carl, S. (2013) 'Intermediate complexity model for Model Predictive Control of Integrated Room Automation', *Energy & Buildings*. Elsevier B.V., 58, pp. 250–262. doi: 10.1016/j.enbuild.2012.12.007.

Ljung, L. (1999) *System identification: theory for the user*. 2nd edn. Upper Saddle River, NJ: Prentice Hall PTR.

Ma, J., Qin, J., Salsbury, T. and Xu, P. (2012) 'Demand reduction in building energy systems based on economic model predictive control', *Chemical Engineering Science*. Elsevier, 67(1), pp. 92–100. doi: 10.1016/j.ces.2011.07.052.

Manz, H., Egolf, P. W., Suter, P. and Geotzberger, A. (1997) 'TIM-PCM External Wall System for Solar Space Heating', 61(6), pp. 369–379.

Martinelli, R. C. (1947) 'Heat transfer to molten metals', *Trans. ASME*, 69(8), pp. 947–959.

May-Ostendorp, P., Henze, G. P., Corbin, C. D., Rajagopalan, B. and Felsmann, C. (2011) 'Model-predictive control of mixed-mode buildings with rule extraction', *Building and Environment*. Elsevier Ltd, 46(2), pp. 428–437. doi: 10.1016/j.buildenv.2010.08.004.

Morse, E. S. (1881) *Warming and Ventilating Apartments by the Sun's Rays,* US Patent 246626 A. Available at: http://www.google.ca/patents/US246626

NRCan-OEE (2013) 'Energy Use Data Handbook Tables - 1990 to 2010.' Available at: oee.nrcan.gc.ca/publications/statistics/handbook2010/handbook2013.pdf

Oldewurtel, F., Parisio, A., Jones, C. N., Gyalistras, D., Gwerder, M., Stauch, V., Lehmann, B. and Morari, M. (2012) 'Use of model predictive control and weather forecasts for energy efficient building climate control', *Energy and Buildings*. Elsevier B.V., 45, pp. 15–27. doi: 10.1016/j.enbuild.2011.09.022.

Pedersen, C. O. (1972) 'Enthalpy formulation of conduction heat transfer problems involving latent heat', *Simulation*, 18, pp. 57–59. doi: 10.1177/003754977201800205.

Qin, S. J. and Badgwell, T. a. (2003) 'A survey of industrial model predictive control technology', *Control Engineering Practice*, 11(7), pp. 733–764. doi: 10.1016/S0967-0661(02)00186-7.

Schröder, J. and Gawron, K. (1981) 'Latent heat storage', *International Journal of Energy Research*. Wiley Online Library, 5(2), pp. 103–109.

Straube, J. (2006) *Building Science Digests: BSD-007: Historical Development of the Building Enclosure*, *Buildingscience.com*. Available at: http://www.buildingscience.com/documents/digests/bsd-007-historical-development-of-the-building-enclosure?topic=doctypes/digests.

Streicher, W. (2008) 'Final report of Subtask C " Phase Change Materials " The overview Final report of Subtask C'.

Tabares-Velasco, P. C., Christensen, C. and Bianchi, M. (2012) 'Verification and validation of EnergyPlus phase change material model for opaque wall assemblies', *Building and Environment*. Elsevier Ltd, 54, pp. 186–196. doi: 10.1016/j.buildenv.2012.02.019.

Termodeck (2007) *Thermodeck Reference Projects*. Available at: http://www.termodeck.com/ref.html (Accessed: 1 April 2015).

Trombe, F., Robert, J. F., Cabanot, M. and Sesolis, B. (1977) 'Concrete walls to collect and hold heat', *Solar Age*, 2(8), pp. 13–19.

US DOE (2014) 'EnergyPlus Engineering Reference', *The Reference to EnergyPlus Calculations*.

US National Park Service (2015) *Mesa Verde National Park (U.S. National Park Service)*. Available at: http://www.nps.gov/meve/index.htm (Accessed: 1 April 2015).

Winwood, R., Benstead, R. and Edwards, R. (1997) 'Advanced fabric energy storage I: Review', *Building Services Engineering Research and Technology*, 18, pp. 1–6. doi: 10.1177/014362449701800101.

Zalba, B., Marín, J. M., Cabeza, L. F. and Mehling, H. (2003) 'Review on thermal energy storage with phase change: materials, heat transfer analysis and applications', *Applied Thermal Engineering*, 23, pp. 251–283. doi: 10.1016/S1359-4311(02)00192-8.

Zhou, G., Zhang, Y., Lin, K. and Xiao, W. (2008) 'Thermal analysis of a direct-gain room with shape-stabilized PCM plates', *Renewable Energy*, 33, pp. 1228–1236. doi: 10.1016/j.renene.2007.06.024.

Zmeureanu, R. and Fazio, P. (1988) 'Thermal performance of a hollow core concrete floor system for passive cooling', *Building and Environment*. Elsevier, 23(3), pp. 243–252.

Appendices

A.1 Finite Difference Method Formulation

The following section expands Fourier's Law into the finite difference method. The formulation is reinterpreted from Koschenz and Lehmann (2004).

Starting from Fourier's Law for multi-dimensional heat transfer:

$$\rho \frac{\partial h}{\partial t} + \nabla(-k(T)\nabla T) = 0 \tag{8.1}$$

Simplified to a 1-dimensional system in the *x* direction,

$$\rho \frac{\partial h}{\partial t} + \frac{\partial}{\partial x}(-k(T)\nabla T) = 0 \tag{8.2}$$

The density of the material is assumed to be constant. By performing the inner derivative and applying the product law of calculus, we obtain:

$$\rho \frac{dh}{dT}\frac{\partial T}{\partial t} - k(T)\frac{\partial^2 T}{\partial x^2} - \frac{dk}{dT}\left(\frac{\partial T}{\partial x}\right)^2 = 0 \tag{8.3}$$

The specific heat, C_p, is defined as:

$$C_p(T) \equiv \frac{dh}{dT} \tag{8.4}$$

Rearranging equation (8.3),

$$\frac{\partial T}{\partial t} = \frac{k(T)}{\rho \cdot C_p(T)}\left[\frac{\partial^2 T}{\partial x^2} + \frac{1}{k(T)}\frac{dk}{dT}\left(\frac{\partial T}{\partial x}\right)^2\right] \tag{8.5}$$

If the conductivity is constant, or if the conductivity only changes discreetly per timestep, then equation (8.5) becomes:

$$\frac{\partial T}{\partial t} = \frac{k}{\rho \cdot C_p(T)} \frac{\partial^2 T}{\partial x^2} \tag{8.6}$$

Since the above equation can only be solved analytically for certain cases, a finite difference approximation of the partial differential equation is necessary. Writing the 1st order forward difference equation for the left hand side:

$$\left(\frac{\partial T}{\partial t}\right)_i^t = \frac{T_i^{t+1} - T_i^t}{\Delta t} + O(\Delta t) \tag{8.7}$$

Now, the central difference equation for the right hand side 2nd order differential equation:

$$\left(\frac{\partial^2 T}{\partial x^2}\right)_i^{t+\theta} = \frac{T_{i+1}^{t+\theta} - 2T_i^{t+\theta} + T_{i-1}^{t+\theta}}{\Delta x^2} + O(\Delta x)^2 \tag{8.8}$$

The value of θ is between 0 and 1, typically θ is chosen from the following: {0, ½, 1}, which yield, respectively, the explicit, Crank-Nicholson and implicit schemes. In the explicit case, the future timestep is computed node by node. The last two yield a system of equations which must be solved simultaneously.

Inputting equations (8.7) and (8.8) into (8.6), and rearranging for the future timestep:

$$T_i^{t+1} = T_i^t + \frac{k \cdot \Delta t}{\rho \cdot C_p(T) \cdot \Delta x^2} \left[(1-\theta)\left(T_{i+1}^t - 2T_i^t + T_{i-1}^t\right) + \theta\left(T_{i+1}^{t+1} - 2T_i^{t+1} + T_{i-1}^{t+1}\right)\right] \tag{8.9}$$

Now, let's look at a case where the neighbouring nodes have a fixed boundary temperature, T_{bound}. And assume the initial temperature at the active node is T_{init} and is at a lower temperature than the neighbouring nodes. For the future timestep, physically, the temperature at the active node cannot exceed the boundary temperature since there is no internal heat generation.

$$T_{init} < T_{bound} \tag{8.10}$$

$$T_{i-1}^{t} = T_{i+1}^{t} = T_{i-1}^{t+1} = T_{i+1}^{t+1} = T_{bound} \tag{8.11}$$

$$T_{i}^{t} = T_{init} \tag{8.12}$$

$$T_{i}^{t+1} \leq T_{bound} \tag{8.13}$$

And since,

$$\frac{k \cdot \Delta t}{\rho \cdot C_p(T) \cdot \Delta x^2} = \frac{T_i^{t+1} - T_i^t}{(1-\theta)\left(T_{i+1}^t - 2T_i^t + T_{i-1}^t\right) + \theta\left(T_{i+1}^{t+1} - 2T_i^{t+1} + T_{i-1}^{t+1}\right)} \tag{8.14}$$

$$\therefore \quad \frac{k \cdot \Delta t}{\rho \cdot C_p(T) \cdot \Delta x^2} \leq \frac{1}{2(1-\theta)} \tag{8.15}$$

To assure numerical stability in the solution, the timestep must be chosen according to equation (8.15).

For the implicit case {θ = 0}:

$$\frac{k \cdot \Delta t}{\rho \cdot C_p(T) \cdot \Delta x^2} \leq \frac{1}{2} \tag{8.16}$$

$$\therefore \quad \Delta t \leq \frac{\rho \cdot C_p(T) \cdot \Delta x^2}{2k} \tag{8.17}$$

For the Crank-Nicholson case {θ = ½}:

$$\frac{k \cdot \Delta t}{\rho \cdot C_p(T) \cdot \Delta x^2} \leq 1 \tag{8.18}$$

$$\therefore \quad \Delta t \leq \frac{\rho \cdot C_p(T) \cdot \Delta x^2}{k} \tag{8.19}$$

Finally, for the implicit case {θ = 1}:

$$\frac{k \cdot \Delta t}{\rho \cdot C_p(T) \cdot \Delta x^2} \leq 0 \tag{8.20}$$

$$\therefore \quad \Delta t \leq \infty \tag{8.21}$$

These time steps assure numerical stability. For the implicit case, there is no restriction on the timestep, however, for very large time steps, the solution may oscillate. Although the oscillations will eventually dampen, large time steps do not guarantee physically plausible solutions.

A.2 Model Validation Metrics

The normalized mean bias error (NMBE) and the coefficient of variance of the root mean square error (CV(RMSE)) are defined as (IBPSA US, 2015):

$$NMBE = \frac{\sum_{i=1}^{n} (y_{simulated,i} - y_{measured,i})}{\bar{y}_{measured} \cdot (n-1)} \tag{8.22}$$

$$CV(RMSE) = \frac{1}{\bar{y}_{measured}} \cdot \sqrt{\frac{\sum_{i=1}^{n} \left[(y_{simulated,i} - y_{measured,i})^2 \right]}{n-2}} \tag{8.23}$$

where

y, variable of interest;

$\bar{y}$, average value of y; and,

n, number of data points.

A.3 Code: Energy Balance Uncertainty Analysis

This script is used to calculate the uncertainty (standard deviation) in the energy balance of the air stream. It is based on a Monte Carlo method where the error in measurements follow a normal (Gaussian) distribution. "N·M" simulations were carried out; so for here, the total is 1 million per process.

uncertainty_analysis.m

```
%% Uncertainty analysis in the Energy Balance (Air Stream) using Monte-Carlo
% Based on JCGM 101:2008 Evaluation of measurement data – Supplement 1 to the "Guide to the
expression of uncertainty in measurement" – Propagation of distributions using a Monte Carlo
method

%% Clean start
close all
clear

%% Dependencies
addpath('Data');

%% Load data
load('0320RTR.mat')
T_in  = T_exp.AirIn;    % degC
T_out = T_exp.AirOut;   % degC
clear T_exp

% Heating (Charge) process
T_in  = T_in(1:925);
T_out = T_out(1:925);
% Cooling (Discharge) process
%T_in  = T_in(926:end);
%T_out  = T_out(926:end);

%% Input Arguments
m  = 400/3600;          % kg/s
dt = 60;                % s
Cp = 1.006;             % kJ/kgK
nt = size(T_in,1);      % number of timesteps, experimental data

U_m = 0.02*m;           % +/- kg/s uncertainty of mass flow measurements
U_RTD = 0.06;           % +/- degC uncertainty of RTD measurements

N = 1e5;                % number of runs
M = 10;                 % number of sets of runs

%% Calculate Energy Balance
rng shuffle;            % randomize the seeds

E = zeros(N,1);
for j=1:M;
    for i = 1:N
        % Q = m * Cp * (T_out - T_in)   % per time step (from t = 1 to t = nt)
```

```
        Q = normrnd(m,U_m/1.96) * Cp * (normrnd(T_out,U_RTD/1.96) - ...
            normrnd(T_in,U_RTD/1.96));
        E(i) = sum(Q)*dt;   % Total Energy transfered at end of process, kJ
    end
    clear i

    %% Standard Deviation
    mean_E = mean(E);
    std_E = std(E);
    U_E = 1.96*std_E;   % uncertainty in energy balance @ 95% CI, kJ

    if (M > 1); fprintf('%d: ', j); end;
    fprintf('U_E by Monte-Carlo (N = %d): Mean: %.2f, 1.96*std %.2f\n', N, mean_E, ...
             1.96*std_E);
end
clear j
```

A.4 Code: Single-Channel PCM-TES

The finite difference models were implemented in MATLAB.

A.4.1 Experimental Data Visualization

This script is used to read the experimental data and to prepare certain charts. Not all the charts are presented in this thesis. The following chart plots a histogram of the differences between model and measurement. It was used as a check to determine the models' fit.

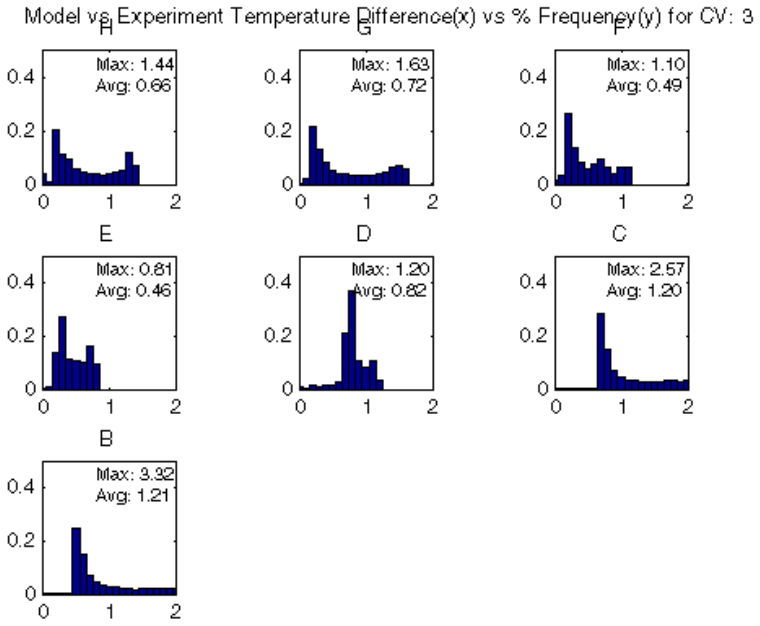

Figure A 1: Temperature difference histogram between model v. experiment for section 3 of the 30th order PCM-TES model.

Plot_ExpData_20150320.m

```
%% Plot Experimental Data, Charging/discharging of PCM with different flow
%-----------------------------------------------
%   Vasken Dermardiros
%   v001:  June 2014
%-----------------------------------------------

%% Dependencies
addpath('Aux Functions');
```

```
%% Get *.txt File and Location
[txtFilename,txtPath] = uigetfile({'*.txt'},'Select the data file');
if txtFilename == 0
    clear txtFilename txtPath
    return
end

%% Parse File
D = dataset('File',txtFilename);
clearvars txtFilename txtPath

%% Plot
pltD = [D.x4eA D.x4eB D.x4eC D.x4eD D.x4eE D.x4eF D.x4eG D.x4eH ...
        D.x4bA D.x4bB D.x4bC D.x4bD D.x4bE D.x4bF D.x4bG D.x4bH ...
        D.x2eA D.x2eB D.x2eC D.x2eD D.x2eE D.x2eF D.x2eG D.x2eH ...
        D.x2bA D.x2bB D.x2bC D.x2bD D.x2bE D.x2bF D.x2bG D.x2bH ]';

pltAvg =[   mean([  D.x4eA  D.x4bA  D.x2eA  D.x2bA  ],2) ...
            mean([  D.x4eB  D.x4bB  D.x2eB  D.x2bB  ],2) ...
            mean([  D.x4eC  D.x4bC  D.x2eC  D.x2bC  ],2) ...
            mean([  D.x4eD  D.x4bD  D.x2eD  D.x2bD  ],2) ...
            mean([  D.x4eE  D.x4bE  D.x2eE  D.x2bE  ],2) ...
            mean([  D.x4eF  D.x4bF  D.x2eF  D.x2bF  ],2) ...
            mean([  D.x4eG  D.x4bG  D.x2eG  D.x2bG  ],2) ...
            mean([  D.x4eH  D.x4bH  D.x2eH  D.x2bH  ],2)]';

pltDA= [D.x4eA D.x4bA D.x2eA D.x2bA]';

pltAir = [D.RTD_in D.RTD_out]';

pltSubCool = [  D.x4eB D.x4bB D.x2aB D.x2bB D.x2eB D.x2fB]';

pltdT = [D.TPR D.TPL]'/3;
pltExtra = [D.x1 D.x3 D.x4 D.x6 D.FANOR D.FANOL D.x2fC D.x2fD D.x2fE]';
pltExtraLabel = {'x1', 'x3', 'x4', 'x6', 'Fanor', 'Fanol', '2fc', '2fD', '2fE'};

pltHeight = [D.RTD_in D.x1 D.x2aD D.x2bD D.x2cD D.x2 D.x2dD D.x2eD D.x2fD D.x3 D.RTD_out]';
pltHeightLabel = {'RTD in','x1','2aD','2bD','2cD','x2','2dD','2eD','2fD','x3','RTD out'};

pltYLabel = {'4eA' '4eB' '4eC' '4eD' '4eE' '4eF' '4eG' '4eH' ...
             '4bA' '4bB' '4bC' '4bD' '4bE' '4bF' '4bG' '4bH' ...
             '2eA' '2eB' '2eC' '2eD' '2eE' '2eF' '2eG' '2eH' ...
             '2bA' '2bB' '2bC' '2bD' '2bE' '2bF' '2bG' '2bH'};

plt3DR =[D.x2fH D.x2fG  D.x2fF  D.x2fE  D.x2fD  D.x2fC  D.x2fB  D.x2fA  ...
        D.x2eH  D.x2eG  D.x2eF  D.x2eE  D.x2eD  D.x2eC  D.x2eB  D.x2eA  ...
        D.x2dH  D.x2dG  D.x2dF  D.x2dE  D.x2dD  D.x2dC  D.x2dB  D.x2dA  ...
        D.x2cH  D.x2cG  D.x2cF  D.x2cE  D.x2cD  D.x2cC  D.x2cB  D.x2cA  ...
        D.x2bH  D.x2bG  D.x2bF  D.x2bE  D.x2bD  D.x2bC  D.x2bB  D.x2bA  ...
        D.x2aH  D.x2aG  D.x2aF  D.x2aE  D.x2aD  D.x2aC  D.x2aB  D.x2aA  ];

plt3DM = reshape(plt3DR',[8 6 length(plt3DR)]);
plt3D = permute(plt3DM, [2 1 3]);
clear plt3DR plt3DM

%%
charge_beg = [1817 13383 16166 20205];   % Each data value was taken at a 1 min interval!
charge_end = [2750 14480 17285 21311];
discharge_beg = [2755 11592 14488 17292]; % 3rd time at 500 kg/h; 4th time at 300 kg/h
discharge_end = [4040 13370 16000 18950];
charge_n = charge_end - charge_beg;
```

```
discharge_n = discharge_end - discharge_beg;
charge_t = (1*charge_n)/60;
discharge_t = (1*discharge_n)/60;

%% Lineplot; Charge average, layer A; Final Version
yLabelN = {'400 kg/h' '400 kg/h' '500 kg/h', '300 kg/h'};
for p = 1:4
    subplot(4,1,p);
    plot(pltAvg(:,charge_beg(p):charge_end(p))');
    hLegend(p) = legend('A','B','C','D','E','F','G','H');
%     plot(pltD([1 9 17 25],charge_beg(p):charge_end(p))');
%     hLegend(p) = legend('4eA','4bA','2eA','2bA');

    set(gca, ...
        'Box'         , 'off'     , ...
        'TickDir'     , 'out'     , ...
        'TickLength'  , [.02 .02] , ...
        'YMinorTick'  , 'on'      , ...
        'XColor'      , [.2 .2 .2], ...
        'YColor'      , [.2 .2 .2]);
    set(gca,'XTick',0:240:3300,...
            'XMinorTick', 'on');
    set(gca,'XTickLabel','');

    grid on
    xlim([1 16*60])
    hYLabel(p) = ylabel(yLabelN(p));
    ylim([15 27])

    if p == 1
        hTitle = title('Heating Line Plot: Layer Average');
    end
    if p == 4
        hXLabel = xlabel('Time, h');
        set(gca,'XTickLabel',0:4:55);
    end
    set(gca,'FontSize'    , 8           );
end
clear p

%% Lineplot; Discharge average, layer A; Final Version
yLabelN = {'400 kg/h' '400 kg/h' '500 kg/h' '300 kg/h'};
for p = 1:4
    subplot(4,1,p);
    plot(pltAvg(:,discharge_beg(p):discharge_end(p))');
    hLegend(p) = legend('A','B','C','D','E','F','G','H');
%     plot(pltD([1 9 17 25],discharge_beg(p):discharge_end(p))');
%     hLegend(p) = legend('4eA','4bA','2eA','2bA');

    set(gca, ...
        'Box'         , 'off'     , ...
        'TickDir'     , 'out'     , ...
        'TickLength'  , [.02 .02] , ...
        'YMinorTick'  , 'on'      , ...
        'XColor'      , [.2 .2 .2], ...
        'YColor'      , [.2 .2 .2]);
    set(gca,'XTick',0:240:3300,...
            'XMinorTick', 'on');
    set(gca,'XTickLabel','');

    grid on
```

```
    xlim([1 20*60])
    hYLabel(p) = ylabel(yLabelN(p));
    ylim([13 27])

    if p == 1
        hTitle = title('Cooling Line Plot: Layer Average');
    end
    if p == 4
        hXLabel = xlabel('Time, h');
        set(gca,'XTickLabel',0:4:55);
    end
    set(gca,'FontSize'   , 8           );
end
clear p

%% Colour Map vs Time; Charging at 2.0 m/s
pltEvolvCharge2ms = figure;
run = 2;

steps = 12;
start = charge_beg(run);
finish = charge_end(run);
stepsize = 60;%floor((finish-start)/(steps-1));

for n = 0:(steps-1)
    subplot(2,6,n+1);
    colormap(jet(256));
    if n == (steps-1)
        imagesc(plt3D(:,:,finish));
        %xlabel(sprintf('t = %.2f', (finish-start)*3/60));
        hXLabel(n+1) = xlabel(sprintf('t = %.2f', (finish-start)/60));
    else
        imagesc(plt3D(:,:,n*stepsize+start));
        %xlabel(sprintf('t = %.2f', n*stepsize*3/60));
        hXLabel(n+1) = xlabel(sprintf('t = %.2f', n*stepsize/60));
    end
    vline([4.5 5.5]);
    set(gca,'YTick',(1:size(plt3D,1)));
    set(gca,'YTickLabel',{'2f','2e','2d','2c','2b','2a'});
    set(gca,'XTick',(1:size(plt3D,2)));
    set(gca,'XTickLabel',{'H','G','F','E','D','C','B','A'});
    caxis([13, 28])
    axis square

end
clear n steps start finish stepsize

%% Colour Map vs Time; Discharging at 2.0 m/s
pltEvolvDischarge2ms = figure;
run = 2;
%plt3D = discharge;

steps = 12;
start = discharge_beg(run);
finish = discharge_end(run);
stepsize = 120;%floor((finish-start)/(steps-1));

for n = 0:(steps-1)
    subplot(2,6,n+1);
    colormap(jet(256));
    if n == (steps-1)
```

```
        imagesc(plt3D(:,:,finish));
        %xlabel(sprintf('t = %.2f', (finish-start)*3/60));
        hXLabel(n+1) = xlabel(sprintf('t = %.2f', (finish-start)/60));
    else
        imagesc(plt3D(:,:,n*stepsize+start));
        %xlabel(sprintf('t = %.2f', n*stepsize*3/60));
        hXLabel(n+1) = xlabel(sprintf('t = %.2f', n*stepsize/60));
    end
    vline([4.5 5.5]);
    set(gca,'YTick',(1:size(plt3D,1)));
    set(gca,'YTickLabel',{'2f','2e','2d','2c','2b','2a'});
    set(gca,'XTick',(1:size(plt3D,2)));
    set(gca,'XTickLabel',{'H','G','F','E','D','C','B','A'});
    caxis([13, 24])
    axis square

end
clear n steps start finish stepsize

%% Profile plot air channel
pltProfileAir = figure;
% pltHeight = [D.x1 D.x2aD D.x2bD D.x2cD D.x2 D.x2dD D.x2eD D.x2fD D.x3]';
% pltHeightLabel = {'x1','2aD','2bD','2cD','x2','2dD','2eD','2fD','x3'};

% start = charge_beg(1);
% finish = charge_end(1);
start = discharge_beg(3);
finish = discharge_end(3);

% start = 1;
% finish = 1120;
% start = 1148;
% finish = length(pltHeight);
% stepsize = floor((finish-start)/(steps-1));
stepsize = 60;
steps = floor((finish-start)/stepsize) - 1;

plotData = pltHeight(:,[start:stepsize:(finish-stepsize) finish]);
hold all
for n = 0:(steps-1)
    if n == (steps-1)
        plot(plotData(:,end));
    else
        plot(plotData(:,n+1))
    end
end
N = [(0:(steps-2))*stepsize (finish-start)]/60;
plotLegend = cellstr(num2str(N', 't = %-.2f'));
legend(plotLegend,'Location','EastOutside');
set(gca,'XTick',1:length(pltHeightLabel));
set(gca,'XTickLabel',pltHeightLabel);
ylabel('Temperature, degC');

%clear n N steps start finish stepsize plotData plotLegend
title('Temperature Profile at air node')
```

Symmetry_Assumption_Run17.m

```
%% Symmetry assumption verification
%------------------------------------------------
%   Vasken Dermardiros
%   v001:  July 2014
%------------------------------------------------

%% Dependencies
addpath('Aux Functions');

%% Get *.txt File and Location
[txtFilename,txtPath] = uigetfile({'*.txt'},'Select the data file');
if txtFilename == 0
    clear txtFilename txtPath
    return
end

%% Parse File
D = tdfread(txtFilename);
clearvars txtFilename txtPath

%% Run 17
% Organize data
rightData = [D.x2bA D.x2bB D.x2bC D.x2bD D.x2bE D.x2bF D.x2bG D.x2bH ...
             D.x2eA D.x2eB D.x2eC D.x2eD D.x2eE D.x2eF D.x2eG D.x2eH ...
             D.TPR D.x1 D.x2 D.x3];

rightLabel = {'2bA' '2bB' '2bC' '2bD' '2bE' '2bF' '2bG' '2bH' ...
              '2eA' '2eB' '2eC' '2eD' '2eE' '2eF' '2eG' '2eH' ...
              'TPR' 'InR' 'MdR' 'ExR'};

leftData = [D.x4bA D.x4bB D.x4bC D.x4bD D.x4bE D.x4bF D.x4bG D.x4bH ...
            D.x4eA D.x4eB D.x4eC D.x4eD D.x4eE D.x4eF D.x4eG D.x4eH ...
            D.TPL D.x4 D.x5 D.x6];

leftLabel = {'4bA' '4bB' '4bC' '4bD' '4bE' '4bF' '4bG' '4bH' ...
             '4eA' '4eB' '4eC' '4eD' '4eE' '4eF' '4eG' '4eH' ...
             'TPL' 'InL' 'MdL' 'ExL'};

botpanelData = [D.x1bA D.x1bC D.x1bD D.x1bE D.x1bH ...
                D.x3bA D.x3bC D.x3bD D.x3bE D.x3bH ];

botpanelLabel = {'1bA' '1bC' '1bD' '1bE' '1bH' ...
                 '3bA' '3bC' '3bD' '3bE' '3bH' };

rightData = rightData(12942:15711,:);
leftData = leftData(12942:15711,:);
botpanelData = botpanelData(12942:15711,:);

%% Plot right data vs left data; calculate correlation
pltCorrelation = figure;
for i = 1:20;
    subplot(4,5,i);
    anaData = [rightData(:,i), leftData(:,i)];

    corr = corr2(anaData(:,1),anaData(:,2));
    nmbe = NMBE(anaData(:,1),anaData(:,2));
    cvrmse = CVRMSE(anaData(:,1),anaData(:,2));
```

```
    hold all
    scatter(anaData(:,1),anaData(:,2),'.');

    p = polyfitZero(anaData(:,1),anaData(:,2),1);
    x = [0 40];
    plot(x,p(1)*x + p(2));

    l1 = sprintf('COR: %.4f', corr);
    l2 = sprintf('NMBE: %.4f', nmbe);
    l3 = sprintf('CV(RMSE): %.4f', cvrmse);
    l4 = sprintf('Slope: %.4f', p(1));
    hText(i,1) = text(10.5,30,{l1;l2},'VerticalAlignment','top','FontSize',6);
    hText(i,2) = text(10.5,10,{l3;l4},'VerticalAlignment','bottom','FontSize',6);
    hTitle(i) = title([rightLabel{1,i} ' vs ' leftLabel{1,i}]);
    axis([10 30 10 30]);
    axis square
    clear anaData p

end
clear i

%% Plot 1b and 3b data vs 2b; calculate correlation
pltCorrBotPanel = figure;
pair = [1 1; 3 2; 4 3; 5 4; 8 5; 1 6; 3 7; 4 8; 5 9; 8 10];
for j = 1:15;
    subplot(3,5,j);
    if j <= 10
        anaData = [rightData(:,pair(j,1)), botpanelData(:,pair(j,2))];
        hTitle(j) = title([rightLabel{1,pair(j,1)} ' vs '
       botpanelLabel{1,pair(j,2)}]);
    else
        anaData = [botpanelData(:,j-10), botpanelData(:,j-5)];
        hTitle(j) = title([botpanelLabel{1,j-10} ' vs ' botpanelLabel{1,j-5}]);
    end

    corr = corr2(anaData(:,1),anaData(:,2));
    nmbe = NMBE(anaData(:,1),anaData(:,2));
    cvrmse = CVRMSE(anaData(:,1),anaData(:,2));

    hold all
    scatter(anaData(:,1),anaData(:,2),'.');

    p = polyfitZero(anaData(:,1),anaData(:,2),1);
    x = [0 40];
    plot(x,p(1)*x + p(2));

    l1 = sprintf('COR: %.4f', corr);
    l2 = sprintf('NMBE: %.4f', nmbe);
    l3 = sprintf('CV(RMSE): %.4f', cvrmse);
    l4 = sprintf('Slope: %.4f', p(1));
    hText(j,1) =      text(10.5,30,{l1;l2},'VerticalAlignment','top','FontSize',6);
    hText(j,2) =      text(10.5,10,{l3;l4},'VerticalAlignment','bottom','FontSize',6);

    axis([10 30 10 30]);
    axis square
    clear anaData p
end
clear j
```

A.4.2 30th Order Model

The following is the script for the 30th order finite difference model. It serves to validate the model against the measured data. The 2nd and 4th order models are very similar to this one and are left out.

thermNet_6CV5C_03.m

```
%% Thermal Network Method

%% Clean start
close all
clear
clc

%% Dependencies
addpath('Aux Functions');
addpath('Data');

%% Input Arguments
% Import pre-processed data from Experiment 17
%load('Run17FullRight.mat')
load('0320RTR.mat')

% PCM Properties and Data Range
phT = 'M';
if phT == 'M'         % Melting range
%   T_exp = T_exp(1:1144,:);    % Run 17
    T_exp = T_exp(1:921,:);     % Run 0320
    skew = -10;       % skew
    T_peak = 23.;    % peak phase change temperature, C; SLIGHTLY OFF 22
    rng = 4.5;        % range of phase change, C
    dh = 11500;       % enthalpy of phase change, J/kg 13100
    Cp_avg = 3200;    % average solid/liquid specific heat (full quality), J/kg
%   Cp-T curve that best fits data
%     skew = -6;        % skew
%     T_peak = 21.4;    % peak phase change temperature, C; SLIGHTLY OFF
%     rng = 4.5;        % range of phase change, C
%     dh = 10000;       % enthalpy of phase change, J/kg
%     Cp_avg = 3200;    % average solid/liquid specific heat (full quality), J/kg
elseif phT == 'F'     % Freezing range
%   T_exp = T_exp(1145:end,:);  % Run 17
    T_exp = T_exp(931:end,:);   % Run 0320
    skew = -4;
    T_peak = 20.8;%20.8;
    rng = 5;
    dh = 13600;
    Cp_avg = 3200;
%   Cp-T curve that best fits data
%     skew = -4;
%     T_peak = 20.6;
%     rng = 5;
%     dh = 11000;
%     Cp_avg = 3200;
end
```

```
% Material Properties
rho = 850;          % kg/m^3
dx = 0.0052;        % m
h_out = 20;
h_chn = 18;         % W/m^2K; Convection coefficient in the air channel
e_chn = 0.90;       % emissivity of painted PCM panels (0.85 to 0.95)
sig = 5.67*10^-8;   % Stefan-Boltzman constant
A = 4.8/6;          % m^2
m_air = 400/3600;   % kg/s; Air massflow rate
Cp_air = 1005;      % J/kgK
R_ins = 0.36;       % m^2K/W 0.6-1.0, 1.32 real; but leaks etc
R_back = 1.00;      % quite well insulated back side
k_fctr = 0.80;      % representing contact resistance applied to the conductivity of PCM
ehAmCp = exp(-h_chn*2*A/(m_air*Cp_air));

% Control
nN = 86;            % Number of nodes
st = 60;            % steps per hour
%H = 12;             % number of hours, simulation only
%nT = st*H;          % number of timesteps, simulation only
nT = size(T_exp,1); % number of timesteps, experimental data
dt = 3600/st;       % s (3600s = 1 hour)
maxItt = 10;        % maximum number of iterations per timestep
maxErr = 1e-3;      % maximum temperature difference between iterations of a given timestep

%T_exp = T_exp(1:nT,:);

% Temperature
% T_ini = 17;         % Initial Temperature
% T_air = 16;         % Air Temperature (at middle; then to be used as entering)
T_room = 21;        % Room Temperature, range: 21.2-22.6

%% Initial Conditions
T = NaN(nT,nN);     % Nodal Temperature
% T(1,:) = T_ini;
T(1,1) = T_exp.AirIn(1);
T(1,[2  4   6   8   9   10  12  14]) = [T_exp.H1(1),    T_exp.G1(1),    T_exp.F1(1),
T_exp.E1(1),    T_exp.D1(1),    T_exp.C1(1),    T_exp.B1(1),    T_exp.A1(1)];
T(1,[16 18  20  22  23  24  26  28]) = [T_exp.H2(1),    T_exp.G2(1),    T_exp.F2(1),
T_exp.E2(1),    T_exp.D2(1),    T_exp.C2(1),    T_exp.B2(1),    T_exp.A2(1)];
T(1,[30 32  34  36  37  38  40  42]) = [T_exp.H3(1),    T_exp.G3(1),    T_exp.F3(1),
T_exp.E3(1),    T_exp.D3(1),    T_exp.C3(1),    T_exp.B3(1),    T_exp.A3(1)];
T(1,[44 46  48  50  51  52  54  56]) = [T_exp.H4(1),    T_exp.G4(1),    T_exp.F4(1),
T_exp.E4(1),    T_exp.D4(1),    T_exp.C4(1),    T_exp.B4(1),    T_exp.A4(1)];
T(1,[58 60  62  64  65  66  68  70]) = [T_exp.H5(1),    T_exp.G5(1),    T_exp.F5(1),
T_exp.E5(1),    T_exp.D5(1),    T_exp.C5(1),    T_exp.B5(1),    T_exp.A5(1)];
T(1,[72 74  76  78  79  80  82  84]) = [T_exp.H6(1),    T_exp.G6(1),    T_exp.F6(1),
T_exp.E6(1),    T_exp.D6(1),    T_exp.C6(1),    T_exp.B6(1),    T_exp.A6(1)];
% T(1,:) = T_charge(end, :);
T(1,86) = T_room;
T(1,:) = inpaint_nans(T(1,:));  % Fill Gaps
E = zeros(nT,nN);   % Energy Balance per Node

%% Outer Loop
tic
for t = 2:nT

    %% First Run?
    itt = 1;
    error = inf;
    Tlast = NaN(1,nN);
```

```
%% Inner Loop
while (error > maxErr) && (itt <= maxItt)

    %% Node Connections
    RC = zeros(nN);

    % How are nodes connected? "0"s is for when they are not (K/W)
    if itt == 1
        ti = t-1;
    else
        ti = t;
    end

    % Radiation exchange in the channel
    for rad = [8, 22, 36, 50, 64, 78]
        TfK = T(ti,rad) + 273.15;
        TbK = T(ti,rad+2) + 273.15;
        Urad = A*sig*(TfK^2+TbK^2)*(TfK+TbK) / (1/e_chn + 1/e_chn - 1);
        RC(rad,rad+2) = 1/Urad;
    end
    clear rad TfK TbK Urad

    % node 1: inlet of 1st cv
    RC(2,3) = dx/(2*A*k_fctr*fK_erfc([T(ti,2) T(ti,3)]));
    RC(3,4) = dx/(2*A*k_fctr*fK_erfc([T(ti,3) T(ti,4)]));
    RC(4,5) = dx/(2*A*k_fctr*fK_erfc([T(ti,4) T(ti,5)]));
    RC(5,6) = dx/(2*A*k_fctr*fK_erfc([T(ti,5) T(ti,6)]));
    RC(6,7) = dx/(2*A*k_fctr*fK_erfc([T(ti,6) T(ti,7)]));
    RC(7,8) = dx/(2*A*k_fctr*fK_erfc([T(ti,7) T(ti,8)]));
    RC(8,9) = 1/(h_chn*A);
    RC(9,10) = 1/(h_chn*A);
    RC(10,11) = dx/(2*A*k_fctr*fK_erfc([T(ti,10) T(ti,11)]));
    RC(11,12) = dx/(2*A*k_fctr*fK_erfc([T(ti,11) T(ti,12)]));
    RC(12,13) = dx/(2*A*k_fctr*fK_erfc([T(ti,12) T(ti,13)]));
    RC(13,14) = dx/(2*A*k_fctr*fK_erfc([T(ti,13) T(ti,14)]));
    % node 15: oulet of 1st cv, inlet of 2nd cv
    RC(16,17) = dx/(2*A*k_fctr*fK_erfc([T(ti,16) T(ti,17)]));
    RC(17,18) = dx/(2*A*k_fctr*fK_erfc([T(ti,17) T(ti,18)]));
    RC(18,19) = dx/(2*A*k_fctr*fK_erfc([T(ti,18) T(ti,19)]));
    RC(19,20) = dx/(2*A*k_fctr*fK_erfc([T(ti,19) T(ti,20)]));
    RC(20,21) = dx/(2*A*k_fctr*fK_erfc([T(ti,20) T(ti,21)]));
    RC(21,22) = dx/(2*A*k_fctr*fK_erfc([T(ti,21) T(ti,22)]));
    RC(22,23) = 1/(h_chn*A);
    RC(23,24) = 1/(h_chn*A);
    RC(24,25) = dx/(2*A*k_fctr*fK_erfc([T(ti,24) T(ti,25)]));
    RC(25,26) = dx/(2*A*k_fctr*fK_erfc([T(ti,25) T(ti,26)]));
    RC(26,27) = dx/(2*A*k_fctr*fK_erfc([T(ti,26) T(ti,27)]));
    RC(27,28) = dx/(2*A*k_fctr*fK_erfc([T(ti,27) T(ti,28)]));
    % node 29: oulet of 2nd cv, inlet of 3rd cv
    RC(30,31) = dx/(2*A*k_fctr*fK_erfc([T(ti,30) T(ti,31)]));
    RC(31,32) = dx/(2*A*k_fctr*fK_erfc([T(ti,31) T(ti,32)]));
    RC(32,33) = dx/(2*A*k_fctr*fK_erfc([T(ti,32) T(ti,33)]));
    RC(33,34) = dx/(2*A*k_fctr*fK_erfc([T(ti,33) T(ti,34)]));
    RC(34,35) = dx/(2*A*k_fctr*fK_erfc([T(ti,34) T(ti,35)]));
    RC(35,36) = dx/(2*A*k_fctr*fK_erfc([T(ti,35) T(ti,36)]));
    RC(36,37) = 1/(h_chn*A);
    RC(37,38) = 1/(h_chn*A);
    RC(38,39) = dx/(2*A*k_fctr*fK_erfc([T(ti,38) T(ti,39)]));
    RC(39,40) = dx/(2*A*k_fctr*fK_erfc([T(ti,39) T(ti,40)]));
    RC(40,41) = dx/(2*A*k_fctr*fK_erfc([T(ti,40) T(ti,41)]));
```

```
        RC(41,42) = dx/(2*A*k_fctr*fK_erfc([T(ti,41) T(ti,42)]));
        % node 43: oulet of 3rd cv, inlet of 4th cv
        RC(44,45) = dx/(2*A*k_fctr*fK_erfc([T(ti,44) T(ti,45)]));
        RC(45,46) = dx/(2*A*k_fctr*fK_erfc([T(ti,45) T(ti,46)]));
        RC(46,47) = dx/(2*A*k_fctr*fK_erfc([T(ti,46) T(ti,47)]));
        RC(47,48) = dx/(2*A*k_fctr*fK_erfc([T(ti,47) T(ti,48)]));
        RC(48,49) = dx/(2*A*k_fctr*fK_erfc([T(ti,48) T(ti,49)]));
        RC(49,50) = dx/(2*A*k_fctr*fK_erfc([T(ti,49) T(ti,50)]));
        RC(50,51) = 1/(h_chn*A);
        RC(51,52) = 1/(h_chn*A);
        RC(52,53) = dx/(2*A*k_fctr*fK_erfc([T(ti,52) T(ti,53)]));
        RC(53,54) = dx/(2*A*k_fctr*fK_erfc([T(ti,53) T(ti,54)]));
        RC(54,55) = dx/(2*A*k_fctr*fK_erfc([T(ti,54) T(ti,55)]));
        RC(55,56) = dx/(2*A*k_fctr*fK_erfc([T(ti,55) T(ti,56)]));
        % node 57: oulet of 4th cv, inlet of 5th cv
        RC(58,59) = dx/(2*A*k_fctr*fK_erfc([T(ti,58) T(ti,59)]));
        RC(59,60) = dx/(2*A*k_fctr*fK_erfc([T(ti,59) T(ti,60)]));
        RC(60,61) = dx/(2*A*k_fctr*fK_erfc([T(ti,60) T(ti,61)]));
        RC(61,62) = dx/(2*A*k_fctr*fK_erfc([T(ti,61) T(ti,62)]));
        RC(62,63) = dx/(2*A*k_fctr*fK_erfc([T(ti,62) T(ti,63)]));
        RC(63,64) = dx/(2*A*k_fctr*fK_erfc([T(ti,63) T(ti,64)]));
        RC(64,65) = 1/(h_chn*A);
        RC(65,66) = 1/(h_chn*A);
        RC(66,67) = dx/(2*A*k_fctr*fK_erfc([T(ti,66) T(ti,67)]));
        RC(67,68) = dx/(2*A*k_fctr*fK_erfc([T(ti,67) T(ti,68)]));
        RC(68,69) = dx/(2*A*k_fctr*fK_erfc([T(ti,68) T(ti,69)]));
        RC(69,70) = dx/(2*A*k_fctr*fK_erfc([T(ti,69) T(ti,70)]));
        % node 71: oulet of 5th cv, inlet of 6th cv
        RC(72,73) = dx/(2*A*k_fctr*fK_erfc([T(ti,72) T(ti,73)]));
        RC(73,74) = dx/(2*A*k_fctr*fK_erfc([T(ti,73) T(ti,74)]));
        RC(74,75) = dx/(2*A*k_fctr*fK_erfc([T(ti,74) T(ti,75)]));
        RC(75,76) = dx/(2*A*k_fctr*fK_erfc([T(ti,75) T(ti,76)]));
        RC(76,77) = dx/(2*A*k_fctr*fK_erfc([T(ti,76) T(ti,77)]));
        RC(77,78) = dx/(2*A*k_fctr*fK_erfc([T(ti,77) T(ti,78)]));
        RC(78,79) = 1/(h_chn*A);
        RC(79,80) = 1/(h_chn*A);
        RC(80,81) = dx/(2*A*k_fctr*fK_erfc([T(ti,80) T(ti,81)]));
        RC(81,82) = dx/(2*A*k_fctr*fK_erfc([T(ti,81) T(ti,82)]));
        RC(82,83) = dx/(2*A*k_fctr*fK_erfc([T(ti,82) T(ti,83)]));
        RC(83,84) = dx/(2*A*k_fctr*fK_erfc([T(ti,83) T(ti,84)]));
        % node 85: oulet of 6th cv

        % Towards the room air, node 86
        RC(14,86) = R_back/A + 1/(h_out*A); % Back side to room
        RC(28,86) = R_back/A + 1/(h_out*A); % Back side to room
        RC(42,86) = R_back/A + 1/(h_out*A); % Back side to room
        RC(56,86) = R_back/A + 1/(h_out*A); % Back side to room
        RC(70,86) = R_back/A + 1/(h_out*A); % Back side to room
        RC(84,86) = R_back/A + 1/(h_out*A); % Back side to room

        RC(2,86) = R_ins/A + 1/(h_out*A); % Front side to room
        RC(16,86) = R_ins/A + 1/(h_out*A); % Front side to room
        RC(30,86) = R_ins/A + 1/(h_out*A); % Front side to room
        RC(44,86) = R_ins/A + 1/(h_out*A); % Front side to room
        RC(58,86) = R_ins/A + 1/(h_out*A); % Front side to room
        RC(72,86) = R_ins/A + 1/(h_out*A); % Front side to room

        % Copy upper triangle to lower
        RC = RC + RC';
```

```
        % Air nodes
        RC(1,1) = 1; % CV1 in
        RC(15,15) = 1; % CV2 in
        RC(29,29) = 1; % CV3 in
        RC(43,43) = 1; % CV4 in
        RC(57,57) = 1; % CV5 in
        RC(71,71) = 1; % CV6 in
        RC(85,85) = 1; % CV6 out

        % Thermal Capacitance (K/W)
        RC(3,3) = dt/(rho*A*dx*fCp_skewnormal(T(t-1,3), skew, T_peak, rng, dh, Cp_avg));
        RC(5,5) = dt/(rho*A*dx*fCp_skewnormal(T(t-1,5), skew, T_peak, rng, dh, Cp_avg));
        RC(7,7) = dt/(rho*A*dx*fCp_skewnormal(T(t-1,7), skew, T_peak, rng, dh, Cp_avg));
        RC(11,11) = dt/(rho*A*dx*fCp_skewnormal(T(t-1,11), skew, T_peak, rng, dh, Cp_avg));
        RC(13,13) = dt/(rho*A*dx*fCp_skewnormal(T(t-1,13), skew, T_peak, rng, dh, Cp_avg));
        RC(17,17) = dt/(rho*A*dx*fCp_skewnormal(T(t-1,17), skew, T_peak, rng, dh, Cp_avg));
        RC(19,19) = dt/(rho*A*dx*fCp_skewnormal(T(t-1,19), skew, T_peak, rng, dh, Cp_avg));
        RC(21,21) = dt/(rho*A*dx*fCp_skewnormal(T(t-1,21), skew, T_peak, rng, dh, Cp_avg));
        RC(25,25) = dt/(rho*A*dx*fCp_skewnormal(T(t-1,25), skew, T_peak, rng, dh, Cp_avg));
        RC(27,27) = dt/(rho*A*dx*fCp_skewnormal(T(t-1,27), skew, T_peak, rng, dh, Cp_avg));
        RC(31,31) = dt/(rho*A*dx*fCp_skewnormal(T(t-1,31), skew, T_peak, rng, dh, Cp_avg));
        RC(33,33) = dt/(rho*A*dx*fCp_skewnormal(T(t-1,33), skew, T_peak, rng, dh, Cp_avg));
        RC(35,35) = dt/(rho*A*dx*fCp_skewnormal(T(t-1,35), skew, T_peak, rng, dh, Cp_avg));
        RC(39,39) = dt/(rho*A*dx*fCp_skewnormal(T(t-1,39), skew, T_peak, rng, dh, Cp_avg));
        RC(41,41) = dt/(rho*A*dx*fCp_skewnormal(T(t-1,41), skew, T_peak, rng, dh, Cp_avg));
        RC(45,45) = dt/(rho*A*dx*fCp_skewnormal(T(t-1,45), skew, T_peak, rng, dh, Cp_avg));
        RC(47,47) = dt/(rho*A*dx*fCp_skewnormal(T(t-1,47), skew, T_peak, rng, dh, Cp_avg));
        RC(49,49) = dt/(rho*A*dx*fCp_skewnormal(T(t-1,49), skew, T_peak, rng, dh, Cp_avg));
        RC(53,53) = dt/(rho*A*dx*fCp_skewnormal(T(t-1,53), skew, T_peak, rng, dh, Cp_avg));
        RC(55,55) = dt/(rho*A*dx*fCp_skewnormal(T(t-1,55), skew, T_peak, rng, dh, Cp_avg));
        RC(59,59) = dt/(rho*A*dx*fCp_skewnormal(T(t-1,59), skew, T_peak, rng, dh, Cp_avg));
        RC(61,61) = dt/(rho*A*dx*fCp_skewnormal(T(t-1,61), skew, T_peak, rng, dh, Cp_avg));
        RC(63,63) = dt/(rho*A*dx*fCp_skewnormal(T(t-1,63), skew, T_peak, rng, dh, Cp_avg));
        RC(67,67) = dt/(rho*A*dx*fCp_skewnormal(T(t-1,67), skew, T_peak, rng, dh, Cp_avg));
        RC(69,69) = dt/(rho*A*dx*fCp_skewnormal(T(t-1,69), skew, T_peak, rng, dh, Cp_avg));
        RC(73,73) = dt/(rho*A*dx*fCp_skewnormal(T(t-1,73), skew, T_peak, rng, dh, Cp_avg));
        RC(75,75) = dt/(rho*A*dx*fCp_skewnormal(T(t-1,75), skew, T_peak, rng, dh, Cp_avg));
        RC(77,77) = dt/(rho*A*dx*fCp_skewnormal(T(t-1,77), skew, T_peak, rng, dh, Cp_avg));
        RC(81,81) = dt/(rho*A*dx*fCp_skewnormal(T(t-1,81), skew, T_peak, rng, dh, Cp_avg));
        RC(83,83) = dt/(rho*A*dx*fCp_skewnormal(T(t-1,83), skew, T_peak, rng, dh, Cp_avg));

        %% Heat Flux
        Q = zeros(nN,1);

%       % How much heat is going into the node? (W)
        % Q(Node) = # Watts;
        % Air channel modelled as a current source where q_in comes from
        % the air stream's energy balance
        Q(9) = -m_air*Cp_air*(T(ti,15)-T(ti,1));
        Q(23) = -m_air*Cp_air*(T(ti,29)-T(ti,15));
        Q(37) = -m_air*Cp_air*(T(ti,43)-T(ti,29));
        Q(51) = -m_air*Cp_air*(T(ti,57)-T(ti,43));
        Q(65) = -m_air*Cp_air*(T(ti,71)-T(ti,57));
        Q(79) = -m_air*Cp_air*(T(ti,85)-T(ti,71));

        % Due to capacitance
        for i = 1:nN
            if RC(i,i) ~= 0
                Q(i) = Q(i) + T(t-1,i)/RC(i,i);
            end
        end
```

```
        clear i

%       % Node 8 due to convection with known temperature
        % Air channel modelled as a voltage source where T_channel comes
        % from the air stream's average temperature; don't forget to add
        % parameters in N-matrix
        % Q(1) = T_air;
        Q(1) = T_exp.AirIn(t);
        Q(86) = T_room;

        %% Node Temperature: N*T=Q
        N = zeros(nN);

        % 1/R
        N(RC~=0) = -1./RC(RC~=0);

        % Calculate diagonal term
        for j = 1:nN
            N(j,j) = -sum(N(j,:));
        end
        clear j

%       % Uncomment for Nodes due to convection with known temperature
        % N(node,:) = zeros(1,nN);
        % N(node, node) = 1;
        N(1,:) = zeros(1,nN);
        N(1,1) = 1;
        N(86,:) = zeros(1,nN);
        N(86,86) = 1;
        %%%

        %% Solve
        T(t,:) = N\Q;

        %% Solve for special nodes
        T(t,15) = T(t, 1)*ehAmCp + 0.5*(T(t, 8)+T(t,10))*(1-ehAmCp);
        T(t,29) = T(t,15)*ehAmCp + 0.5*(T(t,22)+T(t,24))*(1-ehAmCp);
        T(t,43) = T(t,29)*ehAmCp + 0.5*(T(t,36)+T(t,38))*(1-ehAmCp);
        T(t,57) = T(t,43)*ehAmCp + 0.5*(T(t,50)+T(t,52))*(1-ehAmCp);
        T(t,71) = T(t,57)*ehAmCp + 0.5*(T(t,64)+T(t,66))*(1-ehAmCp);
        T(t,85) = T(t,71)*ehAmCp + 0.5*(T(t,78)+T(t,80))*(1-ehAmCp);

        %% Calculate Error
        if itt ~= 1
            error = max(abs(T(t,:) - Tlast));
        end
        Tlast = T(t,:);

        %% Iterate
        if itt == maxItt
            warning('progr:Nneg','Maximum iteration attained for t = %d',t)
        end
        itt = itt+1;
    end

    %% Energy Balance
    % E = m*Cp*dT in Joules
    for m = 1:nN
        if RC(m,m) ~= 0
            E(t,m) = dt/RC(m,m)*(T(t,m)-T(t-1,m));
        end
```

```
    end
    clear m

end
fprintf('Simulation took %.1f seconds\n', toc)

%% Energy Transfer PCM
% E_PCM = E(:,[3    5   7   11  13  17  19  21  25  27  31  33  35  39  41  45  47  49  53
55  59  61  63  67  69  73  75  77  81  83]); % Take only the PCM layers
% E_total = sum(E_PCM);               % J
% E_total_cum = cumsum(E_PCM,1);      % J
% E_total_kJ_kg = E_total/(1000*A*rho*dx);
% E_total_system_cum = sum(E_total_cum,2);

E_air = [0; -m_air.*Cp_air.*T_exp.dT(2:end)*dt];
% E_air = [0; -m_air.*Cp_air.*(T(2:end,85)-T(2:end,1))*dt];
E_air_cum = cumsum(E_air,1);
E_air_total = E_air_cum(end,:);

% Energy Balance at air node
Q_air_conv = zeros(nT,13);
Q_air_conv(:,1) = h_chn*A*(T(:,9)-T(:,8));
Q_air_conv(:,2) = h_chn*A*(T(:,9)-T(:,10));
Q_air_conv(:,3) = h_chn*A*(T(:,23)-T(:,22));
Q_air_conv(:,4) = h_chn*A*(T(:,23)-T(:,24));
Q_air_conv(:,5) = h_chn*A*(T(:,37)-T(:,36));
Q_air_conv(:,6) = h_chn*A*(T(:,37)-T(:,38));
Q_air_conv(:,7) = h_chn*A*(T(:,51)-T(:,50));
Q_air_conv(:,8) = h_chn*A*(T(:,51)-T(:,52));
Q_air_conv(:,9) = h_chn*A*(T(:,65)-T(:,64));
Q_air_conv(:,10) = h_chn*A*(T(:,65)-T(:,66));
Q_air_conv(:,11) = h_chn*A*(T(:,79)-T(:,78));
Q_air_conv(:,12) = h_chn*A*(T(:,79)-T(:,80));
Q_air_conv(:,13) = sum(Q_air_conv(:,1:12),2);

E_air_conv = dt*Q_air_conv;
E_air_conv_cum = cumsum(E_air_conv);

%% Plot Energy Balance
EBalanceAir = figure();
hold all
plot(E_air_cum/(3.6e6),'--','Color',[.4392 .6784 .2784],'LineWidth',2);
plot(E_air_conv_cum(:,13)/(3.6e6),'k','LineWidth',2);
plot(E_air_conv_cum(:,1)/(3.6e6),'r');
plot(E_air_conv_cum(:,2)/(3.6e6),'b');
plot(E_air_conv_cum(:,3:2:end-1)/(3.6e6),'r');
[ax, h] = plot2axes(E_air_conv_cum(:,4:2:end-1)/(3.6e6), 'b','yscale', 3.41214163);
set(ax, 'XTick', 0);
l1 = sprintf('Air Energy: %.2f kWh', E_air_cum(end)/(3.6e6));
l2 = sprintf('PCM Energy: %.2f kWh', E_air_conv_cum(end,end)/(3.6e6));
if (phT == 'M'), hText = text(20,2.9,{l1;l2},'VerticalAlignment','top','FontSize',10); end;
if (phT == 'F'), hText = text(400,-1,{l1;l2},'VerticalAlignment','top','FontSize',10); end;
xlim([0 size(T,1)])
set(gca,'XTick',0:300:1320);
set(gca,'XTickLabel',0:5:22,'XMinorTick','on');
hXLabel = xlabel(ax(1), 'Time, h');
hYLabel1 = ylabel(ax(1), 'Energy Transfered, kWh');
hYLabel2 = ylabel(ax(2), 'Energy Transfered, MBtu');
plotLegend = {'Air','PCM, Total','PCM, Front Layers','PCM, Back Layers'};
hLegend = legend(plotLegend,'Location','Best');
legend boxoff
```

```
hTitle = title('PCM-TES Energy Balance, 6CV/5C');
movegui(EBalanceAir,'northeast');

%% Plot surface temperatures with height
pltGrad = figure;
times = [1 15 30 60 120 180 240 360 480 720] + 1;
data_fr = flipud(T(times,[8 22  36  50  64  78])');
data_fr_exp = flipud([T_exp.E1(times), T_exp.E2(times), T_exp.E3(times), T_exp.E4(times),
T_exp.E5(times), T_exp.E6(times)]');
data_bk = flipud(T(times,[10    24  38  52  66  80])');
data_bk_exp = flipud([T_exp.C1(times), T_exp.C2(times), T_exp.C3(times), T_exp.C4(times),
T_exp.C5(times), T_exp.C6(times)]');
%dist = [0.2 0.6 1.0 1.4 1.8 2.2];
dist = [0.15 0.6 1.05 1.35 1.8 2.25]; % actual thermocouple locations

subplot(1,2,1)
hold all
for i = 1:length(times)
    plot(data_fr(:,i),dist);
%    plot(data_fr_exp(:,i),dist,'--');
end
ylim([0 2.4])
set(gca,'YTick',[0 dist 2.4])
hXLabel = xlabel('Temperature, °C');
hYLabel = ylabel('Air Stream, m');
plotLegend = {'t = 0',  't = 0.25', 't = 0.50', 't = 1',    't = 2',    't = 3',    't = 4',
't = 6',    't = 8',    't = 12'};
hLegend = legend(plotLegend,'Location','East');
hTitle = title('3-Layer Side');
grid on
set(gca,'FontName'   , 'Helvetica' );
set([hTitle, hXLabel, hYLabel], 'FontName'   , 'AvantGarde');
set(gca,'FontSize'   , 8           );
set([hXLabel, hYLabel],'FontSize'   , 10          );
set( hTitle                    , ...
    'FontSize'   , 12          , ...
    'FontWeight' , 'bold'      );
set(gca, ...
  'Box'         , 'off'     , ...
  'TickDir'     , 'out'     , ...
  'TickLength'  , [.02 .02] , ...
  'YMinorTick'  , 'on'      , ...
  'XColor'      , [.2 .2 .2], ...
  'YColor'      , [.2 .2 .2]);%, ...

subplot(1,2,2)
hold all
for i = 1:length(times)
    plot(data_bk(:,i),dist);
%    plot(data_bk_exp(:,i),dist,'--');
end
ylim([0 2.4])
set(gca,'YTick',[0 dist 2.4])
hXLabel = xlabel('Temperature, °C');
legend boxoff
hTitle = title('2-Layer Side');
grid on
set(gca,'FontName'   , 'Helvetica' );
set([hTitle, hXLabel], 'FontName'   , 'AvantGarde');
set(gca,'FontSize'   , 8           );
set([hXLabel],'FontSize'   , 10          );
```

```
set( hTitle                    , ...
    'FontSize'   , 12          , ...
    'FontWeight' , 'bold'      );
set(gca, ...
  'Box'         , 'off'     , ...
  'TickDir'     , 'out'     , ...
  'TickLength'  , [.02 .02] , ...
  'YMinorTick'  , 'on'      , ...
  'XColor'      , [.2 .2 .2], ...
  'YColor'      , [.2 .2 .2]);%, ...

%% Plot experimental and simulated
for CV = 1%:6
    switch CV
        case 1
            pltExpSim1 = figure;
            simData = T(:,[2    4   6   8   9   10  12  14]);
            expData = [T_exp.H1,    T_exp.G1,   T_exp.F1,   T_exp.E1,   T_exp.D1,
T_exp.C1,   T_exp.B1,   T_exp.A1];
        case 2
            pltExpSim2 = figure;
            simData = T(:,[16   18  20  22  23  24  26  28]);
            expData = [T_exp.H2,    T_exp.G2,   T_exp.F2,   T_exp.E2,   T_exp.D2,
T_exp.C2,   T_exp.B2,   T_exp.A2];
        case 3
            pltExpSim3 = figure;
            simData = T(:,[30   32  34  36  37  38  40  42]);
            expData = [T_exp.H3,    T_exp.G3,   T_exp.F3,   T_exp.E3,   T_exp.D3,
T_exp.C3,   T_exp.B3,   T_exp.A3];
        case 4
            pltExpSim4 = figure;
            simData = T(:,[44   46  48  50  51  52  54  56]);
            expData = [T_exp.H4,    T_exp.G4,   T_exp.F4,   T_exp.E4,   T_exp.D4,
T_exp.C4,   T_exp.B4,   T_exp.A4];
        case 5
            pltExpSim5 = figure;
            simData = T(:,[58   60  62  64  65  66  68  70]);
            expData = [T_exp.H5,    T_exp.G5,   T_exp.F5,   T_exp.E5,   T_exp.D5,
T_exp.C5,   T_exp.B5,   T_exp.A5];
        case 6
            pltExpSim6 = figure;
            simData = T(:,[72   74  76  78  79  80  82  84]);
            expData = [T_exp.H6,    T_exp.G6,   T_exp.F6,   T_exp.E6,   T_exp.D6,
T_exp.C6,   T_exp.B6,   T_exp.A6];
    end
    hold on
    plot(simData);
    plot(expData,'--');
    xlim([0 size(T,1)])
    ylim([15 30])
    xlabel(sprintf('Timestep, (%d seconds)',dt));
    ylabel('Temperature, °C')
    plotLegend = {'H','G','F','E','D','C','B','A'};
    legend(plotLegend,'Location','NorthWest');
    title(sprintf('Experiment (dashed) vs. Simulation (solid), CV: %i', CV));
    movegui(gcf,'south');
end

%% Plot averaged experimental and simulated
for CV = 1:6
    switch CV
```

```
        case 1
            pltAvgExpSim1 = figure;
            simData = T(:,[2    4   6   8   9   10  12  14]);
            expData = [T_exp.H1,    T_exp.G1,   T_exp.F1,   T_exp.E1,   T_exp.D1,
T_exp.C1,   T_exp.B1,   T_exp.A1];
        case 2
            pltAvgExpSim2 = figure;
            simData = T(:,[16   18  20  22  23  24  26  28]);
            expData = [T_exp.H2,    T_exp.G2,   T_exp.F2,   T_exp.E2,   T_exp.D2,
T_exp.C2,   T_exp.B2,   T_exp.A2];
        case 3
            pltAvgExpSim3 = figure;
            simData = T(:,[30   32  34  36  37  38  40  42]);
            expData = [T_exp.H3,    T_exp.G3,   T_exp.F3,   T_exp.E3,   T_exp.D3,
T_exp.C3,   T_exp.B3,   T_exp.A3];
        case 4
            pltAvgExpSim4 = figure;
            simData = T(:,[44   46  48  50  51  52  54  56]);
            expData = [T_exp.H4,    T_exp.G4,   T_exp.F4,   T_exp.E4,   T_exp.D4,
T_exp.C4,   T_exp.B4,   T_exp.A4];
        case 5
            pltAvgExpSim5 = figure;
            simData = T(:,[58   60  62  64  65  66  68  70]);
            expData = [T_exp.H5,    T_exp.G5,   T_exp.F5,   T_exp.E5,   T_exp.D5,
T_exp.C5,   T_exp.B5,   T_exp.A5];
        case 6
            pltAvgExpSim6 = figure;
            simData = T(:,[72   74  76  78  79  80  82  84]);
            expData = [T_exp.H6,    T_exp.G6,   T_exp.F6,   T_exp.E6,   T_exp.D6,
T_exp.C6,   T_exp.B6,   T_exp.A6];
    end
    hold on
%     AvgsimData = [mean(simData(:,1:4),2) mean(simData(:,6:8),2)];
%     AvgexpData = [mean(expData(:,1:4),2) mean(expData(:,6:8),2)];
    AvgsimData = [mean(simData(:,2:3),2) mean(simData(:,7),2)];
    AvgexpData = [mean(expData(:,2:3),2) mean(expData(:,7),2)];
    plot(AvgsimData);
    plot(AvgexpData,'--');
    xlim([0 size(T,1)])
    ylim([15 30])
    xlabel(sprintf('Timestep, (%d seconds)',dt));
    ylabel('Temperature, °C')
    plotLegend = {'Front Layers','Back Layers'};
    legend(plotLegend,'Location','NorthWest');
    title(sprintf('Experiment (dashed) vs. Simulation (solid), CV: %i', CV));
    movegui(gcf,'southwest');
end

%% Plot correlation between simulation and experiment
for CV = 1:6
    switch CV
        case 1
            pltCorrelation1 = figure;
            simData = T(:,[2    4   6   8   9   10  12  14]);
            expData = [T_exp.H1,    T_exp.G1,   T_exp.F1,   T_exp.E1,   T_exp.D1,
T_exp.C1,   T_exp.B1,   T_exp.A1];
        case 2
            pltCorrelation2 = figure;
            simData = T(:,[16   18  20  22  23  24  26  28]);
            expData = [T_exp.H2,    T_exp.G2,   T_exp.F2,   T_exp.E2,   T_exp.D2,
T_exp.C2,   T_exp.B2,   T_exp.A2];
```

```
        case 3
            pltCorrelation3 = figure;
            simData = T(:,[30   32  34  36  37  38  40  42]);
            expData = [T_exp.H3,    T_exp.G3,   T_exp.F3,   T_exp.E3,   T_exp.D3,
T_exp.C3,   T_exp.B3,   T_exp.A3];
        case 4
            pltCorrelation4 = figure;
            simData = T(:,[44   46  48  50  51  52  54  56]);
            expData = [T_exp.H4,    T_exp.G4,   T_exp.F4,   T_exp.E4,   T_exp.D4,
T_exp.C4,   T_exp.B4,   T_exp.A4];
        case 5
            pltCorrelation5 = figure;
            simData = T(:,[58   60  62  64  65  66  68  70]);
            expData = [T_exp.H5,    T_exp.G5,   T_exp.F5,   T_exp.E5,   T_exp.D5,
T_exp.C5,   T_exp.B5,   T_exp.A5];
        case 6
            pltCorrelation6 = figure;
            simData = T(:,[72   74  76  78  79  80  82  84]);
            expData = [T_exp.H6,    T_exp.G6,   T_exp.F6,   T_exp.E6,   T_exp.D6,
T_exp.C6,   T_exp.B6,   T_exp.A6];
    end
    subplotLabel = {'H','G','F','E','D','C','B','A'};
    for i = 1:7;
        subplot(3,3,i);
        anaData = [simData(:,i), expData(:,i)];

        corr = corr2(anaData(:,1),anaData(:,2));
        nmbe = NMBE(anaData(:,1),anaData(:,2));
        cvrmse = CVRMSE(anaData(:,1),anaData(:,2));

        hold all
        scatter(anaData(:,1),anaData(:,2),'.');

        p = polyfitZero(anaData(:,1),anaData(:,2),1);
        x = [0 40];
        plot(x,p(1)*x + p(2));

        l1 = sprintf('COR: %.4f', corr);
        l2 = sprintf('NMBE: %.4f', nmbe);
        l3 = sprintf('CV(RMSE): %.4f', cvrmse);
        l4 = sprintf('Slope: %.4f', p(1));
        text(15.5,30,{l1;l2},'VerticalAlignment','top','FontSize',6)
        text(15.5,15,{l3;l4},'VerticalAlignment','bottom','FontSize',6)
        title(subplotLabel(i));
        axis([15 30 15 30]);
        axis square
        clear anaData p x corr nmbe cvrmse l1 l2 l3 l4
    end
    clear i
    title_val = sprintf('Model(x) vs Experiment(y) Correlations for CV: %i', CV);
    mtit(title_val,'yoff',.035);
    clear simData expData subplotLabel
    movegui(gcf,'northwest');
end

%% Plot difference between simulation and experiment
for CV = 1:6
    switch CV
        case 1
            pltDifference1 = figure;
            simData = T(:,[2    4   6   8   9   10  12  14]);
```

```
            expData = [T_exp.H1,    T_exp.G1,   T_exp.F1,   T_exp.E1,   T_exp.D1,
T_exp.C1,   T_exp.B1,   T_exp.A1];
        case 2
            pltDifference2 = figure;
            simData = T(:,[16   18  20  22  23  24  26  28]);
            expData = [T_exp.H2,    T_exp.G2,   T_exp.F2,   T_exp.E2,   T_exp.D2,
T_exp.C2,   T_exp.B2,   T_exp.A2];
        case 3
            pltDifference3 = figure;
            simData = T(:,[30   32  34  36  37  38  40  42]);
            expData = [T_exp.H3,    T_exp.G3,   T_exp.F3,   T_exp.E3,   T_exp.D3,
T_exp.C3,   T_exp.B3,   T_exp.A3];
        case 4
            pltDifference4 = figure;
            simData = T(:,[44   46  48  50  51  52  54  56]);
            expData = [T_exp.H4,    T_exp.G4,   T_exp.F4,   T_exp.E4,   T_exp.D4,
T_exp.C4,   T_exp.B4,   T_exp.A4];
        case 5
            pltDifference5 = figure;
            simData = T(:,[58   60  62  64  65  66  68  70]);
            expData = [T_exp.H5,    T_exp.G5,   T_exp.F5,   T_exp.E5,   T_exp.D5,
T_exp.C5,   T_exp.B5,   T_exp.A5];
        case 6
            pltDifference6 = figure;
            simData = T(:,[72   74  76  78  79  80  82  84]);
            expData = [T_exp.H6,    T_exp.G6,   T_exp.F6,   T_exp.E6,   T_exp.D6,
T_exp.C6,   T_exp.B6,   T_exp.A6];
    end
    subplotLabel = {'H','G','F','E','D','C','B','A'};
    xvalues = 0:0.1:5;
    for i = 1:7;
        subplot(3,3,i);
        anaData = [simData(:,i), expData(:,i)];

        absDiff = abs(anaData(:,1) - anaData(:,2));
        [nelements, centers] = hist(absDiff,xvalues);
        pelements = nelements./length(absDiff);
        bar(centers,pelements,1);
        axis([0 2.0 0 0.5])
        l1 = sprintf('Max: %.2f',max(absDiff));
        l2 = sprintf('Avg: %.2f',mean(absDiff));

text(0.80,0.49,{l1;l2},'HorizontalAlignment','Left','VerticalAlignment','top','FontSize',6)
        title(subplotLabel(i));
        axis square
        clear anaData absDiff l1
    end
    clear i
    title_val = sprintf('Model vs Experiment Temperature Difference(x) vs %% Frequency(y)
for CV: %i', CV);
    mtit(title_val,'yoff',.035);
    clear simData expData xvalues subplotLabel
    movegui(gcf,'southwest');
end

%% Plot Air in and out
pltAirInOut = figure;
hold all
plot(T(:,1),'b');
plot(T_exp.AirOut,'r');
[ax, h] = plot2axes(T(:,end-1), 'r:', 'yscale', @(y) y*9/5+32);
```

```
set(ax, 'XTick', 0);
xlim([0 size(T,1)])
set(gca,'XTick',0:300:1320);
set(gca,'XTickLabel',0:5:22,'XMinorTick','on');
hXLabel = xlabel(ax(1), 'Time, h');
hYLabel1 = ylabel(ax(1), 'Temperature, °C');
hYLabel2 = ylabel(ax(2), 'Temperature, °F');
plotLegend = {'Inlet','Oulet, Experiment','Outlet, Model'};
hLegend = legend(plotLegend,'Location','Best');
legend boxoff
hTitle = title('Inlet and Oulet Air Temperature');
movegui(gcf,'north');

%% Plot correlation air outlet
pltAirOutCorr = figure;
simData = T(:,85);
expData = T_exp.AirOut;
i = 1;
anaData = [simData(:,i), expData(:,i)];

corr = corr2(anaData(:,1),anaData(:,2));
nmbe = NMBE(anaData(:,1),anaData(:,2));
cvrmse = CVRMSE(anaData(:,1),anaData(:,2));

hold all
scatter(anaData(:,1),anaData(:,2),'.');

p = polyfitZero(anaData(:,1),anaData(:,2),1);
x = [0 40];
plot(x,p(1)*x + p(2));

l1 = sprintf('COR: %.4f', corr);
l2 = sprintf('NMBE: %.4f', nmbe);
l3 = sprintf('CV(RMSE): %.4f', cvrmse);
l4 = sprintf('Slope: %.4f', p(1));
text(15.5,30,{l1;l2},'VerticalAlignment','top','FontSize',10)
text(15.5,15,{l3;l4},'VerticalAlignment','bottom','FontSize',10)
axis([15 30 15 30]);
axis square
clear anaData p x corr nmbe cvrmse l1 l2 l3 l4

clear i
title_val = sprintf('Model(x) vs Experiment(y) Correlations for Outlet Air');
mtit(title_val,'yoff',.035);
clear simData expData subplotLabel
movegui(gcf,'northwest');

%% Average Errors and STD
simData = T(:,[2    4   6   8   9   10  12  14 16   18  20  22  23  24  26  28 30   32  34
36  37  38  40  42 44   46  48  50  51  52  54  56 58   60  62  64  65  66  68  70 72   74
76  78  79  80  82  84]);
expData = [T_exp.H1,    T_exp.G1,   T_exp.F1,   T_exp.E1,   T_exp.D1,   T_exp.C1,
T_exp.B1,   T_exp.A1 T_exp.H2,  T_exp.G2,   T_exp.F2,   T_exp.E2,   T_exp.D2,   T_exp.C2,
T_exp.B2,   T_exp.A2 ...
    T_exp.H3,   T_exp.G3,   T_exp.F3,   T_exp.E3,   T_exp.D3,   T_exp.C3,   T_exp.B3,
T_exp.A3 T_exp.H4,  T_exp.G4,   T_exp.F4,   T_exp.E4,   T_exp.D4,   T_exp.C4,   T_exp.B4,
T_exp.A4 ...
    T_exp.H5,   T_exp.G5,   T_exp.F5,   T_exp.E5,   T_exp.D5,   T_exp.C5,   T_exp.B5,
T_exp.A5 T_exp.H6,  T_exp.G6,   T_exp.F6,   T_exp.E6,   T_exp.D6,   T_exp.C6,   T_exp.B6,
T_exp.A6];
```

```
difference = abs(simData - expData);
difference_v = difference(:);
boxplot(difference,'plotstyle','compact');
figure
boxplot(difference_v,'plotstyle','compact');
```

A.5 Code: Multi-Channel PCM-TES

The multi-channel PCM-TES model was developed modularly. It can analyse any multi-channel configuration sequentially. Parts of the code can be modify depending of the needs of the user. The hysteresis model has not been implemented. Basically, the user will choose to use either the "melting" or "freezing" C_p-curve for the entire run. Future improvements are planned following additional testing of the PCM.

multi_channel_PCM_TES.m

```
%% Multi-Channel PCM-TES
% Vasken Dermardiros
% May 2015

%% Initialize
close all
clear
clc
addpath('Aux Functions')
addpath('Extra')
multi_channel_plot_template()

%% Simulation Input, PCM-TES Configuration and Setup
phase = 'F';
% Here, the user can specify the PCM-TES construction: 1: PCM, 2: Air Channel, 0: Nothing
pTESconf = [1,1,1,1,1,1,2,1,1,1,1,1,1,0,0,0,0,0;...     % 12 layers, {1,2,3,6} air channels
            1,1,1,2,1,1,1,1,1,1,2,1,1,1,0,0,0,0;...
            1,1,2,1,1,1,1,2,1,1,1,1,2,1,1,0,0,0;...
            1,2,1,1,2,1,1,2,1,1,2,1,1,2,1,1,2,1];
if phase == 'M'
    pHours = [36; 20; 14; 10];
    Temp_ini = 10;  % 15-28
    Temp_air = 28;
else
    pHours = [54; 30; 24; 12];
    Temp_ini = 28;
    Temp_air = 10;
end
Temp_env = 22;
pTESheight = [1.2; 2.4; 3.6];
TESwidth = 1;
numbVS = 1;
massflow_air_total = 100*6/3600;   % kg/s; (min: 80 kg/h per channel)

%% Parametric
tic
nTESheight = size(pTESheight,1);
nHours = size(pHours,1);
nTESconf = size(pTESconf,1);
nTEStotal = nTESheight * nTESconf;

count = 1;
for nHeight = 1:nTESheight
```

```
for nConf = 1:nTESconf

    TESheight = pTESheight(nHeight,:);
    TESconf = pTESconf(nConf,:);

    %% Run simulation
    H = pHours(nConf);
    multi_channel_run
    multi_channel_fan_power

    %% Plot Energy Profile
    subplot(nTESheight,nTESconf,count)
    multi_channel_plot
    multi_channel_plot_modify

    %% Plot dT
%     subplot(nTESheight,nTESconf,count)
%     multi_channel_plot_dT
%     multi_channel_plot_modify

    %% Increment
    count = count + 1;
end
end
disp(toc)

%% Save Plot
timestamp = datestr(now(),'yymmddHHMMSS');
filename = {sprintf('%s_%s_parametric',timestamp,phase)};
multi_channel_plot_export
```

multi_channel_plot_template.m

```
function multi_channel_plot_template()
% The new defaults will not take effect if there are any open figures. To
% use them, we close all figures.
close all;

% Defaults
% 4.5 x 3.5 for Cp curves (w x h)
% 6.5 x 2.5 for temp plots - wide
% 5.0 x 1.9 for temp plots - narrow
% 2.5 x 4.0 for temp plots - tall
% 6.5 x 4.5 for charge/discharge plots
% 8.0 x 4.5 for heat maps
% 4.0 x 3.5 for pressure drop
width = 13;    % Width in inches
height = 3.5;  % Height in inches
alw = 0.75;    % AxesLineWidth
fsz = 11;      % Fontsize
lw = 1.;       % LineWidth
msz = 8;       % MarkerSize

% The properties we've been using in the figures
set(0,'defaultLineLineWidth',lw);   % set the default line width to lw
set(0,'defaultLineMarkerSize',msz); % set the default line marker size to msz
```

```
set(0,'defaultLineLineWidth',lw);   % set the default line width to lw
set(0,'defaultLineMarkerSize',msz); % set the default line marker size to msz

% Set the default Size for display
defpos = get(0,'defaultFigurePosition');
set(0,'defaultFigurePosition', [defpos(1) defpos(2) width*100, height*100]);

% Set the defaults for saving/printing to a file
set(0,'defaultFigureInvertHardcopy','on'); % This is the default anyway
set(0,'defaultFigurePaperUnits','inches'); % This is the default anyway
defsize = get(gcf, 'PaperSize');
left = (defsize(1)- width)/2;
bottom = (defsize(2)- height)/2;
defsize = [left, bottom, width, height];
set(0, 'defaultFigurePaperPosition', defsize);
close all
```

multi_channel_run.m

```
%% Load Header file with Cp curve parameters
phT = phase;
multi_header

%% Setup
% PCM-TES configuration
% 0: Front and back are insulated with R_ins and exposed to T_env with h_env
% 1: PCM material of thickness dx
% 2: Air channel
conf = TESconf;
nChn = sum(conf(:) == 2);       % Number of air channels
height = TESheight;
width = TESwidth;
nVS = numbVS;
A = height*width/nVS;          % Surface area per vertical section
m_air_chn = massflow_air_total/nChn;
ehAmCp = exp(-h_chn*2*A/(m_air_chn*Cp_air));
nL = sum(conf(:) ~= 0);         % Number of layers (air channel is a layer)
nN = 2*nL+1;                    % Number of nodes

% Temperatures
T_ini = Temp_ini;         % Initial Temperature
T_air = Temp_air;         % Air Temperature (at middle; then to be used as entering)
T_env = Temp_env;         % Environment Temperature

%% Initial Conditions
T = NaN(nT,nN,nVS);             % Nodal Temperature
T(1,:,:) = T_ini;
Tchn = zeros(nT,nChn,nVS+1);    % Air channel temperatures (time x channel x along channel)
Tchn(:,:,1) = T_air;            % Initial air inlet temperature
Tchn(1,:,:) = T_ini;
E_per_VS = zeros(nT,nN,nVS);    % Energy Balance per Node

%% Outer Loop
for VS = 1:nVS
for t = 2:nT
```

```
    %% First Run?
    itt = 1;
    error = inf;
    Tlast = NaN(1,nN);

    %% Inner Loop
    while (itt <= maxItt) && (error > maxErr)
        if itt == 1
            ti = t-1;
        else
            ti = t;
        end

        %% U-matrix ("U_N")
        U = zeros(nN);      % W/K
        for L = 1:nL
            if conf(L) == 1
                U(2*L-1, 2*L) = 2*A*k_PCM/dx;
                U(2*L, 2*L+1) = 2*A*k_PCM/dx;
            else
                U(2*L-1, 2*L) = A*h_chn;
                U(2*L, 2*L+1) = A*h_chn;
                TfK = T(ti,2*L-1,VS) + 273.15;
                TbK = T(ti,2*L+1,VS) + 273.15;
                U(2*L-1, 2*L+1) = A*sig*(TfK^2+TbK^2)*(TfK+TbK) / (1/e_chn + 1/e_chn - 1);
                clear TfK TbK
            end
        end
        clear L

        %% F-matrix (nodal connections with known temperature sources "U_M")
        F = zeros(nN,1);    % W/K
        F(1) =   (1/(h_out*A) + R_ins/A)^-1;
        F(end) = (1/(h_out*A) + R_ins/A)^-1;    % Front and back insulation could be
               different

        %% C-vector, the default capacitance value can be changed here
        if t ~= 2
            C_prev = C;
        end
        C = zeros(nN,1);    % J/K
        for L = 1:nL
            if conf(L) == 1
                C(2*L) = rho*A*dx*fCp_skewnormal(T(ti,2*L,VS), skew, T_peak, rng, dh,
                                Cp_avg);
                %C(2*L) = rho*A*dx*1000;
            end
        end
        clear L
        if t == 2
            C_prev = C;
        end

        %% Transform U-matrix into standard form (LHS)
        U = -U - U';
        s = -sum(U,2);
        for j = 1:nN
            U(j,j) = s(j) + F(j) + C(j)/dt;
        end
        clear j
```

```
        %% Heat flux into the node
        q = zeros(nN,1);
        q(1) = F(1)*T_env;
        q(end) = F(end)*T_env;
        chn = 1;
        for L = 1:nL
            if conf(L) == 2
                q(2*L) = -m_air_chn*Cp_air*(Tchn(ti,chn,VS+1)-Tchn(ti,chn,VS));
                chn = chn + 1;
            end
        end
        clear L chn

        %% Q-vector (RHS)
        Q = zeros(nN,1);
        for j = 1:nN
            Q(j) = q(j) + C(j)*T(t-1,j)/dt;
        end
        clear j q

        %% Solve
        T(t,:,VS) = U\Q;

        %% Solve for air stream inlet/outlet temperatures
        chn = 1;
        for L = 1:nL
            if conf(L) == 2
%                Tchn(t,chn,1) = T_air;
                Tchn(t,chn,VS+1) = ...
                      Tchn(t,chn,VS)*ehAmCp + 0.5*(T(t,2*L-1,VS)+T(t,2*L+1,VS))*(1-ehAmCp);
                chn = chn + 1;
            end
        end
        clear L chn

        %% Calculate Error
        if (itt ~= 1)   error = max(abs(T(t,:,VS) - Tlast));        end;
        Tlast = T(t,:,VS);

        %% Iterate
        if (itt == maxItt)  warning('progr:Nneg','Maximum iteration attained for t = %d, VS
              = %d',t,VS);    end;
        itt = itt+1;

    end

    %% Energy Balance
    % E = C*dT in Joules
    for m = 1:nN
        E_per_VS(t,m,VS) = (0.5*(C(m)+C_prev(m))) * (T(t,m,VS)-T(t-1,m,VS));
    end
    clear m
end
end

%% Energy Stored in PCM
E_temp = sum(E_per_VS, 3);
E_temp = cumsum(E_temp, 1);
E = E_temp(:, E_temp(2,:)~=0);
clear E_temp E_per_VS
```

```
%% Energy Balance at Air Node, per air channel
Eair_per_t = zeros(nT, nChn);
Eair = zeros(nT, nChn);
for c = 1:nChn
    Eair_per_t(2:end,c) = -m_air_chn.*Cp_air.*(Tchn(2:end,c,end)-Tchn(2:end,c,1))*dt;
    Eair(:,c) = cumsum(Eair_per_t(:,c),1);
end
clear c Eair_per_t

%% Energy transfered to the PCM, per air channel
EtoPCM_per_t = zeros(nT, nChn, nVS);
EtoPCM_cum_t = zeros(nT, nChn, nVS);
for n = 1:nVS
    chn = 1;
    for L = 1:nL
        if conf(L) == 2
            EtoPCM_per_t(:,chn,n) = dt*h_chn*A*(2*T(:,2*L,n) -T(:,2*L-1,n) -T(:,2*L+1,n));
            EtoPCM_cum_t(:,chn,n) = cumsum(EtoPCM_per_t(:,chn,n),1);
            chn = chn + 1;
        end
    end
end
EtoPCM = sum(EtoPCM_cum_t,3);
clear c n chn EtoPCM_per_t EtoPCM_cum_t

%% Energy lost to the environment
Eloss_per_t = zeros(nT, nVS);
Eloss_cum_t = zeros(nT, nVS);
for n = 1:nVS
    Eloss_per_t(2:end,n) = dt*A*(F(1)*(T(2:end,1,n) - T_env) + F(end)*(T(2:end,end,n) -
T_env));
    Eloss_cum_t(:,n) = cumsum(Eloss_per_t(:,n),1);
end
Eloss = sum(Eloss_cum_t,2);
clear n Eloss_per_t Eloss_cum_t
```

multi_header.m

```
% PCM Properties
if phT == 'M'          % Melting range
    skew = -10;        % skew
    T_peak = 23.6;     % peak phase change temperature, C; SLIGHTLY OFF 22
    rng = 4.5;         % range of phase change, C
    dh = 13100;        % enthalpy of phase change, J/kg 13100
    Cp_avg = 3500;     % average solid/liquid specific heat (full quality), J/kg
elseif phT == 'F'      % Freezing range
    skew = -4;
    T_peak = 20.8;
    rng = 4.68;
    dh = 12600;
    Cp_avg = 3500;
end

% Material Properties
rho = 850;             % kg/m^3
dx = 0.0052;           % m
```

```
%gap = 0.030;        %from main program
Lrough = 1.52*10^-6;
h_out = 5;          % W/m^2K; Convection coefficient in the ceiling space
h_chn = 18;         % W/m^2K; Convection coefficient in the air channel (available for 16 or
                      18 W/m^2K)
e_chn = 0.90;       % emissivity of painted PCM panels (0.85 to 0.95)
sig = 5.67*10^-8;   % Stefan-Boltzman constant
rho_air = 1.2;      % kg/m^3
Cp_air = 1005;      % J/kgK
nu_air = 17.6e-6;   % kg/m*s
R_ins = 2;          % m^2K/W, 1.32
k_fctr = 0.80;      % factor representing contact resistance applied to the conductivity of
                      PCM
k_PCM = 0.20*k_fctr;
n_fan = 0.20;       % fan efficiency

% Control
st = 120;           % steps per hour
%H = 36;             % number of hours; from main program
nT = st*H;          % number of timesteps
dt = 3600/st;       % s (3600s = 1 hour)
maxItt = 50;        % maximum number of iterations per timestep
maxErr = 1e-7;      % maximum temperature difference between iterations of a given timestep
```

multi_channel_fan_power.m

```
% For h = 16 W/(m^2*K)
if h_chn == 16
    f_a = 0.295;
    f_b = 0.8171;
    f_c = 0.001974;
% For h = 18 W/(m^2*K)
elseif h_chn == 18
    f_a = 0.2616;
    f_b = 0.8189;
    f_c = 0.001869;
else
    error('channel h-value not studied')
end
gap = f_a*m_air_chn.^f_b + f_c;
clear f_a f_b f_c

velocity = m_air_chn./(rho_air*gap*TESwidth);
Dh = 2*TESwidth*gap/(TESwidth+gap);
Re = velocity*Dh/nu_air;

if Re < 2300
    f = 64/Re;
else
    f = colebrook(Re,Lrough/Dh);
end

dPres = (f*(TESheight/Dh)+0.5+1.0)*(rho_air*velocity^2/2);

fan_power = (TESwidth*gap*velocity*nChn)*dPres/n_fan;
```

```
Efan = fan_power*(1:nT)'*dt;
```

multi_channel_plot.m

```
hold all
if phase == 'F'
    E = -E;
    Eair = -Eair;
    Eloss = -Eloss;
end
plot([sum(E,2), sum(Eair,2), Eloss, Efan]/(3.6e6));
eff = sum(E,2) - Efan;
plot(eff/(3.6e6),'k','LineWidth',2);
if H >= 29
    set(gca,'XTick',0:6*st:nT);
    set(gca,'XTickLabel',0:6:nT/st,'XMinorTick','on');
else
    set(gca,'XTick',0:3*st:nT);
    set(gca,'XTickLabel',0:3:nT/st,'XMinorTick','on');
end
xlim([0 nT]);
% ylimmin = floor(2*max(sum(Eloss,2))/(3.6e6))/2;
ylimmax = ceil(2*max(sum(Eair,2))/(3.6e6))/2;
if ylimmax >= 4
    set(gca,'YTick',0:1:ylimmax);
else
    set(gca,'YTick',0:0.5:ylimmax);
end
ylim([0 ceil(2*max(sum(Eair,2))/(3.6e6))/2]);
hXLabel = xlabel('Time, h');
hYLabel = ylabel('Energy, kWh');
Title = sprintf('H: %.1f, Chns: %.0f, Cap: %.3f kWh', TESheight, sum(TESconf(:)==2),
sum(E(end,:),2)/(3.6e6));
hTitle = title(Title);
hLegend = legend('PCM','Air','Lost','Fan','Effective','Location','Best');
%legend boxoff
grid on

% Percent charge/discharge
PCD_stored_energy = sum(E,2);
PCD_done = PCD_stored_energy(end);

if phase == 'M'
    action = 'charged';
else
    action = 'discharged';
end

PCD_50 = 0.50*PCD_done;
PCD_50_ind = find(abs(PCD_stored_energy) > abs(PCD_50));
PCD_50_ind = PCD_50_ind(1);
PCD_50_val = PCD_stored_energy(PCD_50_ind);
PCD_50_txt = sprintf('50%% %s (%.4f kWh) in %.1f h', action, PCD_50_val/(3.6e6),
PCD_50_ind/st);

PCD_70 = 0.70*PCD_done;
```

```
PCD_70_ind = find(abs(PCD_stored_energy) > abs(PCD_70));
PCD_70_ind = PCD_70_ind(1);
PCD_70_val = PCD_stored_energy(PCD_70_ind);
PCD_70_txt = sprintf('70%% %s (%.4f kWh) in %.1f h', action, PCD_70_val/(3.6e6),
PCD_70_ind/st);

PCD_90 = 0.90*PCD_done;
PCD_90_ind = find(abs(PCD_stored_energy) > abs(PCD_90));
PCD_90_ind = PCD_90_ind(1);
PCD_90_val = PCD_stored_energy(PCD_90_ind);
PCD_90_txt = sprintf('90%% %s (%.4f kWh) in %.1f h', action, PCD_90_val/(3.6e6),
PCD_90_ind/st);

PCD_95 = 0.95*PCD_done;
PCD_95_ind = find(abs(PCD_stored_energy) > abs(PCD_95));
PCD_95_ind = PCD_95_ind(1);
PCD_95_val = PCD_stored_energy(PCD_95_ind);
PCD_95_txt = sprintf('95%% %s (%.4f kWh) in %.1f h', action, PCD_95_val/(3.6e6),
PCD_95_ind/st);

PCD_EFF_ind = find(eff == max(eff));
PCD_EFF_ind = PCD_EFF_ind(1);
PCD_EFF_val = PCD_stored_energy(PCD_EFF_ind);
PCD_EFF_txt = sprintf('Eff: %.1f%% (%.4f kWh) in %.1f h', PCD_EFF_val/PCD_done*100,
PCD_EFF_val/(3.6e6), PCD_EFF_ind/st);

disp([TESheight nConf gap*velocity*TESwidth*rho_air*nChn*3600])
disp([m_air_chn gap velocity dPres])
disp(PCD_50_txt)
disp(PCD_70_txt)
disp(PCD_90_txt)
disp(PCD_95_txt)
disp(PCD_EFF_txt)
disp(' ')
%hText = text(0,0,{PCD_50_txt,PCD_70_txt,PCD_90_txt,PCD_95_txt,PCD_EFF_txt},
       'VerticalAlignment','bottom');
```

multi_channel_plot_modify.m

```
%% Plot adjustments
set(gca,'FontName', 'Helvetica' );
set([hTitle, hXLabel, hYLabel], 'FontName', 'AvantGarde');
if exist('hLegend');    set([hLegend, gca], 'FontSize',8); end;
set(gca,'FontSize', 8);
set([hXLabel, hYLabel],'FontSize', 10);
if exist('hText');    set(hText,'FontName','AvantGarde','FontSize',10); end;
set(hTitle, 'FontSize', 12, 'FontWeight', 'bold');
set(gca, ...
  'Box'         , 'off'     , ...
  'XMinorTick'  , 'off'     , ...
  'TickDir'     , 'out'     , ...
  'TickLength'  , [.02 .02] , ...
  'XColor'      , [.2 .2 .2], ...
  'YColor'      , [.2 .2 .2]);
```

multi_channel_plot_dT.m

```
hold all
dTchn = abs(mean(Tchn(:,:,1) - Tchn(:,:,end),2));
plot(dTchn);
xlim([0 12*st]);
if H >= 29
    set(gca,'XTick',0:6*st:nT);
    set(gca,'XTickLabel',0:6:nT/st,'XMinorTick','on');
else
    set(gca,'XTick',0:3*st:nT);
    set(gca,'XTickLabel',0:3:nT/st,'XMinorTick','on');
end
ylim([0 18]);
hXLabel = xlabel('Time, h');
hYLabel = ylabel('Abs. In-Out Difference, K');
Title = sprintf('H: %.1f, Chns: %.0f', TESheight, sum(TESconf(:)==2));
hTitle = title(Title);
grid on
```

multi_channel_plot_modify.m

```
%% Plot adjustments
set(gca,'FontName', 'Helvetica' );
set([hTitle, hXLabel, hYLabel], 'FontName', 'AvantGarde');
if exist('hLegend');    set([hLegend, gca], 'FontSize',8); end;
set(gca,'FontSize', 8);
set([hXLabel, hYLabel],'FontSize', 10);
if exist('hText');    set(hText,'FontName','AvantGarde','FontSize',10); end;
set(hTitle, 'FontSize', 12, 'FontWeight', 'bold');
set(gca, ...
  'Box'         , 'off'     , ...
  'XMinorTick'  , 'off'     , ...
  'TickDir'     , 'out'     , ...
  'TickLength'  , [.02 .02] , ...
  'XColor'      , [.2 .2 .2], ...
  'YColor'      , [.2 .2 .2]);
```

multi_channel_plot_export.m

```
%% Export EPS
exportFilename = filename;
exportFilename = sprintf('%s.eps',exportFilename{1,1});

set(gcf, 'PaperPositionMode', 'auto');
print -depsc2 dummy.eps
close;
fixPSlinestyle('dummy.eps', exportFilename);
delete('dummy.eps')
movefile(exportFilename,'Figures');
clear exportFilename
```

A.6 PCM-TES Case Study Room Description

The office is among an infinite array of self-similar and similarly behaving south-facing offices. This implies that adjacent rooms have the same thermal profile. When modelling, the underside of the floor becomes the ceiling of the office, and on the opposite side of the left wall, we have the right wall. These walls do not have an adiabatic boundary at their middle. The back wall, however, has to be assumed adiabatic.

The PCM-TES system is assumed not to occupy any space in the office. It draws air from the office room and outputs it back to the office when it is toggled *on*. The PCM-TES is activated at the same time as the morning start-up and is toggled *off* when it no longer supplies energy to the room (discharged). It is assumed that the PCM-TES is recharged at a favourable time with no effect on the peak load. Finally, the PCM-TES follows the multi-channel system design with the most air channels (6) with two systems in series. The boundary layers are assumed to be adiabatic.

A.6.1 Office Geometry

The office has a single large window in the middle of its façade (40% window-to-wall ratio (WWR)). The bottom opaque section of the façade is at 0.8 m which is at the workplane height. The trend for newer "high-performance" buildings is to have a WWR of 90%+. For a more detailed analysis, the window framing should have been considered. Here is a simple rendered image of the office showing relevant dimensions:

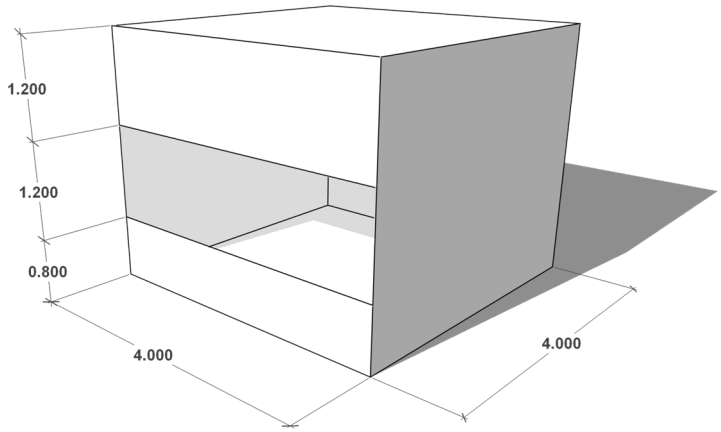

Figure A 2: Rendering of the office with relevant dimensions.

A.6.2 Construction Details

There are four construction details for the office: the window, the exterior opaque wall, the interior walls, the ceiling and the floor. The window consist of a double-glazed low-e insulated glazing unit (IGU) with a 12 mm argon film. A use of interior blinds were planned but left unused. The exterior wall is prefabricated. The interior wall consists of 2 half inch gypsum boards. The building horizontal surfaces are assumed to effectively behave like a 50 mm (2 in.) concrete slab. The concrete is left exposed. The underside of the slab becomes the ceiling. To simplify the modeling, the ceiling was assumed to be fully exposed and without acoustic tiles. Here are the construction detail drawings:

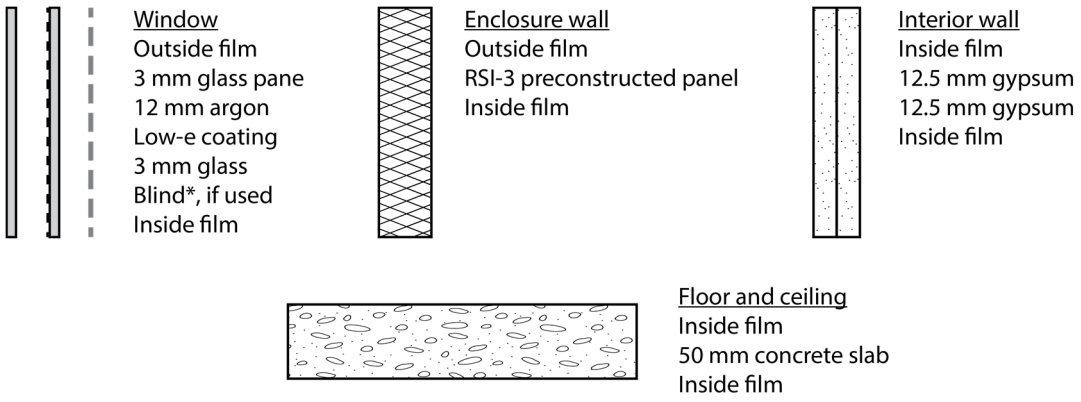

Figure A 3: Construction details.

A.6.3 Numerical Modelling

The implicit finite difference method is used to model the office. The modelling procedure follows the equations from Chapter 3. Full radiation exchange was considered without linearization, but the process had to be iterated for the given timestep until the difference in temperature between iterations were below a set limit. The interior convection rate had a fixed value, but should vary with temperature. The fixed value was assumed since the office is equipped with diffusers and there is always movement in the room, thus encouraging the mixing of the air. The simulation timestep was set to 60 seconds.

A.6.4 Thermal Network and Additional Considerations

To analyse the behaviour of the room, first we draw the thermal network:

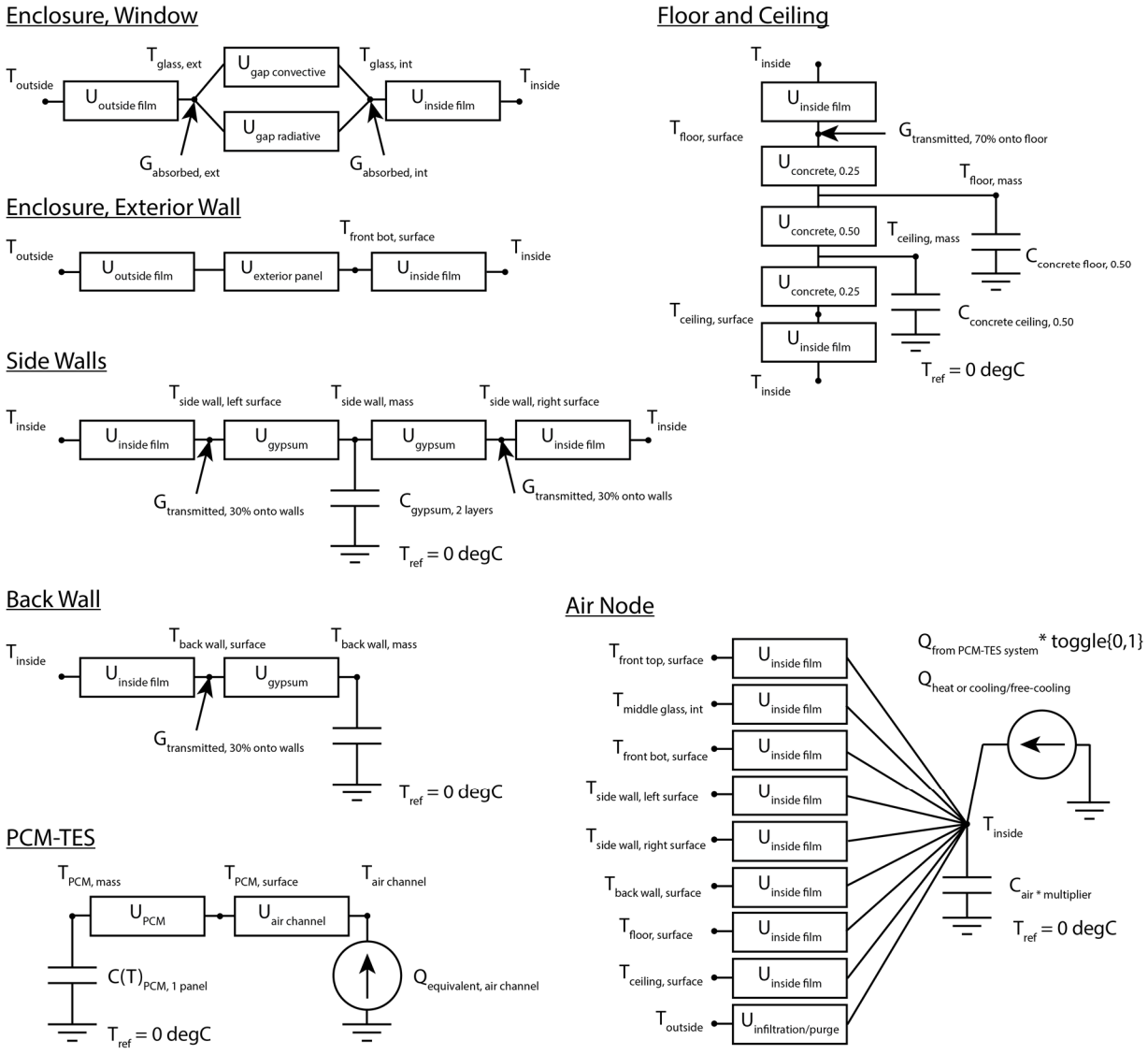

Figure A 4: Office thermal network.

The thermal networks for the window, exterior wall and side walls are straightforward. The floor/ceiling mass is split into two capacitances given its thickness. There is a heat source on the top side which is used in the last part of this study. 70% of the solar radiation falls on the floor. The rest is equally distributed on the side walls. The air node network has a capacitance for the air mass and a

multiplier (set to 20) in order to consider the added capacitance due to furniture. Some infiltration is considered (set to 0.2 air changes per hour).

Radiation exchange between all internal surfaces are considered using the radiosity method. It is not drawn in the thermal network since it would be hard to represent it clearly. The reasoning behind the implementation of this detail is that the floor or ceiling might be used for radiant heating and cooling and will results in large thermal asymmetries in the zone. Radiation exchange within the glass panes in the IGU is also considered.

The view factors, $F_{i->j}$, were estimated using EnergyPlus. The method is limited to convex floor plans. The results can be found in the attached script in the view factor section. For example, the view factor between the side wall and the back wall should be equal to 0.2; EnergyPlus had it calculated as 0.177.

The inside convective rate was fixed to 3 $W \cdot m^{-2} \cdot K^{-1}$. In a more detailed study, this rate should change depending on the surface and air temperatures. In cases where there is no air mixing by the HVAC diffusers, a cool floor would promote stratification and after some time, the only path of heat transfer would be through conduction. The heat transfer rate would be reduced to k_{air} = 1 $W \cdot m^{-2} \cdot K^{-1}$.

Convection in the IGU is governed by natural convection. The method to calculate this value is detailed in §5.3.3 of ISO 15099:2003 and will not be expanded in this report. For a 12 mm argon film, the convective coefficient is around 1.5 $W \cdot m^{-2} \cdot K^{-1}$ for practically the whole temperature range in this study.

A.6.5 Input Profiles

The solar radiation transmitted and absorbed is calculated for Montreal for an overcast sky:

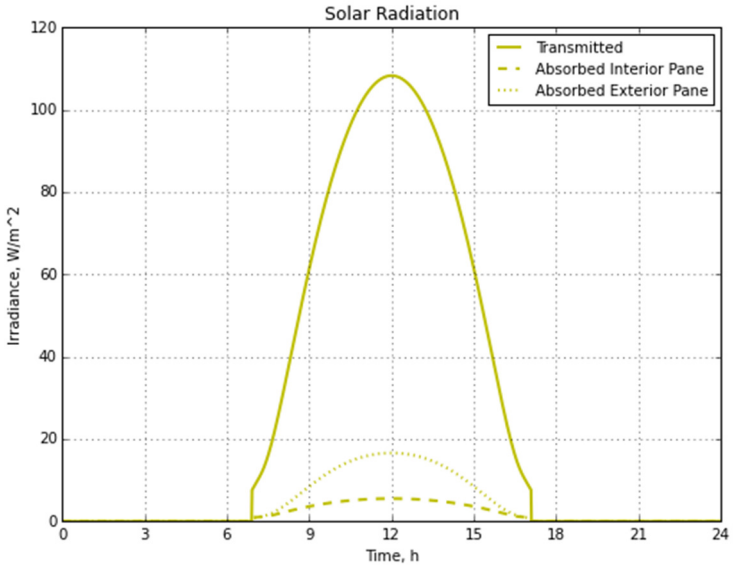

Figure A 5: Solar radiation distribution on a south-facing vertical IGU.

The outside temperature follows a perfect sinusoidal curve for a day in February. The peak is set at 3:00 PM with a 10°C ΔT and a -15°C mean temperature. The weather need not be sinusoidal.

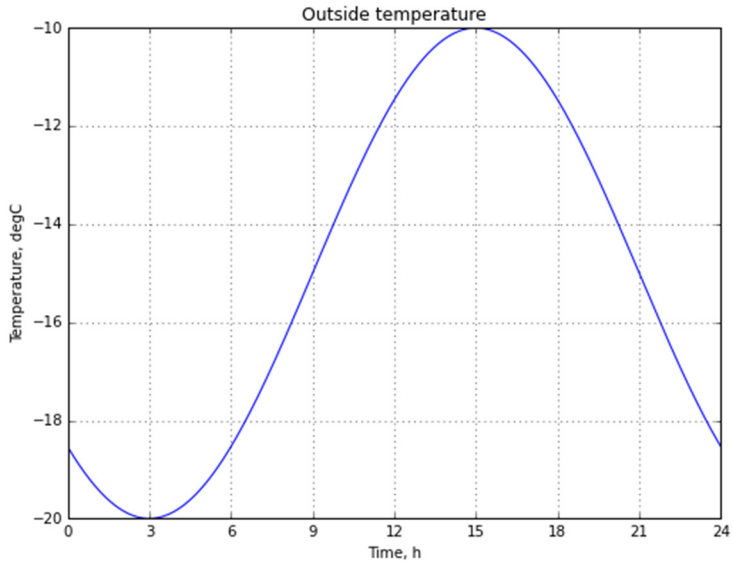

Figure A 6: Outside temperature profile.

Heating and cooling is injected directly and 100% efficiently into the air node. In reality, the HVAC system may need some time to react to newer setpoints or temperature swings. To do a full energy consumption analysis, the COP of the heat pump, fan energy, heater efficiency, etc. have to be all considered.

To simplify the analysis, the office was assumed to be unoccupied at all times.

A.6.6 Control Strategy

The heater is controlled using proportional control. As the room temperature comes closer to the setpoint, less heating is supplied. There is no offset included to counter the resulting temperature bias. A proportional-integral term would remedy this shortcoming.

Algorithm 1 *Proportional control: heating*

given room temperature, heating setpoint, Kp and maximum capacity

repeat:

calculate error = (setpoint - room temperature)$^{+}$

heating required = Kp * error

if heating required > maximum capacity

supply maximum capacity

else

supply heating required

The Kp-value is set to {capacity*2} in order to have a fast-acting system. There are more detailed ways of obtaining the proportionality constant, but this proved sufficient.

During the evening and night, a temperature setback is considered. The code is written so that the setback can be ramped. Basically, during the night, the heating setpoint temperature is lowered to, theoretically, save on heating.

Algorithm 2 *Setpoint setback*

given the setpoint, setback dT, ramp duration and occupied period

repeat:

    if occupied

        use room setpoint

    if unoccupied

        use room setpoint – setback dT

    else

        room setpoint +/- setback dT / ramp duration

And finally, here is the algorithm of the PCM-TES system:

Algorithm 3 *PCM-TES system*

given toggle *on* and *off* times, fully charged temperature, room temperature

repeat:

    if current time >= toggle *on* time & current time < toggle *off*

        if first time

            reset PCM-TES temperature = fully charged temperature

        else

            room air is drawn into the PCM-TES inlet

            heat output from PCM-TES is output towards the office

    else

        heat output from PCM-TES is diverted away from the office

To summarize, the objective here is to study how the PCM-TES can be used to reduce the heating peak load. The base scenario will be the office without the PCM-TES. The office is subjected to a few days of the same solar and temperature profiles described above until a steady periodic state is achieved. In the morning, there is a sudden step change in the setpoint profile. The heater will be turned on to its maximum capacity in order to try to close the setpoint error gap. This will result in a large heating usage. For the second scenario, during the morning start up, the PCM-TES will be discharged of its stored energy alongside the power delivered from the heating system. The energy from the fans to draw the room air into the PCM-TES is minimal compared to the electrical demand needed for the electric heaters, and so a reduction of the peak heating demand is expected.

A.7 Code: PCM-TES Case Study

The PCM-TES case study was analysed in Python and the computer script/code is given below:

PCM_TES_case_study.py

```
# ================================================================================
#  Prepared by Vasken Dermardiros, (C) 2015
# ================================================================================

# PCM-TES Case Study: How it behaves in a small low thermal capacitance office

###### Load Dependencies:
import math
import numpy as np
import matplotlib.pylab as plt
import matplotlib as mpl
mpl.rc('figure', figsize=(8, 6))
import pickle
#import os

#%% User-Defined Functions
# Cp(T) function based on the skewed normal distribution
def fCp(Temp, skew, T_peak, rng, dh, Cp_avg):
    Tx = (Temp-T_peak)/rng
    return dh*mpl.mlab.normpdf(Tx,0,1)*(1+math.erf(skew*Tx/np.sqrt(2))) + Cp_avg

#%%
# U: Conductance matrix (symmetrical) with added capacitance for diagonal term
# C: Capacitance vector
# F: Conductance vector of nodes connected to a known temperature source
# T: Temperature vector
# q: Heat flow, only external sources
# Q: Heat flow vector, external sources + capacitance from previous timestep
# nN: Number of nodes
# VF: View factor matrix; values only for room side surface
# *Node that indexing starts at "0" in python (not "1" like in Matlab)

# Node Number: Surface
# 0: left surface
# 1: right surface
# 2: back surface
# 3: front wall, top -> opaque
# 4: front wall, middle -> transparent
# 5: front wall, bottom -> opaque
# 6: floor surface
# 7: ceiling surface
# 8: air node
# 9: side inside; node connected to left and right surfaces
# 10: floor inside; node connected to ceiling inside
# 11: ceiling inside
# 12: back inside; behind of this layer considered adiabatic
# 13: middle window, outside pane
# 14: PCM, node, first set
# 15: PCM, surface, first set
# 16: PCM, air stream, first set
# 17: PCM, node, second set
```

```
# 18: PCM, surface, second set
# 19: PCM, air stream, second set
# P0: air temp at inlet of PCM
# P1: air temp after first set of PCM
# P2: air temp after second set of PCM

# Geometry and other properties
A_sid = 12.8
A_cei = 16.0
A_bck = 12.8
A_ftp = 4.8
A_ftm = 4.8
A_fbt = 3.2
A = np.array([A_sid, A_sid, A_bck, A_ftp, A_ftm, A_fbt, A_cei, A_cei, 0, A_sid, A_cei,
A_cei, A_bck, A_ftm])
Vol = 51.2
A_total = 2*(A_sid + A_bck + A_cei)
R_curt = 3.     # m^2K/W
purge = 0       # nightime ventilation, on/off control

# View factors; precalculated using EnergyPlus (approximate method)
VF = np.array([ [0,         0.1827, 0.1491, 0.0685, 0.0685, 0.0457, 0.2429, 0.2429], \
                [0.1827,    0,      0.1491, 0.0685, 0.0685, 0.0457, 0.2429, 0.2429], \
                [0.1766,    0.1766, 0,      0.0662, 0.0662, 0.0442, 0.2350, 0.235],  \
                [0.1827,    0.1827, 0.1491, 0,      0,      0,      0.2429, 0.2429], \
                [0.1827,    0.1827, 0.1491, 0,      0,      0,      0.2429, 0.2429], \
                [0.1827,    0.1827, 0.1491, 0,      0,      0,      0.2429, 0.2429], \
                [0.1944,    0.1944, 0.1588, 0.0729, 0.0729, 0.0486, 0,      0.2582], \
                [0.1944,    0.1944, 0.1588, 0.0729, 0.0729, 0.0486, 0.2582, 0] ])
nR = np.size(VF,0)

# Radiosity
sig = 5.67e-8
e_surf = 0.9
e_glas = 0.868
e_lowe = 0.013
emis = np.ones((nR,1))*e_surf   # emissivity vector
emis[4] = e_glas
uRad = np.zeros((nR,nR))
for iR in range(0,nR):
    for jR in range(0,nR):
        if VF[iR,jR] != 0:
            uRad[iR,jR] = ((1-emis[iR])/(A[iR]*emis[iR]) + 1/(A[iR]*VF[iR,jR]) + (1-
                           emis[jR])/(A[jR]*emis[jR]))**-1

# Solar radiation
#with open('direct.pkl') as f:
with open('direct_60.pkl') as f:
    q_st, q_sa_ext_pane, q_sa_int_pane = pickle.load(f)
# Overcast
q_st_overcast = 0.20 * q_st
# Assume Overcast sky
q_st = q_st_overcast
q_sa_ext_pane = 0.20*q_sa_ext_pane
q_sa_int_pane = 0.20*q_sa_int_pane

# ASHRAE values; h-values are convection, conduction and radiation combined
h_out = 34.     # W/m^2K
#h_gap = 3.35    # W/m^2K
h_int = 4.      # W/m^2K
#k_gla = 1.      # W/mK
```

```
#x_gla = 0.004   # m; thickness of glass 4 mm
h_gap_conv = 1.50

# Material properties
# Concrete
k_conc = 1.731       # W/(m*K)
rho_conc = 2240      # kg/m^3
Cp_conc = 840        # J/(kg*K) where J = kgm^2/s^2
dx_conc = 0.050/2    # m, effective slab thickness 50 mm (2"), split into 2 nodes

# Gypsum
k_gyps = 0.810       # W/(m*K)
rho_gyps = 1680      # kg/m^3
Cp_gyps = 840        # J/(kg*K) where J = kgm^2/s^2
dx_gyps = 0.025      # m, 2 layers of gympsum 25 mm total (1"), 1 node

# Air
k_air = 0.0255       # W/(m*K)
rho_air = 1.184      # kg/m^3
Cp_air = 1006        # J/(kg*K)
multi = 20.          # Mass multiplier

# DuPont Energain PCM
use_PCM = True       # use the PCM-TES Option?
time_on_PCM = 6.     # time to turn On PCM-TES system
time_off_PCM = 10.   # time to turn Off PCM-TES system
toggle = 0           # toggle "1" or "on" for PCM-TES fan to be active, "0" otherwise
k_PCM = 0.20         # W/(m*K)
rho_PCM = 850.       # kg/m^3
dx_PCM = 0.0052      # m
T_PCM = 28.          # degC, PCM-TES temperature when fully charged (hot)
h_PCM = 18.          # W/m^2K, convection in PCM-TES channel
n_PCM = 10           # number of PCM panels * 2
m_PCM = 50./3600.    # kg/s, massflow rate per PCM
m_PCM_total = n_PCM*m_PCM   # kg/s, total massflow rate in PCM-TES
A_PCM = 1.2          # m^2, area of PCM panel
ehAmCp = np.exp(-h_PCM*2*A_PCM/(m_PCM*Cp_air))
# Melting Cp Parameters
PCMm_skew = -10.     # skew
PCMm_T_peak = 23.6   # peak phase change temperature, C
PCMm_rng = 4.5       # range of phase change, C
PCMm_dh = 13100.     # enthalpy of phase change, J/kg 13100
PCMm_Cp_avg = 3500.  # average solid/liquid specific heat (full quality), J/kg
# Freezing Cp Parameters
PCMf_skew = -4.
PCMf_T_peak = 20.8
PCMf_rng = 4.68
PCMf_dh = 12600.
PCMf_Cp_avg = 3500.

# Simulation control
nN = 20
st = 60         # steps per hour
H = 24          # hr; number of hours simulated
nt = int(st*H)  # number of timesteps-1
dt = 3600/st    # s (3600 sec = 1 hour)
days = 3        # number of days simulated
maxItt = 20.    # maximum number of iterations
maxErr = 1e-5   # maximum temperature difference from iteration to the next

# Known temperatures
```

```
T_out = np.zeros((nt*days,1))   # degC
T_out_m = -15.                  # degC; Exterior temperature
dT_out = 10.
T_out_theta = -5*np.pi/4
w = 2*np.pi/86400

# Temperature setpoint
# Heating
T_SP = np.zeros((nt,1))         # degC; Interior temperature setpoint per timestep Heating
T_SP_day = 22.
T_SP_dT = 4.
setback_beg = 18.
setback_end = 6.
ramp_dur = 0.1                  # hours
for t in range(0,nt):
    time = t*dt/3600.
    if (setback_beg <= time and time < (setback_beg+ramp_dur)):             # begin setback
        T_SP[t] = T_SP_day - (time-setback_beg)*T_SP_dT/ramp_dur
    elif ((setback_beg+ramp_dur) <= time or time < (setback_end-ramp_dur)): # night time
        T_SP[t] = T_SP_day - T_SP_dT
    elif ((setback_end-ramp_dur) <= time and time < setback_end):           # revert setback
        T_SP[t] = T_SP_day - (setback_end-time)*T_SP_dT/ramp_dur
    else:                                                                   # day time
        T_SP[t] = T_SP_day
# Cooling
T_SP_Cool = np.zeros((nt,1))    # degC; Interior temperature setpoint per timestep Cooling
T_SP_day_Cool = 24.
T_SP_dT_Cool = -2.
setback_beg_Cool = 18.
setback_end_Cool = 6.
ramp_dur_Cool = 0.             # hours
for t in range(0,nt):
    time = t*dt/3600.
    if (setback_beg_Cool <= time and time < (setback_beg_Cool+ramp_dur_Cool)):
        T_SP_Cool[t] = T_SP_day_Cool - (time-setback_beg_Cool)*T_SP_dT_Cool/ramp_dur_Cool
    elif ((setback_beg_Cool+ramp_dur_Cool) <= time or time < (setback_end_Cool-
              ramp_dur_Cool)):
        T_SP_Cool[t] = T_SP_day_Cool - T_SP_dT_Cool
    elif ((setback_end_Cool-ramp_dur_Cool) <= time and time < setback_end_Cool):
        T_SP_Cool[t] = T_SP_day_Cool - (setback_end_Cool-time)*T_SP_dT_Cool/ramp_dur_Cool
    else:
        T_SP_Cool[t] = T_SP_day_Cool

# Heating/Cooling system
q_aux = np.zeros((nt*days,1))   # W
SP_Err = np.zeros((nt*days,1))  # degC
max_Cap = 2500.                 # W; Heater size
min_Cap = 0.                    # W; minimum heat
Kp = max_Cap/0.5
Ki = 0.
iTerm = 0.
delay_nt = 5
heat_output = np.zeros((delay_nt,1))
heat_aux = 0.
SP_Err_Cool = np.zeros((nt*days,1))  # degC
max_Cap_Cool = 3000.
min_Cap_Cool = 0.
Kp_Cool = max_Cap_Cool/2
Ki_Cool = 0.0
iTerm_Cool = 0.
cool_aux = 0.
```

```
# Infiltration
ACH = 0.2

# Occupancy, internal loads
q_int = np.zeros((nt,1))
q_occup = 0.
q_unoccup = 0.    # Internal load reduction during unoccupied hour
occup_start = 9.
unoccup_start = 17.
ramp_dur = 1.5
for t in range(0,nt):
    time = t*dt/3600.
    if (unoccup_start <= time and time < (unoccup_start+ramp_dur)):
        q_int[t] = q_occup - (time-unoccup_start)*q_unoccup/ramp_dur
    elif ((unoccup_start+ramp_dur) <= time or time < (occup_start-ramp_dur)):
        q_int[t] = q_occup - q_unoccup
    elif ((occup_start-ramp_dur) <= time and time < occup_start):
        q_int[t] = q_occup - (occup_start-time)*q_unoccup/ramp_dur
    else:
        q_int[t] = q_occup

#%%
# Declare variables
C = np.zeros((nN,1))        # J/K
T = np.zeros((nt*days,nN))  # degC
P0 = np.zeros((nt*days,1))  # degC
P1 = np.zeros((nt*days,1))  # degC
P2 = np.zeros((nt*days,1))  # degC
q_PCM = np.zeros((nt*days,1))

# Nodes with capacitance
C[8] = rho_air*Cp_air*(Vol*multi)
C[9] = rho_gyps*Cp_gyps*(dx_gyps*A[9])
C[10] = rho_conc*Cp_conc*(dx_conc*A[10])
C[11] = rho_conc*Cp_conc*(dx_conc*A[11])
C[12] = rho_gyps*Cp_gyps*(dx_gyps*A[12])

# Initial condition
#T[0,] = 20.
T[0,] = T_SP_day - T_SP_dT

#%%
# Loop for number of days
for d in range(0,days):

    # Loop for all time in a day
    for t in range(0,nt):

        Itt = 1.
        Err = 100.
        Tp = T[d*nt+t,]

        time = t*dt/3600.
        # Turn on PCM-TES system
        if (use_PCM == True and time >= time_on_PCM  and time < time_off_PCM and toggle ==
              0):
            toggle = 1
            T[d*nt+t,14:20] = T_PCM      # re-initialize temperatures
        # Turn off PCM-TES system
        if (use_PCM == True and time >= time_off_PCM and toggle == 1):
```

```
            toggle = 0

        while(Itt <= maxItt and Err > maxErr):

            # Declare variables
            U = np.zeros((nN,nN))       # W/K
            F = np.zeros((nN,1))        # W/K

            # How are the nodes connected?
            # Radiation exchange between inside surfaces
            TR = T[d*nt+t,] + 273
            for jR in range(0,nR):
                for iR in range(0,jR):
                    if uRad[iR,jR] != 0:
                        U[iR,jR] = sig*uRad[iR,jR]*(TR[iR]**4-TR[jR]**4) / (TR[iR]-TR[jR])
            i_NaN = np.isnan(U)     # if both surfaces are at the exact same temperature,
                                    # results in a NaN: 0/0
            U[i_NaN] = 0            # replace NaN with 0: no heat transfer bet surfaces
            del i_NaN, iR, jR
            # Radiation exchange between glass panes
            h_gap_mid_rad = sig*(TR[4]**2+TR[13]**2)*(TR[4]+TR[13]) / (1/e_glas+1/e_lowe-1)
            # Connected to air node
            for i in range(0,8):
                U[i,8] = (1/(h_int*A[i]))**-1
            # Side walls
            U[0,9] = (dx_gyps/(2*k_gyps*A[0]))**-1
            U[1,9] = (dx_gyps/(2*k_gyps*A[1]))**-1
            # Floor and ceiling
            U[6,10] = (dx_conc/(2*k_conc*A[6]))**-1
            U[7,11] = (dx_conc/(2*k_conc*A[7]))**-1
            U[10,11] = (dx_conc/(k_conc*A[10]))**-1
            # Back wall
            U[2,12] = (dx_gyps/(2*k_gyps*A[2]))**-1
            # Window, middle
            h_gap_mid = h_gap_conv + h_gap_mid_rad
            U[4,13] = (1/(h_gap_mid*A[4]))**-1

            # Connected to temperature sources
            F[3] = (1/(h_out*A[3]) + R_curt/A[3])**-1
            F[5] = (1/(h_out*A[5]) + R_curt/A[5])**-1
            F[8] = ACH*Vol*rho_air*Cp_air/3600
            F[13] = (1/(h_out*A[4]))**-1

            # PCM-TES
            U[14,15] = 2*A_PCM*k_PCM/dx_PCM     # first set
            U[15,16] = A_PCM*h_PCM
            U[17,18] = 2*A_PCM*k_PCM/dx_PCM     # second set
            U[18,19] = A_PCM*h_PCM
            C[14] = rho_PCM*A_PCM*dx_PCM*fCp(T[d*nt+t,14], PCMf_skew, PCMf_T_peak, PCMf_rng,
                      PCMf_dh, PCMf_Cp_avg)
            C[17] = rho_PCM*A_PCM*dx_PCM*fCp(T[d*nt+t,16], PCMf_skew, PCMf_T_peak, PCMf_rng,
                      PCMf_dh, PCMf_Cp_avg)
            P0[d*nt+t] = T[d*nt+t,8]
            P1[d*nt+t] = P0[d*nt+t]*ehAmCp + T[d*nt+t,15]*(1-ehAmCp)
            P2[d*nt+t] = P1[d*nt+t]*ehAmCp + T[d*nt+t,18]*(1-ehAmCp)
            q_PCM[d*nt+t] = toggle*m_PCM_total*Cp_air*(P2[d*nt+t]-P0[d*nt+t])

            # U-matrix and its inverse
            U = -U - U.T # U is symmetrical, non-diagonals are -ve
            s = -np.sum(U,1)
            for i in range(0,nN):
```

```
                U[i,i] = s[i] + F[i] + C[i]/dt
            del i, s

            # Auxiliary heat, PI control
            SP_Err[d*nt+t] = (np.abs(T_SP[t]-T[d*nt+t,8]) + (T_SP[t]-T[d*nt+t,8]))/2
#            iTerm += Ki*SP_Err[d*nt+t]
            output = Kp*SP_Err[d*nt+t] # + iTerm
            if output > max_Cap:
#                iTerm -= output - max_Cap
                output = max_Cap
            if output < min_Cap:
#                iTerm += min_Cap - output
                output = min_Cap
            heat_output[-1] = output
            heat_aux = np.mean(heat_output)

            # Heat flow into the node
            T_out[d*nt+t] = T_out_m + dT_out/2*np.cos(w*t*dt + T_out_theta)     # Outside T
            q = np.zeros((nN,1))
            q[0] = A[0]/(A[0]+A[1]+A[2]) * 0.30 * (A[4]*q_st[t]) # 30% of total solar
                                                    radiation falls on sides walls
            q[1] = A[1]/(A[0]+A[1]+A[2]) * 0.30 * (A[4]*q_st[t]) # 30% of total solar
                                                    radiation falls on sides walls
            q[2] = A[2]/(A[0]+A[1]+A[2]) * 0.30 * (A[4]*q_st[t]) # 30% of total solar
                                                    radiation falls on sides walls
            q[3] = F[3]*T_out[d*nt+t]
            q[4] = A[4]*q_sa_int_pane[t]
            q[5] = F[5]*T_out[d*nt+t]
            q[6] = 0.70 * (A[4]*q_st[t])    # 70% of total solar radiation falls on floor
            q[8] = heat_aux - cool_aux + q_int[t] + q_PCM[d*nt+t]
            q[10] = 0.                  # Heated floor, off
            q[11] = 0.                  # Radiant ceiling, off
            q[13] = F[13]*T_out[d*nt+t] + A[13]*q_sa_ext_pane[t]
            q[16] = -m_PCM*Cp_air*(P1[d*nt+t]-P0[d*nt+t])
            q[19] = -m_PCM*Cp_air*(P2[d*nt+t]-P1[d*nt+t])

            # Q-vector
            Q = np.zeros((nN,1))
            for i in range(0,nN):
                Q[i] = q[i] + C[i]*T[d*nt+t,i]/dt
            del i

            # Compute temperature
            if (days*nt) > (d*nt+t+1):
                T[d*nt+t+1,] = np.linalg.solve(U,Q).T

            # Store auxilary heat data
                q_aux[d*nt+t+1,] = heat_aux - cool_aux
                if heat_aux > 20 and cool_aux > 20:
                    print "Both heating and cooling are on at timestep: %i, heating: %.0f W,
                             cooling: %.0f W" % (d*nt+t, heat_aux, cool_aux)

            # Compute iteration error
                Err = np.max(np.abs(T[d*nt+t+1,]-Tp))
                Tp = T[d*nt+t+1,]

            # Iterate
            Itt += 1

            if Itt == maxItt:
                print "Max iteration occured at timestep: %i" % (d*nt+t)
```

```
        # Adjust heat output delay: move everything up by a timestep, add a 0 at the end
        heat_output = np.append(heat_output[-(delay_nt-1):],0)

#%%
# Setpoints with internal temperature
fig = plt.figure()
ax = fig.add_subplot(1,1,1)
plt.hold(True)
plt.plot(np.dot(dt/3600.,range(0,nt)),T_SP,'r')
plt.plot(np.dot(dt/3600.,range(0,nt)),T_SP_Cool,'b')
plotT = T[(days-1)*nt:(days)*nt:]
plt.plot(np.dot(dt/3600.,range(0,nt)),plotT[:,8],'g')
plt.xlim([0,24])
ticks = np.arange(0,25,3)
ax.set_xticks(ticks)
plt.ylim([15,28])
plt.grid()
plt.legend(['Heating setpoint','Cooling setpoint','Room air'], loc='lower right',
fontsize='medium')
plt.xlabel('Time, h')
plt.ylabel('Temperature, degC')
plt.title('Zone Temperature')

#%%
# Heating/cooling
plotQ = q_aux[(days-1)*nt:(days)*nt:]
fig = plt.figure()
ax = fig.add_subplot(1,1,1)
plt.hold(True)
plt.plot(np.dot(dt/3600.,range(0,nt)),plotQ)
plt.xlim([0,24])
ticks = np.arange(0,25,3)
ax.set_xticks(ticks)
plt.xlabel('Time, h')
plt.ylabel('Auxiliary Heat or Cooling, W')
plt.title('Auxiliary heating or cooling supplied to air node')
plt.grid(True)
plt.show()
#fig.savefig('test.eps')
#fig = plt.figure()
#plt.plot(q_aux)
#plt.ylim([-2000,1100])

#%%
## Outside temperature
plotTout = T_out[(days-1)*nt:(days)*nt:]
fig = plt.figure()
ax = fig.add_subplot(1,1,1)
plt.hold(True)
plt.plot(np.dot(dt/3600.,range(0,nt)),plotTout)
plt.xlim([0,24])
ticks = np.arange(0,25,3)
ax.set_xticks(ticks)
plt.xlabel('Time, h')
plt.ylabel('Temperature, degC')
plt.title('Outside temperature')
plt.grid(True)
plt.show()
##fig.savefig('test.eps')
```

```
#%%
## Solar radiation transmitted
fig = plt.figure()
ax = fig.add_subplot(1,1,1)
plt.hold(True)
#plt.plot(np.dot(dt/3600.,range(0,nt)),[q_st, q_sa_ext_pane],'y', linewidth=2)
plt.plot(np.dot(dt/3600.,range(0,nt)),q_st,'y', linewidth=2)
plt.plot(np.dot(dt/3600.,range(0,nt)),q_sa_int_pane,'y--', linewidth=2)
plt.plot(np.dot(dt/3600.,range(0,nt)),q_sa_ext_pane,'y:', linewidth=2)
plt.xlim([0,24])
ticks = np.arange(0,25,3)
ax.set_xticks(ticks)
plt.xlabel('Time, h')
plt.ylabel('Irradiance, W/m^2')
plt.legend(['Transmitted', 'Absorbed Interior Pane', 'Absorbed Exterior Pane'],loc='best',
fontsize='medium')
plt.title('Solar Radiation')
plt.grid(True)
plt.show()
##fig.savefig('test.eps')

#%%
plotT = T[(days-1)*nt:(days)*nt:]
fig = plt.figure()
ax = fig.add_subplot(1,1,1)
plt.hold(True)
plt.plot(np.dot(dt/3600.,range(0,nt)),plotT[:,[0,1,2,6,7,10,11]])
plt.xlim([0,24])
#plt.ylim([19.2,20])
ticks = np.arange(0,25,3)
ax.set_xticks(ticks)
plt.xlabel('Time, h')
plt.ylabel('Temperature, degC')
plt.title('Office temperature: periodic steady state')
plt.grid(True)
plt.legend(['Left Surface', 'Right Surface', 'Back Surface', 'Floor Surface',\
            'Ceiling Surface','Floor Inside','Ceiling Inside'],loc=0)
plt.show()
```